Semiconductor Laser Signals and Noise in Fiber Grating Systems

Thesis by

Matthew S. McAdams

In Partial Fulfillment of the Requirements

for the Degree of

Doctor of Philosophy

California Institute of Technology

Pasadena, California

1998

(Defended December 8, 1997)

Acknowledgments

I would like to thank my advisor, Professor Amnon Yariv, for inviting me to study as a member of his research group. His keen physical intuition and decades of accumulated knowledge make him a more valuable reference than any collection of textbooks. The quality of his group serves as a magnet for funding and intellectual talent, both of which made my tenure as a graduate student much more pleasant.

I owe thanks to Dr. Bill Marshall for introducing me to laser noise and fiber propagation experiments, and for explaining a large volume of physics to me, often patiently. Dan Provenzano helped me build equipment and collect data, and rented me a bed in his apartment. Eva Peral refined our experimental and numerical techniques, and cheerfully tolerated my teasing. Ali Gaffari urged me to watch my diet and Jana Mercado fascinated me with many stories. Without the collaboration of T.R. Chen and ORTEL Corp., which provided state-of-the-art laser diodes, none of these experiments would have happened. I'm appreciative of all the other students in Prof. Yariv's group with whom I've spent years conversing, for scientific edification and otherwise: Dr. John O'Brien, Roger Koumans, Dr. Boaz Salik, Reginald Lee, and the others who know who they are.

Most of all I thank my beautiful wife Jennifer, who had a perfect sense for when to be patient and when to be...well, less patient.

Finally, the research described herein was supported financially by the Defense Advanced Research Projects Agency, the Office of Naval Research, and the Air Force

Office of Scientific Research. I greatly appreciate the willingness of these funding agencies, and through them the American taxpayers, to support basic research in science and engineering.

For Gwen Bowers

1943 - 1997

Thanks, Mom.

Abstract

This thesis describes the effect of transmission through a fiber Bragg grating on the signal and noise properties of semiconductor laser light. We show that fiber gratings can be used to increase the modulation response of a laser, to improve the response of a laser/fiber system, or to decrease the intensity noise of a continuous-wave laser signal. The effects are the result of dispersive propagation and frequency discrimination, and depend on the nature of the grating and the laser dynamic properties. This connection is developed first by deriving the dynamic properties of semiconductor lasers, including the direct current modulation response, frequency chirp, and laser noise. The effect of propagation through an arbitrary medium is derived, with the conclusion that both dispersion and frequency discrimination result in conversion of frequency modulation into amplitude modulation and vice versa. These general results are applied to laser modulation and noise spectra to derive the transfer functions for dispersive optical fiber. Next we detail the experimental characterization of laser dynamics, from which we can determine the important laser parameters. We follow this with a discussion of fiber Bragg gratings and show that the phase of the grating transmittance, which is important in changing the characteristics of the signals being transmitted, can be inferred numerically from a measurement of the intensity transmission. Finally, we unite these topics with the demonstration of a 7 dB increase in the laser response at frequencies up to 25 GHz in transmission through a fiber grating. The result is well predicted by a numerical Fourier-

domain analysis of the laser signal and fiber grating. In addition, we investigate the effect of a fiber grating on the relative intensity noise (RIN) of a laser, showing that a model of grating as a linear frequency discriminator is sufficient for explaining much of the results. We show there exist conditions under which a grating can reduce the RIN, which depend on the phase relationship between correlated intensity and frequency fluctuations. We demonstrate a 2 dB reduction in RIN at frequencies up to 15 GHz. The combination of these effects is used in calculating signal-to-noise ratios for real systems incorporating gratings, and in showing that gratings can re-narrow pulses broadened by fiber dispersion.

Chapter 1 -- Introduction

This thesis describes research done for the degree of Doctor of Philosophy in Physics at the California Institute of Technology. The main theme is the use of fiber Bragg gratings to increase the modulation response and decrease the intensity noise of semiconductor laser light, and the thesis revolves around work published by the author [1, 2]. In this chapter we put the topic in context by giving a brief overview of optical telecommunications, and then we survey the coming chapters.

1.1 Optical telecommunication

The technical field in which this work was performed is that of optical telecommunications: generating high-speed optical signals with semiconductor lasers, transmitting them over long distances along optical fibers, and detecting them with high-speed photodiodes. Common applications include long-distance telephony, cable television, computer data transmission as in the Internet, and microwave (GHz frequency) relay links for satellite transmitters and receivers. Data transmission speeds of 2.5 Gbit/s are common, with advanced systems operating at 10 Gbit/s. An excellent introduction to optical communication can be found in the textbook by Agrawal [3] and a thorough

survey of the current technological issues is found in the recent volumes by Kaminow and Koch [4,5].

The semiconductor lasers of choice in today's systems are made of InGaAsP and emit light with a wavelength of 1.55 μm, chosen to take advantage of the low-loss wavelength band of silica optical fiber. The lasers consist of a horizontal active region of InGaAsP sandwiched between InP regions above and below, n-doped on one side and p-doped on the other. When a current is passed thorough this modified p-n junction, electrons and holes injected from either side get trapped in the active region, by virtue of its lower bandgap, which serves as a one-dimensional potential well. There they sit until they either decay spontaneously or interact with photons. The lower bandgap in the active region is accompanied by a higher index of refraction (compared to the surrounding InP), which serves as a dielectric waveguide, confining the laser optical mode. The exact designs of the confining heterostructures vary among manufacturers and are often not publicly disclosed. Photons travel up and down the laser cavity, reflected at either end by the semiconductor-air interface, and stimulate the annihilation of an electron-hole pair and the generation of a photon. By modulating the current injected into the active region, we can modulate the density of electron/hole pairs, and thus change the optical gain and output optical power. Thus we can convert electrical signals into optical signals, with efficiencies as high as 90%.

To control the laser wavelength more carefully, high-speed lasers typically employ distributed feedback (DFB) reflectors. This is a corrugation of the index of refraction along the cavity which serves as a Bragg reflector, continually coupling forward-going

photons into the backward-going direction and vice versa. Thus the cavity reflectivity is provided not by mirrors at the cavity ends, but by the Bragg grating along its entire length. Such cavities have only two degenerate modes instead of the infinite spectrum for Fabry-Perot cavities, and the two can be reduced to one by inserting a quarter-wavelength spacer in the center of the grating, or by corrugating the optical gain instead of the index of refraction. (Neither of these is obvious—see [6] for a good treatment of Bragg reflectors with optical gain.) DFB lasers are for this reason referred to as single-mode lasers, as they avoid launching multiple optical modes down the fiber.

The optical fibers are made of silica glass, with a center core typically 6 μm in diameter and a surrounding cladding 125 μm in diameter. The core has been doped with germanium, which increases its index of refraction and forms a cylindrical step-index waveguide. Usually one uses single-mode fiber, which has a core small enough to support only the lowest order transverse mode at the 1.55 μm wavelength, thereby preventing modal dispersion (a difference in propagation velocity among the different excited waveguide modes). Losses at 1.55 μm are typically 0.2 dB/km, and when combined with optical amplifiers, permit communication distances of hundreds of kilometers.

By an unfortunate coincidence, the most important technical flaw in semiconductor lasers happens to reinforce, negatively, the most important flaw in optical fiber. Optical fiber is dispersive—the group velocity of light traveling down the fiber depends on the wavelength of that light. This means that the different Fourier

components of a signal will get out of phase with each other as they propagate, distorting the signal and, in the case of digital modulation, broadening the individual pulses until they overrun each other. This is worsened by the fact that diode lasers are chirped: modulation of the injection current modulates not only the output power but also the lasing frequency. This broadens the spectrum beyond the Fourier-transform-limited minimum width, and hastens dispersive distortion. The two phenomena in concert produce a roughly 50 km propagation limit on a laser modulated at 10 GHz. For this reason, the 10 Gbit/s systems referenced above usually employ external optical modulators, which have far less chirp.

One of the most important innovations in optical fiber technology in the last decade is the construction of fiber gratings, which are small periodic perturbations of the index of refraction of the fiber core along the fiber axis. This forms a Bragg grating which reflects light with a wavelength of twice the corrugation period, thereby serving as a very wavelength-sensitive optical filter. Applications include remote sensing, forming add/drop devices for wavelength division multiplexing, and compensation of fiber dispersion. These are described more in Chapter 6.

1.2 In this thesis

In Chapter 2 we develop the theory of the dynamics of semiconductor lasers. The features of optical gain which lead to laser chirp and non-linear gain are discussed

physically, and the laser rate equations are presented. A small signal expansion of these equations allows us to derive the AM and FM response to direct current modulation, analyzing them in terms of laser chirp. A Langevin force analysis is used to derive the intensity and frequency noise spectra of the lasers and detail the correlations between them.

In Chapter 3 we analyze the effect of propagation through an arbitrary medium on an optical signal. We first present a general formalism for describing signals with both amplitude modulation and frequency modulation. We analyze the effect of dispersive propagation and apply it to laser modulation and noise, and then we analyze the effect of frequency discrimination. The uniting theme is that of FM-to-AM conversion in a dispersive or discriminating medium. We present an intuitive time-domain model and finally a Fourier-domain numerical calculation, which is the only way to analyze the most general combination of the above.

In Chapter 4 we detail the experimental characterization of lasers. The basic measurements are that of the laser modulation response and the laser intensity noise. We show the results of typical measurements and compare them to the theory presented in Chapter 2. Then we measure the change in the modulation response and intensity noise due to dispersive fiber, and compare those to the theory presented in Chapter 3. We discuss how the above measurements can be used in concert to extract many of the important laser dynamic parameters.

Chapter 5 is devoted to Bragg fiber gratings. We introduce the applications and fabrication of gratings, and derive the coupled mode theory that is used very successfully

to model a grating's optical properties. We present the properties of analytical solutions for uniform gratings, and numerical solutions for apodized and chirped gratings. Finally we present a Kramers-Kronig relationship between the magnitude and phase of a gratings transmission spectrum, which allows us to infer the very important phase information of a grating by measuring only its intensity transmittance.

In Chapter 6 we report on the use of a fiber grating to improve the modulation response of a laser/fiber system. We find that the laser response can be increased by over 7 dB at all frequencies up to 25 GHz, as a consequence of converting laser FM into additional laser AM. When combined with 25 or 50 km of dispersive optical fiber, the grating produces a system response that is larger, flatter, and has a larger bandwidth. This is a result of both optical filtering and dispersion compensation. This experiment combines the themes presented in previous chapters: the observed results are in good agreement with the numerical calculation of Chapter 3, using the laser parameters which were fit with the techniques of Chapter 4, and for the most accurate prediction we need the Kramers-Kronig calculation described in Chapter 5.

Chapter 7 investigates the effect of transmission through a fiber grating on the intensity noise of semiconductor laser light. We show that in many cases the grating acts as a linear frequency discriminator, converting laser frequency noise into excess intensity noise, increasing the latter by as much as 30 dB at low frequencies, with an inverse-square frequency dependence. We show that there are conditions under which the grating can reduce the intensity noise, and that these are determined by the phase relationship between the correlated intensity and frequency fluctuations. We demonstrate 2 dB of

noise reduction and show that this is fairly well predicted by a numerical calculation that incorporates the phase of the grating.

Chapter 8 combines the ideas of Chapters 6 and 7 to describe when a fiber grating can both increase the signal and decrease the noise, or at least increase their ratio. Requirements for practical use in systems is discussed, including the role played by shot noise and amplifier noise in the total signal-to-noise ratio. Then pulsed modulation schemes are considered, and we find that a fiber grating can be used to re-narrow pulses broadened by fiber dispersion, as a consequence of frequency discrimination alone, independent of grating dispersion.

Chapter 2 -- Dynamics of Semiconductor Lasers

The important dynamic effects of semiconductor lasers have their roots in the physics of optical gain. A study of this physics is a thesis in itself and is not the topic of this chapter. Instead, in the first section we will merely introduce the phenomena behind non-linear gain and amplitude-phase coupling, which will turn out to be important in studying the propagation of laser signals.

By expanding the gain as a function of carrier density and photon density, we will, in the following sections, write a set of rate equations for those quantities that predict most laser dynamic effects. For example, we will use these equations to derive the AM and FM response of the laser, the characteristics of laser chirp, and the spectra of and correlations between intensity and frequency noise. The results will be the basis for experimental characterization of the laser, explained in Chapter 5, whose goal is to measure the laser dynamic parameters. The dynamics also become inextricably linked with the effect of propagation through dispersive fiber and fiber gratings, explored in the remainder of the thesis.

2.1 Origin of gain in semiconductors

Optical gain in semiconductors results from the stimulated transition of an electron from the conduction band to the valence band or, equivalently, the stimulated recombination of an electron-hole pair. The photon momentum involved in the transition is small compared to the carrier momentum, so only transitions between states with the same wavevector $\vec{k}$ are allowed by momentum conservation. This means the entire collection of carriers in the conduction and valence band can be considered as an ensemble of independent two-level systems, and the total gain is the sum of contributions from each system. Indexing these two-level systems by the frequency ω' of the transition, and integrating over all the systems, gives the gain at optical frequency ω,

$$G(\omega) \propto \int_{E_{gap}/\hbar}^{\infty} \rho(\omega')\left[f_c(\omega') - f_v(\omega')\right] g(\omega,\omega')d\omega' \qquad (2.1)$$

Here $\rho(\omega')$ is the joint density of states of the conduction and valance bands at a separation energy $\hbar\omega'$. The difference of the conduction and valance band occupation functions $f_c(\omega')$-$f_v(\omega')$ varies between +1 and -1, and produces either gain or absorption, depending on the quasi-Fermi levels in each band and the separation energy $\hbar\omega'$. $g(\omega, \omega')$ is the Lorentzian lineshape function of a two-level system, which gives the response of the two-level system with resonant frequency ω' to the optical field at frequency ω. The width of the Lorentzian is determined by the dephasing time T_2, which is the intra-band scattering time for carriers, on the order of picoseconds. The constant of

proportionality in (2.1) includes a transition matrix element, which for quantum well lasers includes a spatial wavefunction [7].

The quasi-Fermi levels in the conduction and valence band are determined by the total number of carriers N, and with no optical power present, the occupation functions have the usual Fermi-Dirac form. The gain integral (2.1) is a functional of the distributions $f_c(\omega')$ and $f_v(\omega')$ of those N carriers, that is, it is a function of the occupation of each two-level system ω'. To a good approximation, however, the gain can be written as a function of the total number of carriers N instead of their distributions. Such functions are usually determined by evaluating (2.1) for a given total carrier number, using the details of the band structure and the carrier scattering, repeating for different values of N, and fitting the results versus N. The change in gain with N at some fixed point N_0 is called the differential gain, and is fundamentally important in laser modulation.

Non-linear gain compression

At high photon densities, the rate of stimulated transitions is large, and the carriers at ω may be depleted faster than they can be replaced by other carriers scattered in from different energies. In this case the occupation function is decreased in the vicinity of ω', and we say that a spectral hole has been burned in the occupation function [8, 9]. Density matrix equations for the semiconductor predict a form of the suppression similar to that of gain saturation in a 2-level system [10],

$$f_c(\omega') - f_v(\omega') \rightarrow \frac{f_c(\omega') - f_v(\omega')\big|_{P=0}}{1 + (\pi / T_2) g(\omega, \omega') P / P_{sat}} \tag{2.2}$$

which gives the shape of the spectral hole. The width of the hole is the same as the width of the Lorenztian response g(ω, ω') and the depth depends on the stimulated emission rate and the scattering rate. When a spectral hole is burned in the carrier distributions, the number of carriers within a resonant width of the optical frequency is decreased, and thus the gain is decreased. G(ω) therefore decreases with optical power, and this spectral hole burning is the leading candidate explanation for so-called gain suppression or gain compression. The suppression is usually represented in the form

$$G(N,P) \rightarrow G(N)[1 - \varepsilon P] \tag{2.3}$$

The gain suppression parameter ε has an important effect on laser dynamics [11], as we shall see.

Amplitude/phase coupling and α

Just as each two-level system contributes to the gain of the medium, each also contributes to the index of refraction. In a single two-level system the refractive index perturbation Δn is an odd function of the detuning from the resonant frequency, ω – ω', and Δn is zero exactly on resonance, which coincides with the gain peak. In a semiconductor, the density of states increases with photon energy, leaving more states above the resonance than below; and the occupation functions decrease with energy, leaving fewer carriers per state above the resonance than below. Furthermore, in DFB

lasers and vertical cavity lasers, in which the optical feedback in the cavity is strongly peaked about a single wavelength, lasing need not occur at the gain peak. The result of all this is that at the gain peak there may be a net non-zero index perturbation Δn. This is not so bad in itself, except that Δn can change with carrier density. Thus the index of refraction can change along with the optical gain. The proportionality is measured by the amplitude-phase coupling factor, also know as the linewidth-enhancement factor or simply the α parameter:

$$\alpha = -\frac{\partial n_r / \partial N}{\partial n_i / \partial N} \tag{2.4}$$

For small changes in n_r and n_i, (2.4) is the same as

$$\alpha = -\frac{\partial \chi_r / \partial N}{\partial \chi_i / \partial N} \tag{2.5}$$

where χ is the electric susceptibility. (2.5) is sometimes used as the definition of the parameter. Some authors do not include the minus sign in the definition; the ratio of derivatives itself is negative for semiconductor lasers, and the minus sign makes α positive. To avoid confusion, in this thesis we'll use $|\alpha|$ in formulae, which is easy to interpret by both camps. This phenomenon is the origin of laser chirp.

Finally, we should note that these phenomena are material phenomena, and may be compounded by similar effects related to the laser cavity. For example, in a DFB laser the photon density is strongly concentrated at the center of the grating. Thus the stimulated depletion of carriers is fastest there, and may be faster than the diffusion of carriers from neighboring regions. This leads to a spatial hole burning, which also lowers

the total gain at high photon densities. This may also change the local refractive index of the grating, producing a grating chirp which can change the phase of the output field. So the material chirp may be complimented by a cavity chirp, and both contribute to the measured value of the α parameter [12, 13].

2.2 The laser rate equations

The majority of laser dynamic phenomena, including frequency chirp and noise, can be explained well by using rate equations for the photon density and carrier density in the laser active region. There is some variety of definition and form among the rate equations; derivation of the main results can be found in many texts [14] and a thorough treatment can be found in [15].

We start by writing the time rate of change of photon and carrier density in the active region of the laser:

$$\frac{dP(t)}{dt} = G(N,P)v_g P(t)\Gamma - \frac{P(t)}{\tau_{ph}} + \frac{\Gamma F_{\|}(t)}{V} \tag{2.6}$$

$$\frac{dN(t)}{dt} = \frac{I(t)}{eV} - \frac{N(t)}{\tau} - G(N,P)v_g P(t) + \frac{F_N(t)}{V} \tag{2.7}$$

Here P and N are the number densities in the active region of the laser, with units of cm^{-3}. The first term on the right side of (2.6) describes the stimulated emission of photons into the lasing mode. G(N,P) is the active region gain, explicitly a function of carrier and photon density, with units of cm^{-1}, and the group velocity v_g converts G to a gain per unit

time. Γ is the confinement factor of the active region, defined as the fraction of the optical power in the laser mode that is confined within the active region. τ_{ph} is the photon lifetime, describing both mirror and internal losses. For a Fabry-Perot laser,

$$\tau_{ph} = v_g\left(\frac{1}{2L}\ln\left(\frac{1}{R_1R_2}\right)+\alpha_{int\,enal}\right) \tag{2.8}$$

where L is the cavity length, R_1 and R_2 the mirror reflectivities, and $\alpha_{internal}$ is the internal loss coefficient describing scattering and absorption losses of the waveguide, with a typical value of 5 cm^{-1}. For DFB lasers the photon density is non-uniform along the cavity and the reflectivity is distributed along the cavity length--in this case the photon lifetime has some effective value which is most often measured experimentally. $F_{||}(t)$ and $F_N(t)$ are Langevin noise forces describing, respectively, the spontaneous emission of photons into the lasing mode, and the spontaneous decay of carriers, discussed further below. The first three terms on the right side of (2.7) describe the injection of carriers due to the driving current I(t), with V the volume of the active region and e the electron charge; the loss of carriers due to spontaneous emission and non-radiative carrier decay, with a carrier lifetime τ; and loss of carriers due to stimulated emission. Some fraction $n_{sp} \sim 10^{-5}$ of the spontaneously emitted carriers will by chance enter the laser mode and also contribute to dP/dt. This spontaneous emission factor is mostly important near threshold and will be ignored here. Note the stimulated emission term in (2.7) is not modified by Γ since all of the electron-hole pairs on resonance with the laser field are confined to the active region by the heterostructure.

Gain conventions

G(N,P) is a complicated and largely unknown function of N and P, as discussed in the previous section, and to make the rate equations useful we have to linearize G with respect to N and P. It is primarily in this step that treatments of the rate equations differ in the literature, and it is important because all of the observable dynamic phenomena, such as relaxation resonance, damping, and chirp, are determined by how G changes with N and P. The most general expansion of G(N,P) about a continuous wave (CW) operating point N_0 and P_0 would take the form

$$G(N,P) = G(N_0,P_0) + \left(\frac{\partial G}{\partial N}\bigg|_{N_0,P_0}\right)\Delta N + \left(\frac{\partial G}{\partial P}\bigg|_{N_0,P_0}\right)\Delta P + \left(\frac{\partial G}{\partial N \partial P}\bigg|_{N_0,P_0}\right)\Delta N \Delta P + \ldots \quad (2.5)$$

The first term on the right side is the total gain at N_0 and P_0, the second describes the differential gain, and the third describes the non-linear gain or gain compression. (Here $\Delta N \equiv N - N_0$ and $\Delta P \equiv P - P_0$.) For small-signal applications in which $\Delta N << N_0$ and $\Delta P << P_0$, the fourth term and all higher order terms are ignored because they involve products of small quantities. These are all functions of N_0 and P_0 and can be defined

$$G_0 = G(N_0,P_0) \quad (2.10a)$$

$$A = A(N_0,P_0) \equiv \frac{\partial G}{\partial N}\bigg|_{N_0,P_0} \quad (2.10b)$$

$$\varepsilon = \varepsilon(N_0,P_0) \equiv -\frac{1}{G(N_0,P_0)}\left(\frac{\partial G}{\partial P}\bigg|_{N_0,P_0}\right) \quad (2.10c)$$

Then the gain used in the rate equation becomes

$$G(N,P) = G_0(1-\varepsilon\Delta P) + A\Delta N \tag{2.11}$$

The advantage of this convention is that it is defined in terms of the physical quantities that are actually measured in a small signal modulation response or noise measurement--namely, the differential and nonlinear gain *at the operating point used in the experiment.* It does not presume to describe how G varies with N starting from the threshold carrier density N_{th}, or how G varies with P starting from P = 0. Rather G_0, A, and ε are all explicitly functions of N_0 and P_0 (and for that matter that τ and τ_{ph} are too), and if we wish to study how A and ε depend on N_0 and P_0 we can repeat a single dynamics measurement for different laser powers.

Unfortunately (2.11) is not the most common convention for the rate equations. Most authors use [15]

$$G(N,P) = \left[G_0' + A'\Delta N\right](1-\varepsilon' P) \tag{2.12}$$

or the equivalent, where the primes denote the conventional use of the variables. This expansion contains questionable assumptions that (2.11) does not. The first is that the gain compression (1-ε'P) is independent of the operating point P_0, that is, the compression of the gain from P = 0 to P = ΔP as the same as the compression of the gain from P = P_0 to P = P_0 + ΔP. This is not likely to be true, and in general the gain compression mechanism will have some higher order dependence on P, which is implied in our first approach. Second, it assumes the compression (1-ε'P) applies to the differential gain A' as well. The differential gain is surely compressed by P, and for spectral hole burning it

may well be that the coefficient of compression is the same for G_0' as for A'. But in a DFB laser there are many non-linear effects, including longitudinal hole burning and carrier heating effects, that might not be so simply described [9]. Furthermore, compression of the differential gain will not affect the nature of the dynamics but only how the dynamics change with P_0. This is because we will eventually ignore the second-order term $A'\varepsilon'\Delta N\,\Delta P$ in the rate equations, so the term $A'(1-\varepsilon'P)$ only defines how A' changes as P_0 increases. Since the dynamics at high-powers are affected as much by temperature and detuning effects as by gain compression [16], it is not clear that it is helpful to assume a form $A'(1-\varepsilon'P_0)$.

In the end, only the quantities (2.10) are observable in a modulation response or noise measurement, and these quantities relate to those in (2.12) by

$$G_0 = G_0'(1-\varepsilon' P_0) \tag{2.13a}$$

$$\varepsilon = \frac{\varepsilon'}{1-\varepsilon' P_0} \tag{2.13b}$$

$$A = A'(1-\varepsilon' P_0) \tag{2.13c}$$

which we find by equating the first-order "small" terms of (2.11) and (2.12). If we analyze the dynamics using the primed variables, we will only be doing more algebra than necessary--e.g., everywhere ε would appear we will instead have $\varepsilon'/(1-\varepsilon'P_0)$. For these reasons we shall describe the gain by (2.11).

Putting (2.11) into (2.6) and (2.7), assuming $F_{\|}(t) = F_N(t) = 0$, and setting the time derivatives to zero, we get the steady-state conditions at N_0, P_0, and I_0,

$$G_0 \Gamma v_g = \frac{1}{\tau_{ph}} \tag{2.14}$$

$$\frac{I_0}{eV} = G_0 v_g P_0 + \frac{N_0}{\tau} \tag{2.15}$$

The first of these is the "gain equals loss" condition, and the second says the rate at which carriers are injected into the active region equals the rate at which they are removed, either through stimulated emission or non-radiative or spontaneous decay.

Small signal equations

The small-signal laser dynamics are determined by putting

$$N(t) = N_0 + \Delta N(t) \tag{2.16a}$$

$$P(t) = P_0 + \Delta P(t) \tag{2.16b}$$

$$I(t) = I_0 + \Delta I(t) \tag{2.16c}$$

into the rate equations and neglecting any products of small quantities (second order in Δ's), which gives us

$$\frac{d}{dt}\Delta P = \Gamma v_g A P_0 \Delta N - \frac{\varepsilon P_0}{\tau_{ph}}\Delta P + \frac{\Gamma F_{\parallel}(t)}{V} \tag{2.17}$$

$$\frac{d}{dt}\Delta N = \frac{\Delta I}{eV} - \frac{\Delta N}{\tau} - v_g A P_0 \Delta N - \frac{1-\varepsilon P_0}{\Gamma \tau_{ph}}\Delta P + \frac{F_N(t)}{V} \tag{2.18}$$

where we used the steady-state conditions to simplify the result.

The final rate equation we need describes how the lasing frequency ω changes with carrier density N. We use the chain rule to write

$$\frac{d\omega}{dN} = \frac{d\omega}{dn_r}\frac{dn_r}{dn_i}\frac{dn_i}{dG}\frac{dG}{dN} \tag{2.19}$$

The physics is contained only in the dn_r/dn_i term, through the α parameter,

$$\alpha \equiv -\frac{\partial n_r / \partial N}{\partial n_i / \partial N} \tag{2.20}$$

and the rest are purely mathematical conversions. With an $e^{i\omega t}$ time dependence, the imaginary part of the refractive index is related to material intensity gain G by

$$n_i = G\lambda_{air} / 4\pi \tag{2.21}$$

A change in the real part of the effective mode refractive index $n_{mode,r}$ will change the resonant frequency of the laser by $\Delta\omega / \omega = -\Delta n_{mode,r} / n_{mode,r}$. However, α describes the index change in the active region only, and the optical mode is not entirely confined in the active region. The mode index $n_{mode,r}$ (which is what the mode frequency ω responds to) will change less than the material index n_r, and the correct weighting factor is the same confinement factor Γ as in the rate equations. (This can be shown rigorously by applying perturbation theory to the mode condition [17].) Thus

$$\Delta\omega = -\Delta n_r \Gamma \omega / n_{mode,r} \tag{2.21}$$

Finally, dG/dN is just the differential gain A. Combining all of this, (2.19) becomes

$$\frac{d\omega}{dN} = \left(\frac{-\Gamma\omega}{n_{mode,r}}\right)(-\alpha)\left(\frac{\lambda_{air}}{4\pi}\right)A \tag{2.22}$$

Recognizing that the group velocity is $v_g = \omega\lambda_{air} / 2\pi n_{mode,r}$ we arrive at the frequency deviation rate equation

$$\Delta\omega(t) \equiv \frac{d}{dt}\Delta\phi(t) = \frac{|\alpha|}{2}\Gamma A v_g \Delta N(t) + F_\perp(t) \qquad (2.23)$$

We have tacked on another Langevin noise term describing spontaneous emission into the lasing mode. The relation of $\Delta\omega$ to $d(\Delta\phi)/dt$ is the definition of instantaneous frequency.

The small-signal dynamic equations (2.17), (2.18) and (2.23) are the basis for deriving the modulation response and noise properties. They are not valid for large-signal (e.g., digital) modulation because of the assumptions (2.16). In general, digital modulation dynamics must be analyzed by numerically integrating the rate equations with some model of how G(N,P) depends on large changes in N and P [18].

2.3 Direct modulation

In many applications the laser injection current I(t) is modulated with the desired signal. Then the driving term of the rate equations is ΔI, and we derive the frequency response by assuming a harmonic time dependence, $\Delta I = ie^{i\Omega t}$, $\Delta P = pe^{i\Omega t}$, $\Delta N = ne^{i\Omega t}$, and $\Delta\phi = \beta e^{i\Omega t}$. We can solve the rate equations for any variable of interest, and since we will postpone the discussion of noise to the next section, we'll take $F_{\parallel}(t) = F_N(t) = 0$ here.

AM response

Putting these into (2.17) and (2.18) and eliminating n gives the photon density response p,

$$\frac{p}{(i/eV)} = \frac{Av_g \Gamma P_0}{-\Omega^2 + i\Omega\gamma + {\Omega_0}^2} \tag{2.24}$$

The output power response is related to the photon density by the mirror losses (in later chapters P will refer to output power itself instead of photon density). The modulation response is measured by a detector photocurrent, and the laser response is usually taken to be the detector electrical power normalized to the DC (Ω=0) response:

$$R(\Omega) \equiv \left| \frac{(p/i)_\Omega}{(p/i)_{\Omega=0}} \right|^2 = \frac{{\Omega_0}^4}{\left(\Omega^2 - {\Omega_0}^2\right)^2 + \Omega^2\gamma^2} \tag{2.25}$$

Here Ω_0 is the resonant frequency (also called the relaxation oscillation resonant frequency), given by

$${\Omega_0}^2 \equiv \frac{v_g A P_0}{\tau_{ph}} + \frac{\varepsilon P_0}{\tau_{ph}\tau} \tag{2.26}$$

and the γ is the damping frequency, given by

$$\gamma \equiv \frac{1}{\tau} + v_g A P_0 + \frac{\varepsilon P_0}{\tau_{ph}} \tag{2.27}$$

Note that these frequencies are in radians per second, not Hz.

The AM response is flat at low frequencies, then has a resonance at $\Omega = \Omega_0$, typically several GHz. Above Ω_0 the response falls off dramatically, by 40 dB per

decade. The damping frequency, also several GHz, widens the resonance and lower its peak. Thus γ flattens the response and makes it more desirable for transmitting broadband signals without distortion. Both Ω_0 and γ increase with P_0, and in communication systems the lasers are usually run at high bias for optimum high-speed performance. This is discussed more in Chapter 4.

$I - I_{threshold}$	20 mA
fiber coupled optical power	3 mW
$\Omega_0 / 2\pi$	7.7 GHz
$\gamma / 2\pi$	2.4 GHz
$\lvert\alpha\rvert$	4.1
τ_{ph}	5 ps
τ	0.4 ns
$\varepsilon P_0 / \tau_{ph} 2\pi$	1.6 GHz
$v_g A P_0$	1.2×10^{10} 1/s
εP_0	0.05

Table 2.1. Typical values of laser parameters measured as described in Chapter 5 for a DFB laser at fairly low bias. The gain compression (last value) is only 5%.

Typical values of these constants are given in Table 2.1, measured as described in Chapter 5. We see from them that it is a good approximation to neglect the second term of (2.26) and use

$$\Omega_0 \approx \sqrt{\frac{v_g A P_0}{\tau_{ph}}} \tag{2.28}$$

FM response

The FM response, $\Delta\omega$, can be gotten by noting that for $F_{II}(t) = 0$ we can solve (2.17) for ΔN and substitute into (2.23), giving [19]

$$\Delta\omega = \frac{|\alpha|}{2P_0}\left(\frac{d}{dt}\Delta P + \frac{\varepsilon P_0}{\tau_{ph}}\Delta P\right) \tag{2.29}$$

Using the harmonic time dependence and the solution (2.24) for p/i, we get the FM response,

$$\left|\frac{\Delta\omega}{(i/eV)}\right|^2 = \left(|\alpha| A v_g \Gamma / 2\right)\frac{\Omega^2 + \left(\varepsilon P_0 / \tau_{ph}\right)^2}{\left(\Omega^2 - \Omega_0{}^2\right)^2 + \gamma^2\Omega^2} \tag{2.30}$$

This is also resonant at Ω_0 and damped by γ, but at high frequencies it rolls off at 20 dB per decade, less quickly than the AM response.

Adiabatic and transient chirp

The result (2.29) gives us more insight into the frequency response of the laser than (2.30) and is an oft-quoted result, valid without the harmonic assumption of (2.30). We see the laser chirp $\Delta\omega$ is directly proportional to the α parameter, as advertised. The contribution of the first term is referred to as transient chirp and is important when $\Delta P(t)$ changes quickly, for example in digital modulation schemes where P(t) has a sharp

square-wave turn on. The second term is the adiabatic chirp contribution, more often important in analog or linear systems such as cable television.

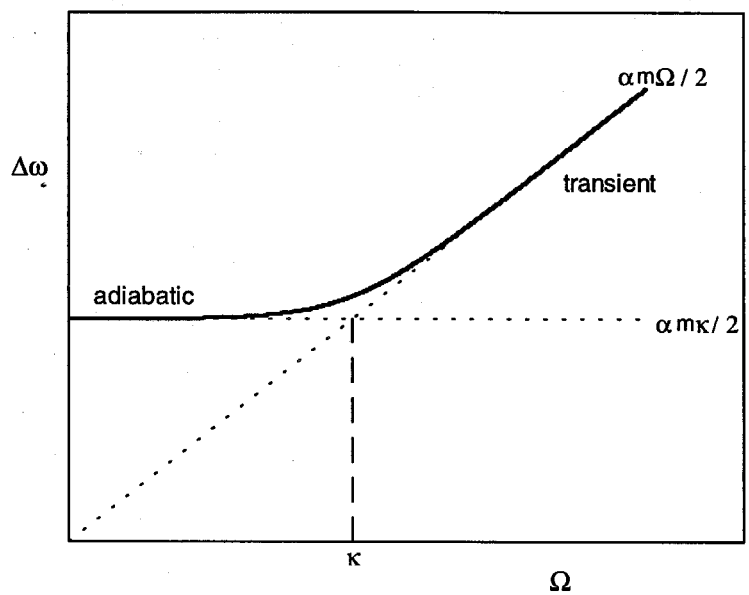

Figure 2.1. Optical frequency chirp $\Delta\omega$ versus modulation frequency Ω, showing the adiabatic regime, in which $\Delta\omega$ is constant, and the transient regime, in which it is linear, and the characteristic frequency $\kappa = \varepsilon P_0 / \tau_{ph}$ separating them.

For a sinusoidal modulation of the form $P(t) = P_0(1 + \Delta P e^{i\Omega t})$ we can write

$$\beta\Omega \equiv \Delta\omega = \frac{|\alpha|}{2} m(i\Omega + \kappa) \tag{2.31}$$

where $m = \Delta P/P_0$ is the optical power modulation index, or AM index, and β is defined as the phase modulation index. Here $\kappa = \varepsilon P_0 / \tau_{ph}$ is a characteristic frequency separating the transient and chirp regimes, typically a few GHz, and is linear with P_0. The magnitude of frequency deviations goes as $\sqrt{\Omega^2 + \kappa^2}$, shown in Figure 2.1, and the phase of the FM with respect to the AM is

$$\theta_{FM} - \theta_{AM} = \tan^{-1}\left(\frac{\Omega}{\kappa}\right) \tag{2.32}$$

as shown in Figure 2.2. This phase will become important when discussing dispersive propagation. Note that both the adiabatic and transient chirp are directly proportional to the output power modulation index m.

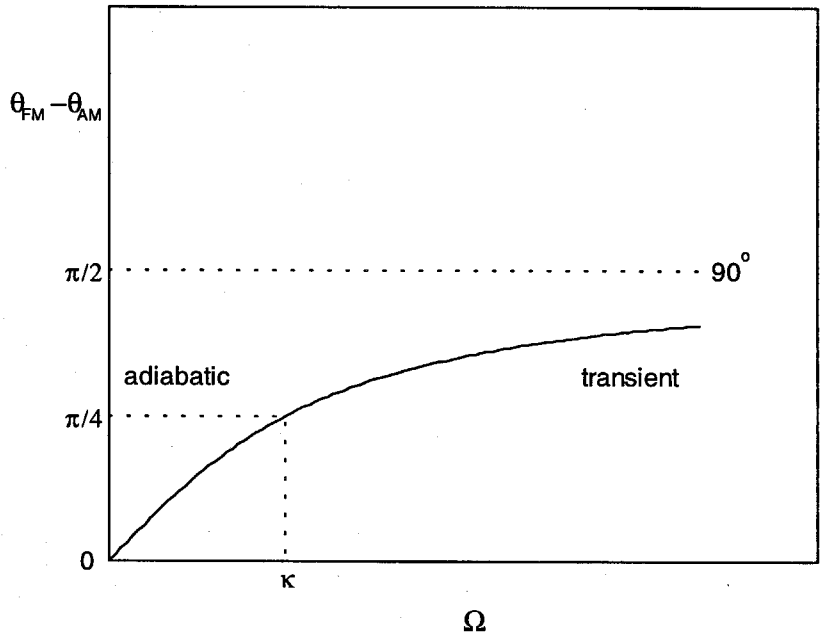

Figure 2.2. Phase by which the FM leads the AM, versus modulation frequency, for direct current modulation. In the adiabatic regime they are in phase; in the transient regime they approach 90° degrees out of phase.

2.4 Laser noise

The small-signal rate equations can also be used to derive the intensity and frequency noise spectra of the laser. In this section we shall use a semi-classical model in which noise is driven by spontaneous emission [20, 21].

Langevin force analysis

We return to the rate equations and examine the Langevin noise terms. $F_N(t)$ is associated with the random decay of carriers, due to spontaneous emission and non-radiative decay. $F_{\parallel}(t)$ and $F_{\perp}(t)$ are associated with spontaneous emission into the laser optical mode. $F_{\parallel}(t)$ is the component of the spontaneous emission field that is in phase with the laser field, perturbing only the laser intensity. $F_{\perp}(t)$ is the other quadrature of the spontaneous emission field, perturbing only the laser phase. In a phasor diagram, $F_{\parallel}(t)$ and $F_{\perp}(t)$ are the spontaneous emission phasor projections parallel to and perpendicular to the laser field phasor. In the Markovian approximation, spontaneous emission is a "memoryless" process, in the sense that the spontaneous noise term $F_{\parallel}(t)$ has an autocorrelation function

$$C_{F_{\parallel}F_{\parallel}}(\tau) \equiv \left\langle F_{\parallel}(t)F_{\parallel}(t+\tau)^{*}\right\rangle_{t} = S_{F_{\parallel}F_{\parallel}}\delta(\tau) \tag{2.33}$$

where the number $S_{F_{\parallel}F_{\parallel}}$ is the correlation strength, and similarly for $F_{\perp}(t)$. Spontaneous emission is assumed to be both stationary and ergodic, which means that the time average

is the same as an ensemble average. The spectral density is the Fourier transform of (2.32), and is "white,"

$$S_{F_{\parallel}F_{\parallel}}(\Omega) \equiv S_{F_{\parallel}}(\Omega) = \int_{-\infty}^{\infty} C_{F_{\parallel}F_{\parallel}}(\tau) e^{-i\Omega\tau} d\tau = S_{F_{\parallel}F_{\parallel}} \tag{2.34}$$

Note we suppress the double subscript identifying S when we are talking about autocorrelations. For the shot noise model of noise, which simplifies the quantum mechanical description of laser noise, a correlation strength is equal to twice the average rate of the events it describes, in number per unit time.

Despite the fact that both spontaneous emission projections come from the same physical events, they are uncorrelated, in the sense that

$$C_{F_{\parallel}F_{\perp}}(\tau) = \left\langle F_{\parallel}(t) F_{\perp}(t+\tau)^* \right\rangle_t = S_{F_{\parallel}F_{\perp}} \delta(\tau) \tag{2.35}$$

This is a weaker statement than statistical independence between the two, but is sufficient for treating them separately as driving terms of the rate equations.

The noise term $F_N(t)$ represents spontaneous decay of carriers, both by radiative and non-radiative means, and includes spontaneous emission into the lasing mode. Thus $F_N(t)$ is correlated with $F_{\parallel}(t)$ and we cannot treat them as independent noise sources. The simplest solution is to write explicitly the part of $F_N(t)$ that does not involve spontaneous emission into the lasing mode.. We define this Langevin force to be $F'_N(t)$, in terms of which $F_N(t)$ becomes

$$F_N(t) = -F_{\parallel}(t) + F'_N(t) \tag{2.36}$$

The minus sign in front of $F_{\|}(t)$ is because the carrier density decreases by the same number the photon density increases due to these events. Now $F'_N(t)$, $F_{\|}(t)$, and $F_{\perp}(t)$ are explicitly mutually uncorrelated, and equation (2.18) becomes

$$\frac{d}{dt}\Delta N = \frac{\Delta I}{eV} - \frac{\Delta N}{\tau} - v_g A P_0 \Delta N - \frac{1-\varepsilon P_0}{\Gamma \tau_{ph}}\Delta P + \frac{-F_{\|}(t) + F'_N(t)}{V} \tag{2.37}$$

To derive the response of the laser to any of one of these sources at frequency Ω, we can take the other two to be zero and use (2.17), (2.23), and (2.37) as our rate equations. For example, since $F'_N(t)$ acts just like current modulation in the rate equations, it produces an intensity noise spectral density $S^{N'}_{\Delta P}(\Omega)$ and frequency noise spectral density $S^{N'}_{\Delta\omega}(\Omega)$ with the same form as the AM response (2.25) and FM response (2.30). It turns out that $F'_N(t)$ is not the dominant source of intensity or frequency noise in semiconductor lasers and can usually be ignored.

Spontaneous emission $F_{\|}$

The response due to $F_{\|}(t)$ is gotten by setting $\Delta I = F'_N(t) = F_{\perp}(t) = 0$, assuming the same harmonic dependence as above, and eliminating ΔN from (2.17) and (2.37). The result is the spectral density of the photon density fluctuations due to $F_{\|}$,

$$S^{\|}_{\Delta P}(\Omega) = S_{F_{\|}}(\Omega)\frac{\Gamma^2}{V^2}\frac{\Omega^2 + 1/\tau^2}{\left(\Omega^2 - \Omega_0^{\,2}\right)^2 + \gamma^2\Omega^2} \tag{2.38}$$

The spectral density of the source is just a constant,

$$S_{F_{\parallel}}(\Omega) = \frac{4n_{sp}KP_0V}{\Gamma\tau_{ph}} = 8K\omega_{ST}\left(P_0V/\Gamma\right)^2 \tag{2.39}$$

where n_{sp} is the spontaneous emission factor, K is the Petermann enhancement factor of DFB lasers, and ω_{ST} is the Schawlow-Townes linewidth [22, 23]. The noise spectrum has a resonance at Ω_0, damped by γ, and is the same form as the FM response, reflecting the fact that the fluctuations in photon density are coupled into carrier fluctuations by the dynamics of the rate equations. These carrier fluctuations chirp the laser frequency through (2.23), and we can find the chirp relation by returning to (2.37) and (2.17) and eliminating $F_{\parallel}(t)$, then using (2.23) to replace ΔN to get

$$\frac{d}{dt}\Delta\omega_{\parallel}(t) + \frac{1}{\tau}\Delta\omega_{\parallel}(t) = -\frac{|\alpha|}{2}v_gA\left[\frac{d}{dt}\Delta P_{\parallel}(t) + \frac{1}{\tau_{ph}}\Delta P_{\parallel}(t)\right] \tag{2.40}$$

This is the equivalent of (2.29) but for variations in frequency and photon density driven by $F_{\parallel}(t)$ rather than by $\Delta I(t)$. For a harmonic time dependence it reduces to

$$\Delta\omega_{\parallel} = -\frac{|\alpha|}{2}v_gA\left[\frac{i\Omega + 1/\tau_{ph}}{i\Omega + 1/\tau}\right]\Delta P_{\parallel} \tag{2.41}$$

From this it follows that the spectral density of the frequency fluctuations caused by $F_{\parallel}$ is

$$S^{\parallel}_{\Delta\omega}(\Omega) = \left(\frac{|\alpha|\Omega_0{}^2}{2P_0\Omega}\right)^2\left[\frac{(\tau_{ph}\Omega)^2 + 1}{(1/\tau\Omega)^2 + 1}\right]S^{\parallel}_{\Delta P}(\Omega) \tag{2.42}$$

where we used (2.28) for Ω_0 to simplify it. $\Delta\omega_{\parallel}(t)$ leads $\Delta P_{\parallel}(t)$ at frequency Ω by a phase

$$\theta^{\parallel} = \frac{\pi}{2} + \tan^{-1}\left(\frac{(1/\tau\Omega) + \tau_{ph}\Omega}{1 - (\tau_{ph}/\tau)}\right) \tag{2.43}$$

Note $\tau_{ph} << \tau$, so the denominator is nearly 1. Note that (2.43) implies that $\Delta\omega_{\|}(t)$ and $\Delta P_{\|}(t)$ are perfectly correlated. This is true because both are driven by the single noise source $F_{\|}(t)$.

Spontaneous emission $F_{\perp}$

The second noise term $F_{\perp}(t)$ produces no intensity fluctuations because it only perturbs the phase of the laser field. Thus

$$S_{\Delta P}^{\perp}(\Omega) = 0 \tag{2.44}$$

It produces frequency fluctuations given by

$$S_{\Delta\omega}^{\perp}(\Omega) = S_{F_{\perp}}(\Omega) = \frac{n_{sp}K}{P_0(V/\Gamma)\tau_{ph}} = 2K\omega_{ST} \tag{2.45}$$

These are uncorrelated with the fluctuations caused by $F_{\|}$.

The intensity noise of the laser is usually specified by the relative intensity noise (RIN), defined as

$$RIN \equiv 10\ \log_{10}\left(\frac{S_{\Delta P}(\Omega)}{P_0^{\,2}}\right) \tag{2.46}$$

and measured in dB per unit frequency. We use photon density as the variable because its ratio $\Delta P/P_0$ or $S_{\Delta P}/P_0^{\,2}$ has the same value as for output power or optical intensity. The noise terms as constructed are uncorrelated, so we can add their spectral densities,

$$S_{\Delta P}(\Omega) = S_{\Delta P}^{N'}(\Omega) + S_{\Delta P}^{\|}(\Omega) + S_{\Delta P}^{\perp}(\Omega) \tag{2.47}$$

Since the first of these terms is negligible and the last is zero, (2.46) becomes

$$\mathrm{RIN} = 10\ \log_{10}\left(\frac{S^{\parallel}_{\Delta P}(\Omega)}{P_0^{\,2}}\right) \tag{2.48}$$

The shape of the RIN spectrum is shown in Figure 2.3, based on (2.38) and (2.39).

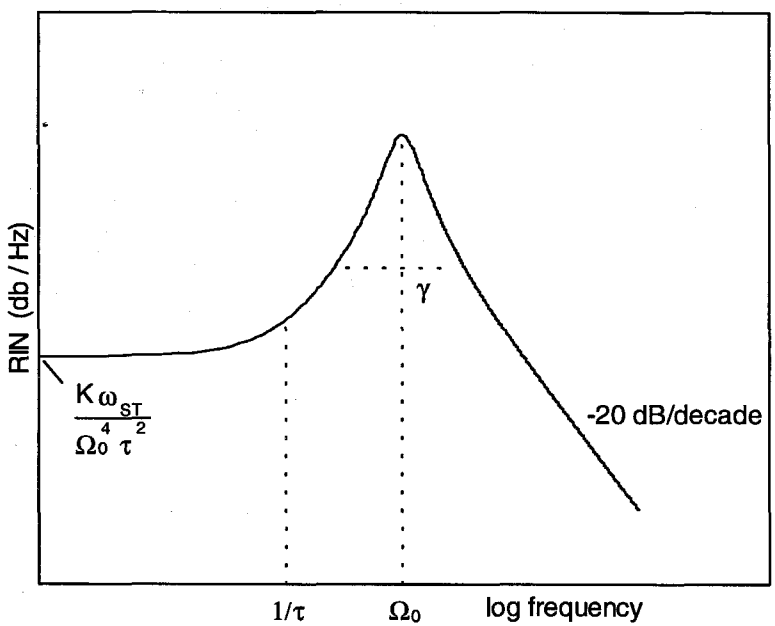

Figure 2.3. Shape of RIN spectrum, with peak at Ω_0 and damped by γ.

In the next chapter we will see how propagation through dispersive or frequency discriminating media can change the characteristics of semiconductor laser signals. In Chapter 4 we will show how measuring the modulation response and noise of a laser, and the change of those quantities in dispersive optical fiber, can let us determine the laser parameters.

Chapter 3 -- Propagation Effects

In this chapter we consider the effect on a general optical signal of propagation through a medium whose properties depend on the optical frequency. In some uses of the word, any physical property that depends on frequency is said to be "dispersive." In this thesis, dispersion refers only to group velocity dispersion, or an optical wavevector $\beta(\omega)$ which depends at least quadratically on the optical frequency. We refer to an optical loss that depends on frequency as "discrimination," in the sense that a frequency discriminator transmits optical signals of different frequencies preferentially, rather than as "dispersive loss."

In some sense, propagation through arbitrary media is a solved problem--we can relate the input and output optical field Fourier transforms by a complex transfer function which describes the medium. In the case of semiconductor lasers and fiber gratings, however, this is unwieldy and lacks insight. The concept of FM-to-AM conversion in fibers and gratings gives us useful heuristics that predict the properties of laser/grating systems without resorting to Fourier transforms.

3.1 Representing AM and FM signals

We start by writing the general form of an optical signal that is both amplitude and frequency modulated:

$$E(t) = E_0\left[1 + m\sin(\Omega t + \theta_{AM})\right]^{1/2} e^{i(\omega_0 t - \beta\cos(\Omega t + \theta_{FM}))} \tag{3.1}$$

The bracketed quantity represents the AM and the exponential the FM. E_0 is chosen to have units of (optical power)$^{1/2}$ so that the intensity is

$$\begin{aligned} P(t) = E * E &= E_0{}^2\left(1 + m\sin\left(\Omega t + \theta_{AM}\right)\right) \\ &= P_0 + \Delta P\sin\left(\Omega t + \theta_{AM}\right) \end{aligned} \tag{3.2}$$

where Ω is the modulation frequency and $m = \Delta P / P_0$ is the AM modulation index for intensity or optical power (as opposed to for the optical field, which for small signals is m/2, or the detected electrical power, which is 2m). The instantaneous optical phase is

$$\phi(t) = \omega_0 t - \beta\cos(\Omega t + \theta_{FM}) \tag{3.3}$$

where β is the phase modulation index. The instantaneous optical frequency is

$$\omega(t) \equiv \frac{d\phi(t)}{dt} = \omega_0 + \beta\Omega\sin(\Omega t + \theta_{FM}) \tag{3.4}$$

where ω_0 is the center optical frequency. We see that a modulation of the optical phase implies a modulation of the optical frequency, and vice versa. The optical frequency deviation (one half peak-to-peak) is clearly

$$\Delta\omega = \beta\Omega \tag{3.5}$$

which is an important basic relation.

θ_{AM} and θ_{FM} are the phase by which the AM and FM modulation *lead* some reference, for example, a sinusoidal modulation of the laser injection current. The form of the phase modulation (3.1) differs among authors but this form has the advantage that when $\theta_{AM} = \theta_{FM}$ the power and frequency are in phase, e.g., for $\theta_{AM} = \theta_{FM} = 0$ both go as $+\sin(\Omega t)$.

General formulae

The signal (3.1) contains discrete frequency components, or harmonics, at intervals of Ω from ω_0,

$$E(t) = E_0 \sum_{q=-\infty}^{\infty} C_q e^{i(\omega_0 + q\Omega)t} \tag{3.6}$$

The harmonics are often referred to as sidebands. In propagation through some medium with a complex transmittance $t(\omega) = |t(\omega)|e^{i\phi_t(\omega)}$, the q^{th} harmonic picks up a factor $t(\omega_0 + q\Omega)$. To analyze the problem analytically, we thus need to find the sideband coefficients C_q for (3.1). We will develop the technique here in order to show why other techniques are necessary.

The AM portion can be written with the Taylor expansion

$$(1+x)^{1/2} = 1 + \sum_{n=1}^{\infty} \frac{x^n}{n!} \prod_{p=0}^{n-1} (1/2 - p) \tag{3.7}$$

which can be reworked into

$$(1+x)^{1/2} = \sum_{n=0}^{\infty} a_n x^n \tag{3.8}$$

with $$a_0 \equiv 1, \quad a_1 \equiv 1/2, \quad a_{n\geq 2} \equiv \frac{(-1)^{n-1}(2n-3)!}{n!4^{n-1}(n-2)!} \tag{3.9}$$

for x<1. For our signal $x = m \sin(\Omega t + \theta_{AM})$, and x^n is evaluated by writing the sine in complex exponential form. For compactness we define the argument of the sine to be $\varphi \equiv \Omega t + \theta_{AM}$, giving

$$(m\sin\varphi)^n = \left(\frac{m}{2i}e^{i\varphi} - \frac{m}{2i}e^{-i\varphi}\right)^n = \left(\frac{m}{2i}\right)^n \sum_{p=0}^{n} (-1)^p e^{i\varphi(n-2p)} \frac{n!}{p!(n-p)!} \tag{3.10}$$

where for $(e^{i\varphi}-e^{-i\varphi})^n$ we used the binomial expansion,

$$(A+B)^n = \sum_{p=0}^{n} A^{n-p}B^n \frac{n!}{p!(n-p)!} \tag{3.11}$$

Combining (3.8) and (3.10) we get the complete analytic expansion for the AM term,

$$(1+m\sin\varphi)^{1/2} = \sum_{n=0}^{\infty} a_n \left(\frac{m}{2i}\right)^n \sum_{p=0}^{n} (-1)^p e^{i\varphi(n-2p)} \frac{n!}{p!(n-p)!} \tag{3.12}$$

The FM term can be written using the Jacobi-Anger expansion [24],

$$e^{-i\beta\cos(\Omega t+\theta_{FM})} = \sum_{n=-\infty}^{\infty} (-i)^n J_n(\beta) e^{-in(\Omega t+\theta_{FM})} \tag{3.13}$$

where $J_n(x)$ is the n^{th} Bessel function of the first kind.

The advantage of the formula (3.13) for the FM sidebands is that it gives explicitly the coefficient $C_{FM,q}$ of the q^{th} harmonic $e^{iq\Omega t}$, whereas the AM formula (3.12) does not. We can deduce the coefficient $C_{AM,q}$ of the q^{th} AM harmonic from (3.12), but

each $C_{AM,q}$ is an infinite sum of a_n in (3.9). Furthermore, a signal with both AM and FM is the product of (3.12) and (3.13), the q^{th} harmonic of which is an infinite sum of $C_{AM,i}$ and $C_{FM,j}$. And to find how dispersive fiber affects the detected signal, for example, we would multiply each sideband by $t(\omega_0+\Omega q)$, take $P(t)=|E(t)|^2$ and find the part of P(t) which goes as $\sin(\Omega t)$.

It should be clear at this point that an analytic treatment is intractable. There are two alternatives. One is to determine the coefficients C_q of (3.1) with a numerical Fourier transform, and analyze the problem completely numerically, as discussed in Section 3.4. The other is to use the small-signal approximation.

Small signal approximation

If we assume $m<<1$ and $\beta<<1$ the expansion simplifies. This is often a good approximation, because to avoid non-linearities in a laser response or optical modulator, the signal is often kept small. Then we can expand the square root and exponential in (3.1) and write the cosine and sine as complex exponentials. If we define

$$\mathcal{M} \equiv m e^{i\theta_{AM}} \tag{3.14}$$

$$\mathcal{B} \equiv \beta e^{i\theta_{FM}} \tag{3.15}$$

and remember that θ_{AM} and θ_{FM} represent phase leads in time, we arrive at

$$E(t) = E_0 e^{i\omega_0 t}\left[1 + e^{+i\Omega t}\left\{\frac{-i}{2}\left(\frac{\mathcal{M}}{2} + \mathcal{B}\right)\right\} + e^{-i\Omega t}\left\{\frac{i}{2}\left(\frac{\mathcal{M}^*}{2} - \mathcal{B}^*\right)\right\}\right] \tag{3.16}$$

This gives the complex amplitude of the upper and lower optical sidebands of E(t) in terms of the size and phase of the AM and FM signals.

Before applying this formula in the next sections, we present a powerful phasor representation of the small signal approximation which can be used to understand the effect of dispersion or discrimination. Suppose we have a generic signal

$$E(t) = E_0 e^{i\omega_0 t}\left[1 + c_1 e^{+i\Omega t} + c_2 e^{-i\Omega t}\right] \tag{3.17}$$

in which c_1 and c_2 are gotten from (3.16). We can draw the amplitudes of the three frequency components as phasors in the complex plane, as in Figure 3.1. As time evolves, the phasors c_1 and c_2 rotate in opposite directions because of their $e^{\pm i\Omega t}$ time dependence (we consider the carrier wave phasor, amplitude 1, to be the fixed reference phase). Note the abscissa in Figure 3.1 serves double duty--it represents the imaginary projection of the phasor and also the frequency axis.

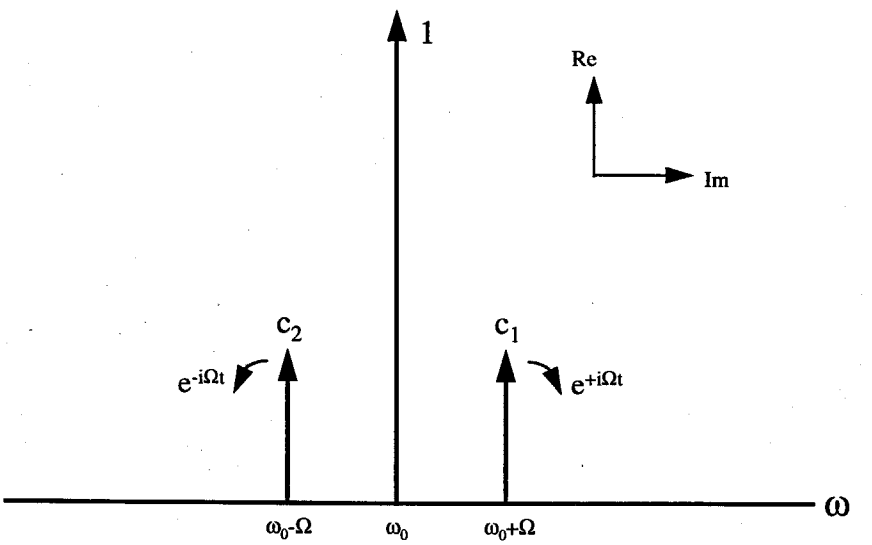

Figure 3.1. Representation of upper and lower sidebands in the complex plane. The sidebands rotate in opposite direction as time progresses, due to the $e^{\pm\Omega t}$ time dependence. This c_1 and c_2 represent pure AM modulation.

The total electric field is the vector sum of these three phasors. We can see that for the c_1,c_2 in Figure 3.1 the horizontal components of the sidebands will always cancel each other, and the time evolution only perturbs the amplitude of total phasor along the real axis. This amounts to pure AM modulation, since the center carrier wave phasor gets sinusoidally longer and shorter with the addition of the rotating sidebands, but doesn't change phase. One half-period later both sidebands point straight down; this configuration also represents AM modulation, but with an AM phase 180° from the original.

Suppose instead the phase of c_1 is opposite c_2, depicted in Figure 3.2. Then as time evolves the real components cancel, and only the imaginary part of the total phasor is perturbed. Assuming $|c_1| << 1$, $|c_2| << 1$, the phasor length is unchanged. This represents pure phase modulation, and hence pure FM. Sidebands that both point left or both point right are also pure FM, but with a different FM phase.

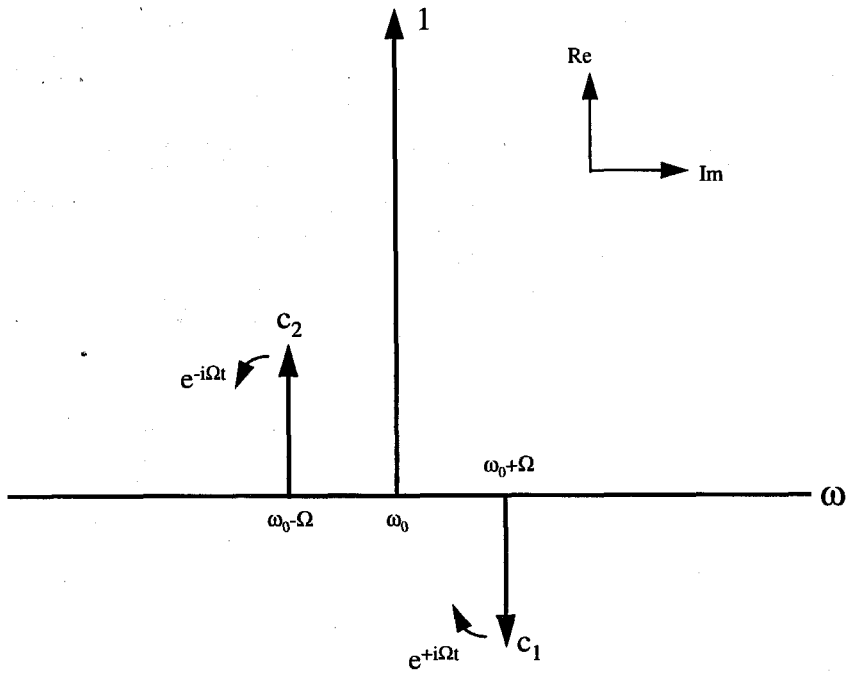

Figure 3.2. Phasor diagram showing pure phase modulation. As the sidebands rotate with time, the real projection cancels and only the phase of the vector sum is perturbed.

The phasor picture is sufficient for representing any arbitrary AM and FM signal in the small-signal approximation. The real and imaginary components of c_1 and c_2 amount to four parameters, adequate for representing m, β, θ_{AM} and θ_{FM}. If $c_2 = 0$, for example, we have only one sideband which perturbs both the length and phase of the carrier wave, producing a signal with equal amounts of AM and FM (in that $\beta = m/2$). If $|c_1|>|c_2|$ we have both AM and FM but in differing amounts--e.g., we could have a mostly AM signal with a slight attendant FM. If $|c_1|=|c_2|$ and both have a phase of $\pi/4$ relative to the real axis, we have equal amounts of AM and FM but with a different relative phase $\theta_{FM}-\theta_{AM}$ between them than if $c_2 = 0$.

The power of this model is that is lets us see immediately the effect of propagation. For example, if a fiber grating blocks the upper sideband and transmits only the carrier wave and lower sideband, we know immediately this will produce an output optical signal with equal amount of AM and FM regardless of whether the input signal was AM or FM modulated or both. A dispersive medium that adds the same phase φ to both sidebands but not the carrier wave (which is essentially what standard optical fiber does) will mix AM and FM components, converting a purely AM input into a purely FM output when $\varphi = \pi/2$. Both of these phenomena will be demonstrated experimentally in subsequent chapters.

3.2 Dispersive propagation

The frequency components of (3.16) are multiplied by $t(\omega)$ in transmission through a medium and knowing $t(\omega)$ we can determine the AM and FM properties of the resulting signal. First we will consider dispersive propagation, by which we mean one in which only the phase of the components is affected, i.e., $t(\omega) = e^{-i\phi(\omega)}$.

General formulae

Suppose the upper and lower sidebands acquire a phase factor $e^{-i\phi_1}$ and $e^{-i\phi_2}$ respectively, with respect to the carrier wave. The resulting signal is, copying (3.16),

$$E(t) = E_0 e^{i\omega_0 t}\left[1 + e^{+i\Omega t}\left(\frac{-i}{2}\right)\left(\frac{\mathcal{M}}{2} + \mathcal{B}\right)e^{-i\phi_1} + e^{-i\Omega t}\left(\frac{i}{2}\right)\left(\frac{\mathcal{M}^*}{2} - \mathcal{B}^*\right)e^{-i\phi_2}\right] \quad (3.18)$$

Note we assigned no phase to the carrier wave. In general the center frequency picks up a phase but it is only the relative phase between it and the sidebands that matters. We can easily pull out an overall phase $e^{-i\phi(\omega_0)}$ so that $\phi_1 = \phi(\omega_0+\Omega)-\phi(\omega_0)$ and $\phi_2 = \phi(\omega_0-\Omega)-\phi(\omega_0)$. The AM and FM of this output signal can be determined by comparing the complex amplitudes of the sidebands in (3.18) with the canonical form (3.16). If we let $\mathcal{M}'$ and $\mathcal{B}'$ represent the AM and FM after the fiber, we see by comparison that

$$\frac{\mathcal{M}'}{2} + \mathcal{B}' = \left(\frac{\mathcal{M}}{2} + \mathcal{B}\right)e^{-i\phi_1} \quad (3.19)$$

and

$$\frac{\mathcal{M}'^*}{2} - \mathcal{B}'^* = \left(\frac{\mathcal{M}^*}{2} - \mathcal{B}^*\right)e^{-i\phi_2} \quad (3.20)$$

Taking the real and imaginary parts of these gives us four equations, from which we can solve for m', β', θ_{AM}' and θ_{FM}' after the fiber. The solution can be expressed succinctly as

$$\mathcal{M}' = \left[\mathcal{M}\cos\phi_a - 2i\mathcal{B}\sin\phi_a\right]e^{-i\phi_b} \quad (3.21)$$

$$\mathcal{B}' = \left[\mathcal{B}\cos\phi_a - \frac{i}{2}\mathcal{M}\sin\phi_a\right]e^{-i\phi_b} \quad (3.22)$$

where

$$\phi_a \equiv (\phi_1 + \phi_2)/2 = \phi(\omega_0 + \Omega) + \phi(\omega_0 - \Omega) - 2\phi(\omega_0) \quad (3.23)$$

$$\phi_b \equiv (\phi_1 - \phi_2)/2 = \phi(\omega_0 + \Omega) - \phi(\omega_0 - \Omega) \quad (3.24)$$

The interpretation of this is that AM and FM get converted into each other by ϕ_a, or any accumulation of phase that is symmetric about the carrier wave. Any anti-

symmetric accumulation of phase, ϕ_b, only serves to add an extra time lag to both the AM and FM phases. The fact that the dispersive effects can be separated into symmetric and anti-symmetric effects follows from our earlier intuitive phasor representation.

Standard optical fiber

For example, in standard single-mode telecommunications fiber, the phase accumulated in traveling a length L is $\beta_{fiber}L$, where $\beta_{fiber}(\omega)$ is the wavenumber of the optical mode. It is often Taylor expanded about the center optical frequency:

$$\beta_{mode}(\omega+\Delta\omega)=\beta_0+\beta'\Delta\omega+\frac{1}{2}\beta''(\Delta\omega)^2+\frac{1}{6}\beta'''\Delta\omega^3+\frac{1}{24}\beta''''\Delta\omega^4+\ldots \quad (3.25)$$

Here $\beta_0=\beta_{mode}(\omega_0)$ and the primes denote derivatives of $\beta(\omega)$ evaluated at ω_0. (Note this β_{mode} is unrelated to the phase modulation index β--we use the awkward subscript "mode" to avoid confusion.) From (3.16) it is obvious that β_0 produces an inconsequential overall phase, and β' produces an extra phase that is linear with frequency, equivalent to a time lag. The second derivative β'' predicts a frequency dependence of the group velocity v_g, defined by

$$\frac{1}{v_{gr}}\equiv\frac{\partial\beta_{mode}}{\partial\omega}=\beta'+\beta''\Delta\omega+\ldots \quad (3.26)$$

v_g is the speed at which a field envelope propagates along the fiber. (For non-dispersive media, $\beta_0 = 0$ and $v_g = 1/\beta'$.) β'' is often measured by the difference in time taken to travel a length of fiber L for two different wavelengths of light, measured in picoseconds

of time difference per kilometer of fiber traveled, per nm of wavelength difference. This is the common dispersion parameter

$$D \equiv \frac{-2\pi c}{\lambda^2}\beta'' \tag{3.27}$$

At the low-loss wavelength of standard optical fiber, around 1550 nm (in air), D has a typical value of 17 ps / nm km ($\beta''<0$ in this region), and the blue components travel faster than the red components. D reaches zero at around 1330 nm and is negative ($\beta''>0$, red components faster) at wavelengths below this.

Including only β'', ϕ_a becomes the mixing angle $\theta(\Omega) = \beta''\Omega^2 L/2$ commonly used for dispersive optical fiber. The root mean square detected electrical power at frequency Ω is, from (3.2), proportional to m^2. After the fiber, we see (by taking the magnitude of (3.25) and some algebra) this becomes

$$(m')^2 = m^2\cos^2\theta + 4\beta^2\sin^2\theta + 4m\beta\sin\theta\cos\theta\sin(\theta_{FM} - \theta_{AM}) \tag{3.28}$$

(Our conventions differ from some authors: for us $\beta''<0$ and $\theta(\Omega)<0$ for standard fiber at 1550 nm.) This is the general formula for the change in an AM signal due to dispersive fiber. The first term describes conversion of the initial AM into FM (and thus represents a decrease of detected signal), and the second the conversion of initial FM into detected AM. The last term is a correction depending on the relative AM-FM phase. The AM phase of the signal, θ_{AM}, will also be changed by the fiber given the complex nature of (3.21), and this can be measured by a network analyzer as easily as m' can.

All of the even-order terms, like β'' and β'''', contribute to ϕ_a or θ in the same way, and they mix the AM and FM nature of a signal as it propagates. The odd-order

dispersion terms like β''' only delay the AM or FM signal. However, we note that just because ϕ_b adds a time delay to AM and FM signals without inter-converting them, this doesn't mean a broadband signal is not distorted by β'''. A broadband or analog signal must be viewed as a superposition of AM and FM components with different frequencies Ω. Each component picks up a phase lag $\phi_b = \beta'''\Omega^3 L/6$ that depends on Ω, and the components get out of phase with respect to each other, which is sufficient to cause distortion. This can be made rigorously correct for a small broadband signal $E(t) = E_0[1 + f(t)]$, where $|f| << 1$, by expanding f(t) into AM and FM components of different frequency, and using (3.25) and (3.26) for each component $\mathcal{M}'(\Omega)$ and $\mathcal{E}'(\Omega)$. In a modulation response experiment, though, we measure $(m')^2$ and θ_{AM} for only a single Ω at a time, and (3.21) is appropriate.

Laser modulation

In the previous chapter we derived the phase modulation index β and the FM phase for direct current modulation of the laser. Using the complex β from (2.31) in (3.21), we get the transfer function for AM laser modulation,

$$H_{AM}(\Omega) \equiv \frac{\mathcal{M}'}{\mathcal{M}} = \cos\theta(\Omega) + |\alpha|\sin\theta(\Omega) - i|\alpha|\frac{\kappa}{\Omega}\sin\theta(\Omega) \qquad (3.29)$$

where $\kappa = \varepsilon P_0 / \tau_{ph}$. The first term on the right side of (3.29) represents the decrease in the initial laser AM as it gets converted into FM by the fiber. The second term represents the creation of new AM from transient chirp FM. But since $\theta < 0$, this term is negative at

low frequencies, and so it serves to cancel the original AM. The third term represents new AM created from adiabatic chirp FM, and it is $\pi/2$ out of phase with both other terms and adds AM power in quadrature.

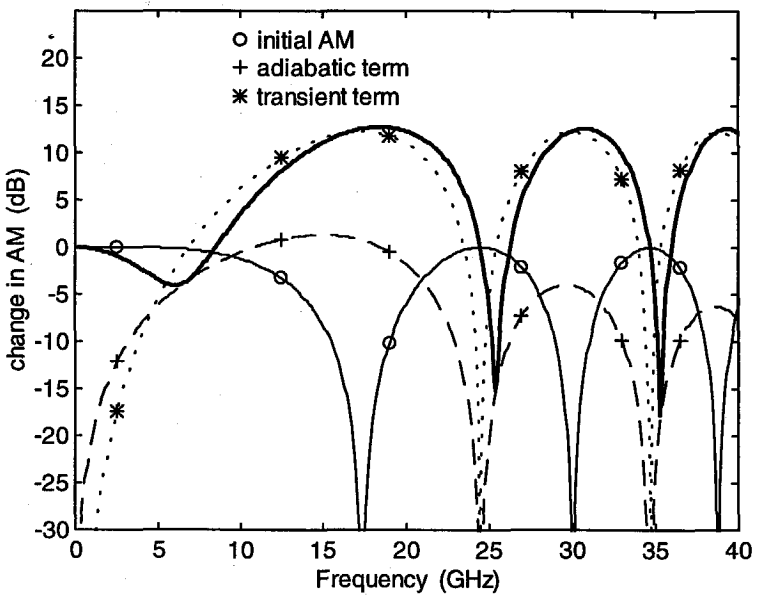

Figure 3.2c. Magnitude of the three terms of equation (3.29). The thick solid line is the total transfer function, and the three component terms are labeled by the symbols.

Figure 3.2c shows the magnitude of these three components for 13.3 km of fiber, with laser parameters $|\alpha| = 4.1$ and $\kappa / 2\pi = 4.6$ GHz. (These parameters were taken from a real measurement, described in Chapter 4, Figure 4.6.) The initial AM term is labeled by the open circles, and shows the zeroes in the AM produced by total conversion into FM when $\cos(\theta) = 0$. At low frequencies the transient term is smaller than the adiabatic term, because the low-Ω expansion of $\sin(\theta)$ goes as Ω^2, whereas the adiabatic term goes

as Ω. The adiabatic and transient terms are equal at $\Omega = \kappa = 4.6$ GHz. The maximum transient contribution (the height of the "bumps" in Figure 3.2c, when $\sin(\theta) = 1$) is larger than the initial AM by a factor of $|\alpha|^2 = 12.3$ dB. Thus the two together can increase the signal by α^2+1. The maximum adiabatic contribution depends on κ and decreases with frequency due to the $1/\Omega$ dependence in (3.29). The thick solid line is the total transfer function,

$$\left|H_{AM}(\Omega)\right|^2 \equiv \frac{m'^2}{m^2} = \cos^2\theta(\Omega) + \left|\alpha\right|^2\left[1+(\kappa/\Omega)^2\right]\sin^2\theta(\Omega) + 2\left|\alpha\right|\cos\theta(\Omega)\sin\theta(\Omega) \tag{3.30}$$

Note in Figure 3.2c that at about 7 GHz the initial AM and the transient term have equal magnitudes and thus cancel each other out exactly, and the total transfer function is equal to the adiabatic component. The depth of this first dip (thick solid line) is determined by the non-linear gain term κ. Fitting (3.30) to an experimental measurement is a good method of measuring the laser parameters $\varepsilon P_0/\tau_{ph}$ and α, as illustrated in the next chapter.

In short, dispersive fiber can increase the AM signal by more than a factor of $|\alpha|^2 + 1$ at some frequencies, and decrease it by several tens of dB at others. It is therefore a major source of distortion in analog signals.

Laser noise

To analyze the change in laser noise with propagation, we need to relate the spectral densities $S_{\Delta P}(\Omega)$ and $S_{\Delta\omega}(\Omega)$ which characterize noise to modulation indices m

and β which we've used to analyze propagation effects. We make an association between mean squared quantities; for the AM index we use get

$$m^2 \equiv \left(\frac{\Delta P}{P_0}\right)^2 \rightarrow \frac{S_{\Delta P}(\Omega)}{P_0{}^2} \tag{3.31}$$

and for phase modulation we have

$$\beta^2 \equiv \left(\frac{\Delta\omega}{\Omega}\right)^2 \rightarrow \frac{S_{\Delta\omega}(\Omega)}{\Omega^2} \tag{3.32}$$

Note that in (3.1), m and β refer only to the single-frequency signal at Ω, and in general can be thought of as functions of frequency just like the spectral densities, which is implied in (3.31) and (3.32).

As remarked in Chapter 2, the relationship between intensity and frequency noise caused by spontaneous carrier decay $F_N'(t)$ is the same as that for direct modulation, and thus the intensity noise $S_{\Delta P}^{N'}(\Omega)$ is modified by the same transfer function (3.30) in propagating through dispersive fiber. Thus

$$S_{\Delta P}^{N'}(\Omega)_{\text{after fiber}} = \left|H_{AM}(\Omega)\right|^2 S_{\Delta P}^{N'}(\Omega) \tag{3.33}$$

The noise driven by $F_{\|}(t)$ at frequency Ω produces a phase modulation index gotten from (2.41),

$$\beta^{\|} = \frac{|\alpha|}{2} m^{\|} \frac{\Omega_0{}^2}{\Omega^2}\left[\frac{(\tau_{ph}\Omega)^2+1}{(1/\tau\Omega)^2+1}\right]^{1/2} \tag{3.34}$$

where

$$m^{\|} = \sqrt{\frac{S_{\Delta P}^{\|}(\Omega)}{P_0{}^2}} \tag{3.35}$$

is the effective noise modulation index. Using this and θ_{FM}-θ_{AM} from (2.42) we get, from (3.21) with much algebra, the transfer function for noise driven by $F_{\|}$,

$$H_{\|}(\Omega) \equiv \frac{\mathcal{M}'}{\mathcal{M}} = \cos\theta(\Omega) + |\alpha| \frac{\Omega_0^{\,2}}{\Omega^2} \left(\frac{1 + i\Omega\tau_{ph}}{1 - i/(\Omega\tau)} \right) \sin\theta(\Omega) \tag{3.36}$$

for which

$$|H_{\|}(\Omega)|^2 = \frac{S^{\|}_{\Delta P}(\Omega)_{\text{after fiber}}}{S^{\|}_{\Delta P}(\Omega)_{\text{before fiber}}} \tag{3.37}$$

The third noise term $F_{\perp}$ produces only a frequency noise, so the initial effective modulation index $m^{\perp}$ is zero, and the phase modulation index is, from (2.45),

$$\beta^{\perp} = \frac{\sqrt{S_{F_{\perp}}(\Omega)}}{\Omega} = \frac{\sqrt{2K\omega_{ST}}}{\Omega} \tag{3.38}$$

Using (3.28) we get

$$\frac{S^{\perp}_{\Delta P}(\Omega)_{\text{after fiber}}}{P_0^{\,2}} = 4 \left(\frac{2K\omega_{ST}}{\Omega^2} \right) \sin^2\theta(\Omega) \tag{3.39}$$

Combining all three of these noise terms, the RIN after the fiber is, by comparison to (2.46) and (2.47),

$$RIN_{\text{after fiber}} = 10\ \log_{10} \left(|H_{AM}(\Omega)|^2 \frac{S^{N'}_{\Delta P}}{P_0^{\,2}} + |H_{\|}(\Omega)|^2 \frac{S^{\|}_{\Delta P}}{P_0^{\,2}} + \frac{8K\omega_{ST}}{\Omega^2} \sin^2\theta(\Omega) \right) \tag{3.40}$$

The first term is still negligible, but we see that the fiber produces a new source of intensity noise--the FM-to-AM conversion phenomenon of dispersion also converts frequency noise into excess amplitude noise [25]. Using the form of $S^{\|}_{\Delta P}(\Omega)$ from the previous chapter, and ignoring the first term above, we get

$$RIN_{\text{after fiber}} = 10\log_{10}\left\{8K\omega_{ST}\left[\left(\frac{\Omega^2 + 1/\tau^2}{\left(\Omega^2 - \Omega_0{}^2\right)^2 + \gamma^2\Omega^2}\right)\left|H_{\|}(\Omega)\right|^2 + \frac{\sin^2\theta(\Omega)}{\Omega^2}\right]\right\} \qquad (3.41)$$

The first term is the usual RIN spectrum modified by the transfer function $H_{\|}$ for "parallel" spontaneous emission, that is, those events whose field is in phase with the laser field. The second term, $\sin^2\theta / \Omega^2$, is the conversion of frequency noise from the "perpendicular" events into excess amplitude noise. These components are plotted in Figure 3.5 for 8.8 km of fiber and laser parameters taken from experimental data (Chapter 7). We see the fiber reduces the RIN by over 10 dB at low frequencies, and is due mostly to the $S^{\|}_{\Delta P}(\Omega)$ term. When $H_{\|}(\Omega)$ is small the $S^{\perp}_{\Delta P}(\Omega)$ term determines the RIN, and the two alternate (due to their cosine and sine behavior) at higher frequencies. Like the modulation response, the change in RIN due to fiber can be positive or negative depending on the frequency, fiber length, and laser parameters.

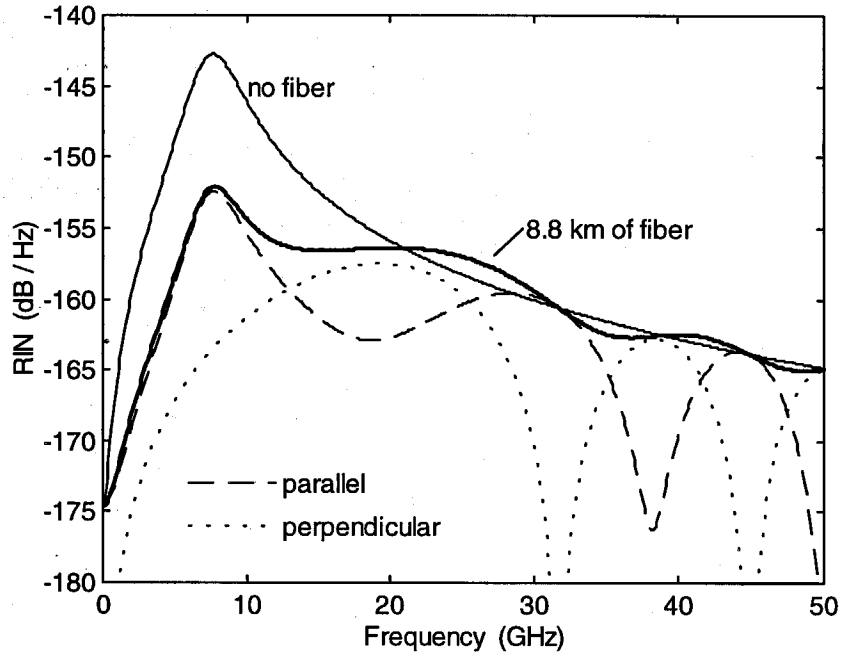

Figure 3.5. RIN before and after 8.8 km of fiber, with the two components of Equation (3.41). The "parallel" line refers to $S^{\parallel}_{\Delta P}(\Omega)$ and the "perpendicular" to $S^{\perp}_{\Delta P}(\Omega)$.

3.3 Frequency discrimination

In this section we let the propagation medium have a frequency-dependent loss, so that $t(\omega)=|t(\omega)|e^{i\phi(\omega)}$. If the magnitude $|t(\omega)|$ is not constant, the medium acts as a frequency discriminator by selectively transmitting some wavelengths more than others.

Single sideband analysis

We can extend our single-sideband analysis to include complex transmittances that are more than just phase factors. Following our previous derivation, the output field becomes

$$E(t) = E_0 e^{i\omega_0 t} t(\omega_0)\left[1 + e^{+i\Omega t}\left(\frac{-i}{2}\right)\left(\frac{\mathcal{M}}{2} + \mathcal{B}\right)t_1 + e^{-i\Omega t}\left(\frac{i}{2}\right)\left(\frac{\mathcal{M}^*}{2} - \mathcal{B}^*\right)t_2\right] \qquad (3.42)$$

where we have factored out the transmittance of the center wave, so $t_1 = t(\omega_0+\Omega)/t(\omega_0)$ and $t_2 = t(\omega_0-\Omega)/t(\omega_0)$. The signal (3.42) is equal to the canonical form (3.16) if we use the new AM and FM parameters

$$\mathcal{M}' = \frac{1}{2}\left[\mathcal{M}(t_1 + t_2^*) + 2\mathcal{B}(t_1 - t_2^*)\right] \qquad (3.43)$$

$$\mathcal{B}' = \frac{1}{2}\left[\mathcal{B}(t_1 + t_2^*) + \frac{\mathcal{M}}{2}(t_1 - t_2^*)\right] \qquad (3.44)$$

These reduce to (3.21) and (3.22) if t_1 and t_2 are purely phase factors. Note that (3.43) predicts the new AM modulation index, which is the optical power at Ω divided by the DC optical power. Because of the $t(\omega_0)$ outside the brackets in (3.39), both the component at Ω and DC power will be reduced by $|t(\omega_0)|^2$ because of the loss.

For a fiber grating, $t(\omega)$ is a complicated function and (3.43) and (3.44) are actually hard to handle analytically. A simple exception is when $|t(\omega)|$ is linear and non-dispersive over the bandwidth of interest, in which case the signal can be more intuitively handled in the time domain.

Time domain model

Suppose we replace our signal (3.1) with one of the form

$$E(t) = \sqrt{P(t)}e^{i\omega_0 t + i\phi(t)} \tag{3.45}$$

which has instantaneous power P(t) and an instantaneous frequency

$$\omega(t) = \omega_0 + \frac{d\phi(t)}{dt} \tag{3.46}$$

Now suppose this signal is incident on a frequency discriminator with a transmittance $T(\omega)$ that responds instantaneously to $\omega(t)$. In this case the transmitted optical power would simply be

$$P_{transmitted}(t) = P(t)T(\omega(t)) \tag{3.47}$$

The problem with this model is that no frequency discriminator responds instantaneously to a change in optical frequency. Indeed, a frequency difference of $\Delta\omega$ between two signals cannot be resolved by any measurement until the signals have gotten out of phase by one cycle, which takes an amount of time on the order of $1/\Delta\omega$. If the characteristic time scale on which P(t) or $\omega(t)$ changes is much longer than the response time of the discriminator, then (3.47) is a reasonable approximation. But if the response time of the discriminator or filter is comparable to the signal bandwidth, we must include the response time in our calculation. This finite response time is manifest as a complex phase of the frequency response of the filter. When the signal bandwidth is comparable

to the filter bandwidth, we must use the Fourier-domain transfer function of the filter to model these phase effects correctly.

Nevertheless, (3.47) offers a simple intuitive explanation of the consequences of frequency discrimination, and is sufficient for explaining many experimental results. For example, consider a directly modulated laser signal $P_{in}(t) = P_{0,in} + \Delta P_{in} \sin(\Omega t)$ incident on a linear frequency discriminator, with a linear transmission $T(\omega) = T + T'\Delta\omega$, where $T = T(\omega_0)$ is the transmission at the center frequency and $T' = dT/d\omega$ is the slope of the transmittance versus frequency. For low frequencies $\Omega << \kappa$ the frequency deviation of the laser is $\Delta\omega = |\alpha|\Delta P_{in}\,\kappa / 2P_{0,in}$ from (2.31), and the FM and AM are in phase. Then, using (3.47),

$$P_{out}(t) = T\left[P_{0,in} + \Delta P_{in} \sin(\Omega t)\right] + \Delta P_{in} T' |\alpha| \kappa / 2 \tag{3.48}$$

where we ignored the $\sin^2$ term. The new output signal at Ω is related to the initial one by

$$\frac{\Delta P_{out}}{\Delta P_{in}} = T + T' |\alpha| \kappa / 2 \tag{3.49}$$

The first term is the initial modulation attenuated by the filter, and the second is new modulated created from the FM by the filter.

The significance of this is two-fold. First, if T' is positive and large enough, the ratio can be greater than 1, meaning the total AM signal is increased in going through the filter. We will see this realized in Chapter 6, with a 14 dB increase in a directly modulated laser signal in transmission through a fiber grating. On the other hand, if T' is

negative, the new AM will cancel some of the original. We will see this in the context of laser noise in Chapter 7, in which a fiber grating reduces the laser RIN by 2 dB.

3.4 Fourier-domain analysis of arbitrary media

Because of the difficulty in calculating the Fourier coefficients of (3.1) outlined in Section 3.1, we were forced to include only the first two sidebands in our analysis. The other alternative is to calculate these coefficients numerically, and treat the entire propagation problem numerically in the Fourier domain.

Figure 3.3 shows a schematic of this approach. For any of the driving terms in the rate equations we can calculate at any frequency Ω the AM and FM signal parameters m, β, and θ_{FM}-θ_{AM} as in Chapter 2. Then from E(t) in (3.1) we calculate the Fourier spectrum $\tilde{E}(\omega)$ before and after the optical device, using the complex transmittance $t(\omega)$. The transfer function is the ratio of the output to input detector power at the modulation frequency Ω. This routine can also be used to calculate the change in a digital signal in the time domain, using a square wave for $E_{in}(t)$ and comparing to $E_{out}(t)$.

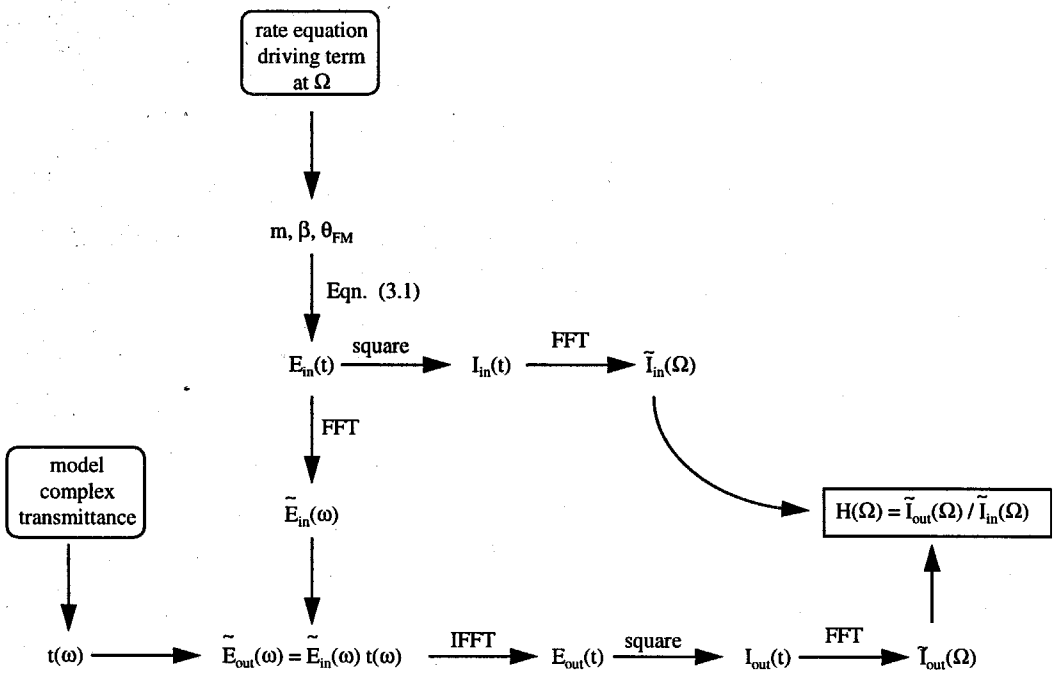

Figure 3.3. Schematic of routine used to numerically calculate the transfer function $H(\Omega)$ of an optical system with transmittance $t(\omega)$. FFT represents a numerical fast Fourier transform and IFFT the inverse transform.

A numerical analysis is the only practical way to analyze fiber gratings, for which the transmittance $t(\omega)$ is either analytically intractable or only available numerically, as we shall see in Chapter 5. In addition, it is valid, when the small signal approximation is not, for signals with large AM or FM modulations, $m \sim 1$ or $\beta \sim 1$.

A listing of a routine for performing this calculation is given in Appendix A.

Chapter 4 -- Characterization of Semiconductor Lasers

We saw in the previous chapter that the laser dynamic parameters α, $\kappa = \varepsilon P_0/\tau_{ph}$, Ω_0 and γ all play a role in the effect of propagation on the laser signals. Thus we need to know these parameters in order to predict the effect of a fiber grating, and in fact measuring the change in noise or modulation response due to a fiber of known length and dispersion can let us measure them. In this chapter we detail the experimental characterization of semiconductor lasers, with the goal of determining these dynamic parameters.

4.1 Experimental setup

A schematic of the experimental setup is shown in Figure 4.1. The laser rests on a home-built probe station that features a two-stage temperature controller, built from plans presented in [26] and modified for our setup, which stabilizes the laser temperature and can be used to temperature-tune the laser wavelength. The DC current is supplied by a low-noise constant current source, built from plans given in [27] and modified for our use, and is delivered to the laser chip via two needle-like DC probes. The output is collimated, sent through an optical isolator, and focused into a fiber pigtail, from which it can be sent through various lengths of standard single-mode telecommunication fiber

(Corning SMF-28) and/or a fiber grating, and into a detector. Often we use a fiber coupler to send some of the light to an optical spectrum analyzer (HP 70950A) to monitor the laser wavelength or measure the grating transmission spectrum.

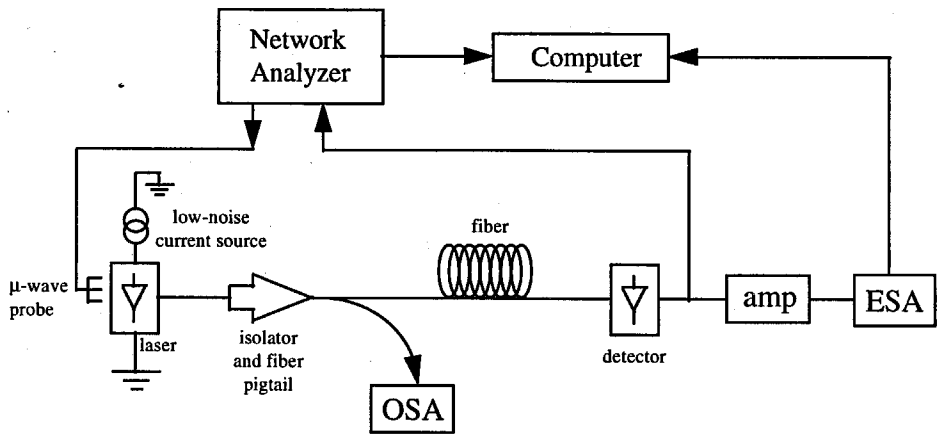

Figure 4.1. Experimental setup. The network analyzer measures the laser modulation response, and the electronic spectrum analyzer measures the intensity noise power.

For a modulation response measurement, the high-frequency signal is provided by an electronic network analyzer (HP 8722C) and delivered to the laser via a custom-ordered microwave probe (Microtech Inc.) with a microstrip contact geometry. This has three planar contact lines, the inner carrying the signal and the two outer ones, separated by 125 μm, serving as grounds. The signal is detected with a high-speed photodiode (Ortel 2516A) with a 20 GHz response. The network analyzer compares the received signal to the sent signal at swept frequencies from 50 MHz to as high as 40 GHz.

For an intensity noise measurements, we provide no high-speed signal and simply bias the laser at some CW operating point. We use a high-power photodiode

(Ortel 2518A) capable of 15 mW of fiber-coupled optical power, and send the high-frequency component (which is by definition all noise) through an electronic amplifier and into an electronic spectrum analyzer (HP 8565E). The network analyzer, electronic spectrum analyzer, and an ammeter that measures the detector photocurrent (not shown in Figure 4.1) are connected to a personal computer programmed to control the data collection.

4.2 Modulation response

Figure 4.2 shows the results of a typical modulation response measurement. The detected signal is more than 40 dB below the sent signal because of electronic losses, which would have to be removed in an imbedded system. The response is shown for six bias points, where $I - I_{threshold}$ is the injection current minus the threshold current. Each curve exhibits an RC rolloff and marked electronic ringing due to electronic reflections at the connectors--the ringing frequencies can be matched to the cable lengths used.

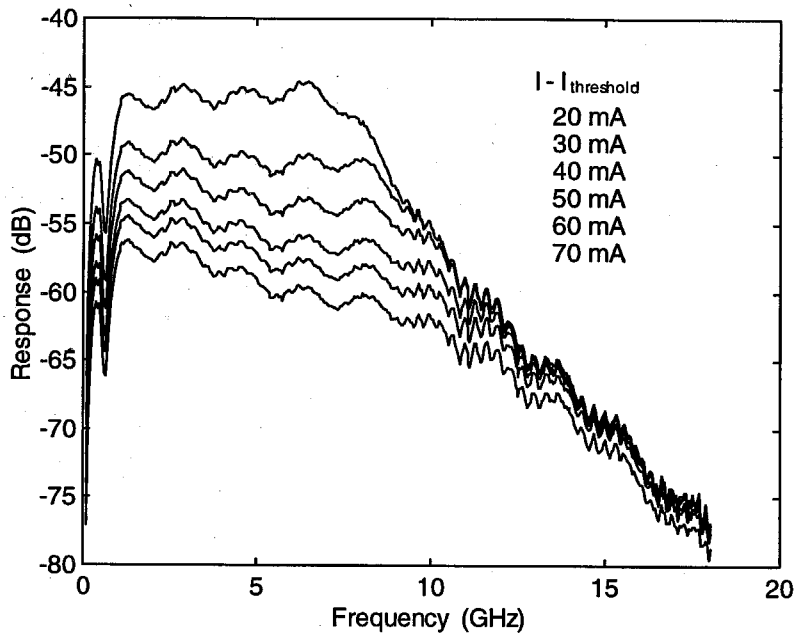

Figure 4.2. Modulation response of the laser at six different bias currents $I-I_{th}$. The largest response was for the lowest current, as indicated in the figure. The electronic ringing and parasitics are obvious.

As the bias level is increased, the bandwidth increases, but the electronic response obscures the details of the intrinsic laser response. This can be remedied by the frequency subtraction technique [28]. Each of the curves in Figure 4.2 can be subtracted from any of the others (subtracted in a dB scale, or dividing on a linear scale), which removes the common electronic response. The result is shown in Figure 4.3 for the top two curves in Figure 4.2. The solid line is a fit to the quotient of equation (2.25) for two sets of peak frequency Ω_0 and damping factor γ, with the results given in the figure caption. By pairing each bias level with each of the others, we can obtain several fit values for each bias level, giving a mean and standard deviation for each one.

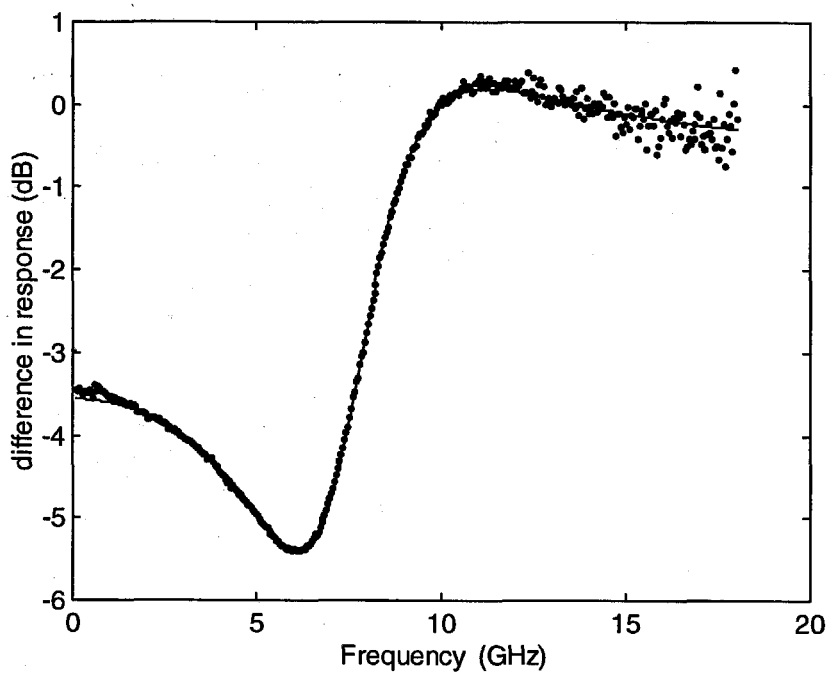

Figure 4.3. The difference of two modulation responses, removing the electronic response. The $I-I_{th} = 20$ mA line of Figure 4.2 is subtracted from the $I-I_{th} = 30$ mA line. The points are experimental data and the solid line is a fit to the theory. The fit parameters at 20 mA are $\Omega_0/2\pi = 7.2$ GHz, $\gamma/2\pi = 3.6$ GHz, and at 30 mA are $\Omega_0/2\pi = 8.5$ GHz, $\gamma/2\pi = 4.8$ GHz.

The resonant frequency increases as the square root of output power according to equation (2.28), and it is straightforward to show from the rate equations that it is also proportional to $\sqrt{I - I_{th}}$. Figure 4.4 shows the fitted resonant frequencies from the frequency subtraction pairings versus $I-I_{th}$. The coefficient of proportionality between Ω_0 and $\sqrt{I - I_{th}}$ is called the modulation efficiency factor, often quoted in GHz per $\sqrt{mA}$, and is a figure of merit for high-speed lasers.

Figure 4.4 clearly shows that Ω_0 does not keep up with $\sqrt{I - I_{th}}$, which is a result of differential gain suppression [29, 30]. This is predicted by the power dependence of A implied by the gain convention of (2.12), which is the main advantage of the choice of that convention. However, in the experience of the author and his colleagues, Ω_0 falls off even faster than this prediction, and may be due to a combination of spatial hole burning and spectral hole burning effects that do not follow the form of (2.13). A study of Ω_0 vs. P_0 might clarify how and why the differential gain A(N,P) and gain compression factor ε(N,P) depend on power and temperature.

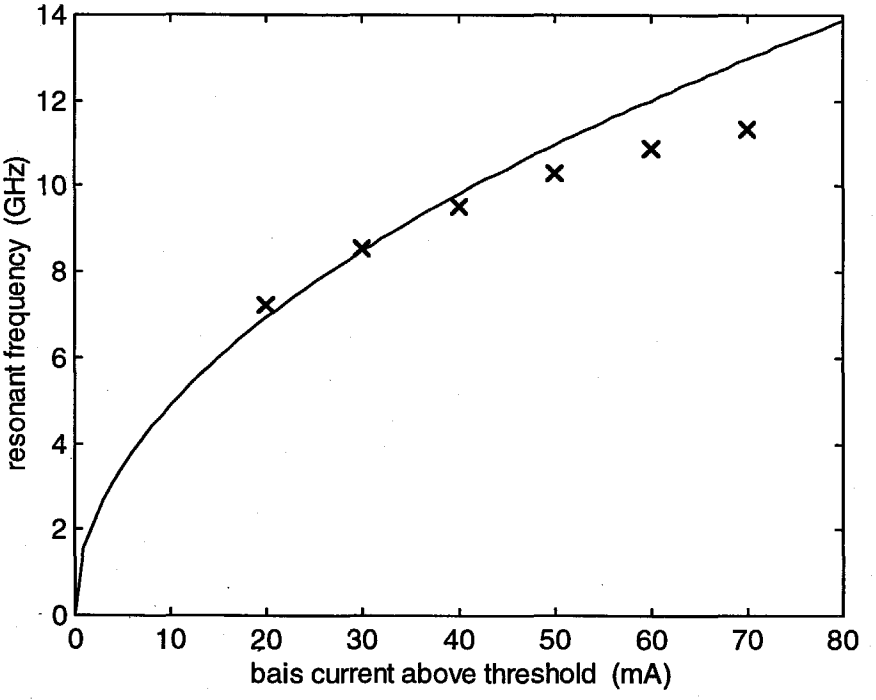

Figure 4.4. W0 vs. I-Ithreshold. The x's are for the six laser biases for Figure 4.2, and the solid line is proportional to $\sqrt{I - I_{th}}$. The decrease below the square-root dependence of equation (2.28) is due to differential gain compression.

The damping factor also increases with output power, and from (2.27) and (2.28) we can see

$$\gamma = \tau_{ph}\Omega_0^{\,2} + \frac{1}{\tau} + \frac{\varepsilon P_0}{\tau_{ph}} \tag{4.1}$$

The damping thus increases as the square of Ω_0, and as power is increased the damping eventually pulls the response down so that the 3 dB frequency occurs before the peak frequency and decreases with further increasing power. Thus the modulation bandwidth has a maximum value, determined by the slope of the γ vs. Ω_0 line, also called the K factor. Had we assumed a form for suppression of the differential gain as in (2.12), the K factor would be τ_{ph} plus some gain suppression corrections.

Figure 4.5 shows a plot of γ vs. Ω_0, showing the accuracy of the linear relationship (4.1). A low K factor means smaller damping and higher maximum bandwidth. It is a common figure of merit for lasers intended for high-speed modulation. The intercept of the linear fit shown in Figure 4.5 can in theory be used to determine $\frac{1}{\tau} + \frac{\varepsilon P_0}{\tau_{ph}}$, but in practice the uncertainty in this number (determined in turn by the standard deviation of the fit values of Ω_0 and γ) makes this an unreliable estimate.

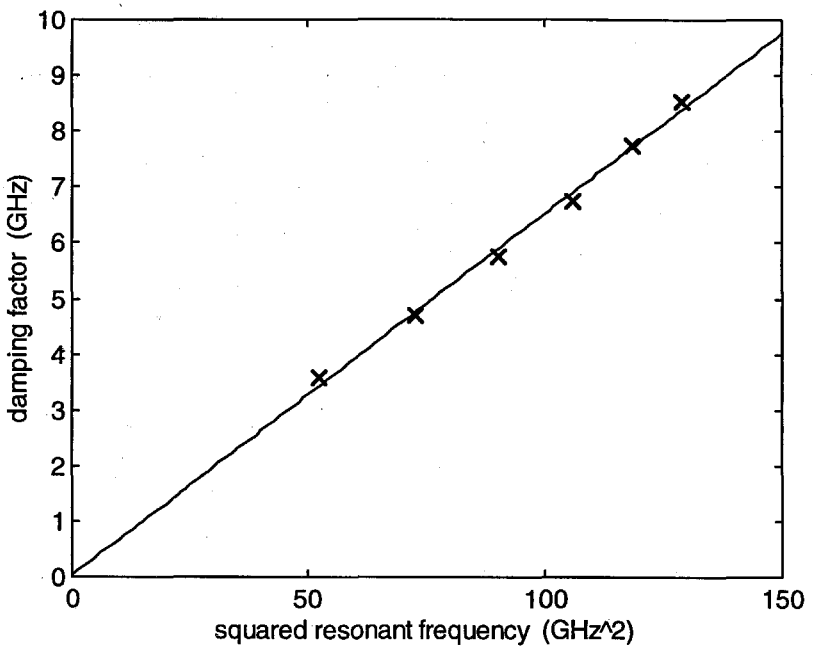

Figure 4.5. γ vs. Ω_0^2 for the six laser biases for Figure 4.6. The slope is the so-called K factor, and is a measure of the maximum 3 dB bandwidth of the laser.

Fiber transfer function

Measuring the change in modulation response due to dispersive optical fiber can let us determine other important laser parameters. Figure 4.6 shows the change in the modulation response for the 6 laser biases of Figure 4.2 due to 13.3 km of fiber (that is, the figure shows the response measured at the end of the fiber minus the response measured with no fiber). The points are experimental data and the solid lines are fits to equation (3.30). Doing this for several lasers and bias levels lets us determine the fiber

dispersion product $\beta''L$ and remove it from any single fit, leaving α and $\varepsilon P_0/\tau_{ph}$ as fit parameters [31, 32]. Results are given in the figure caption.

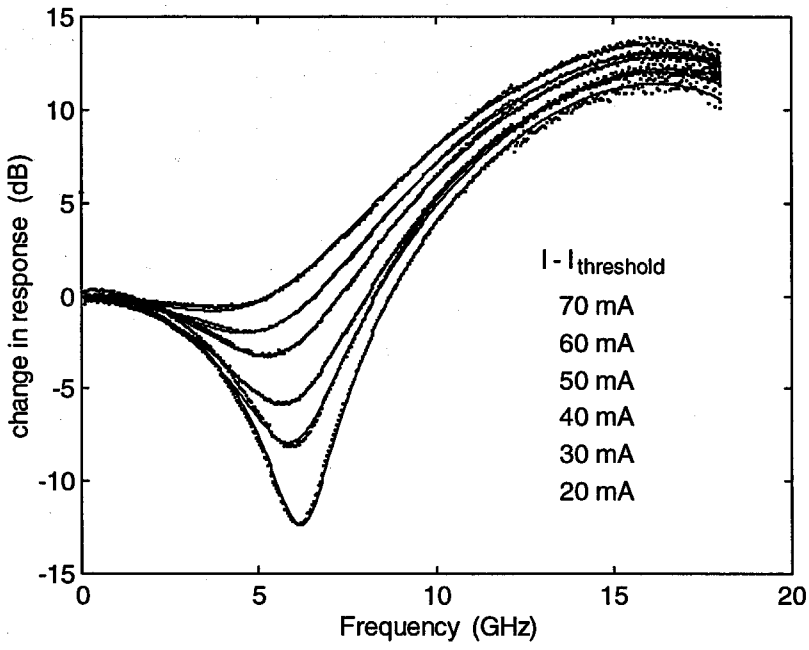

Figure 4.6. Change in modulation response due to 13.3 km of fiber, for the six different bias levels $I-I_{th}$ of Figure 4.2. The fitted α parameter from the six lines was 4.1 ± 0.3, and $\kappa/2\pi = \varepsilon P_0/\tau_{ph}2\pi$ increased very linearly with current, from 1.6 GHz at $I-I_{th} = 20$ mA, to 6.7 GHz at $I-I_{th} = 70$ mA.

The dips in the data at about 6 GHz in Figure 4.6 are caused by a zero in the transfer function for the transient chirp component [33]. As the characteristic frequency $\varepsilon P_0/\tau_{ph}$ increases with bias level, the chirp becomes more adiabatic in nature at 6 GHz, and the dip is lessened. At higher frequencies where the chirp is mostly transient, the transfer function has another dip that can be seen more clearly with longer fiber. Figure 4.7 shows the change in modulation response due to 25 km of fiber, with the same dip that depends on output power and a second dip that does not.

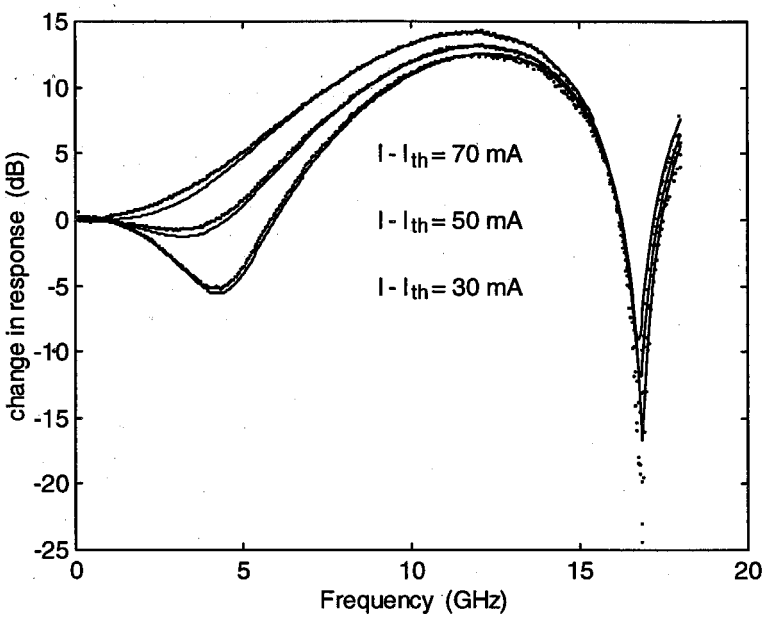

Figure 4.7. Change in modulation response due to 25 km of fiber. The dip at 17 GHz is where H(Ω) of equation (3.30) becomes zero.

4.3 Intensity noise

Measuring the laser relative intensity noise is complicated by the presence of detector thermal noise and shot noise. This means we have to calibrate for the thermal noise and shot noise at any frequency and optical power. We can do this by putting an optical attenuator between the laser and the detector and measuring noise power versus detector photocurrent for different attenuation. The laser is kept at a constant bias and the ESA is kept at a single electronic frequency, so only the attenuation of the light changes. We convert the noise power from dBm into mean squared current fluctuations and use the following relation for the mean squared value of the noise current i_N:

$$\langle i_N^2 \rangle = G(\nu)\Delta\nu\left[f_N(\nu) + 2e\langle i\rangle + [RIN]\langle i\rangle^2\right] \tag{4.2}$$

Here G(ν) is the combined electronic gain of the amplifier and the ESA, which amplifies all noise components equally, and $\Delta\nu$ is the detector bandwidth. f_N is the combined noise figure of the amplifier and detector, which is treated as a pre-amplifier noise source. The second term on the right side is the shot noise, where <i> is the mean photocurrent, and is a basic relation for shot noise [34]. The third follows from the definition of RIN in (2.46), where we've converted optical power to detector current. (Here RIN is measured not in dB but as an absolute ratio.)

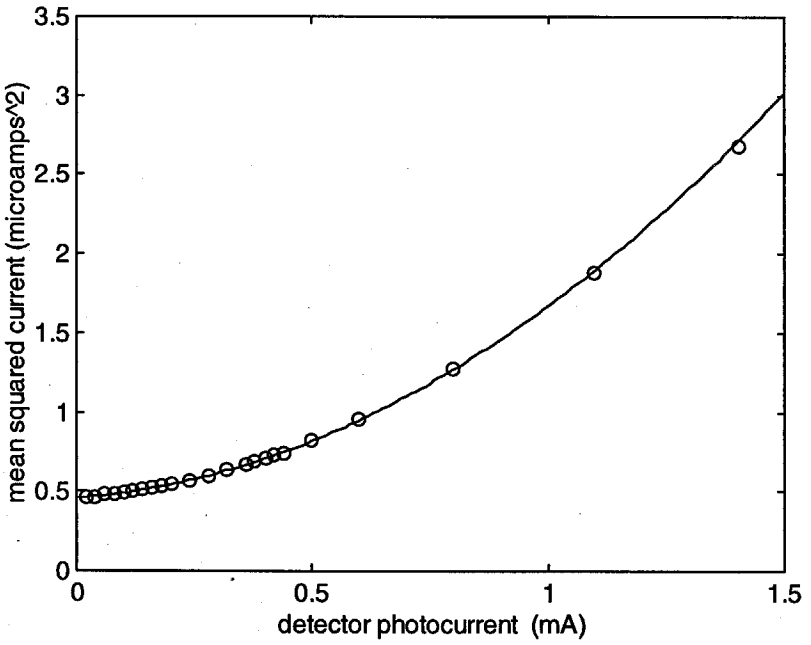

Figure 4.8. Mean squared current fluctuation (proportional to noise power) vs. detector photocurrent, at 12.75 GHz. The fit line extracts the amplifier noise (constant part), shot noise (linear part), and laser noise (quadratic part) at this frequency.

Figure 4.8 shows the result of such a measurement. From (4.2) we see that the constant part of $\langle i_N^2 \rangle$ versus $\langle i \rangle$ corresponds to the thermal noise, the linear part is the shot noise, and the quadratic part is the laser noise. The measurement and fit in Figure 4.8 is repeated as a function of frequency, and since the shot noise spectrum is white, any change in the linear coefficient with frequency must be due to the amplifier gain. Having a calibration of the noise figure and detector response at each frequency lets us extract the RIN from any subsequent measurement. For example, if we call the fitting parameters A, B, and C, as in

$$\langle i_N^2 \rangle = A\langle i \rangle^2 + B\langle i \rangle + C \tag{4.3}$$

then from (4.2),

$$\mathrm{RIN} = \frac{A}{B} 2e \tag{4.4}$$

For example, Figure 4.9 shows the total noise power in dBm versus frequency for a diode laser at a single bias level and no optical attenuation, showing several dB of electronic ringing. Using the results of the

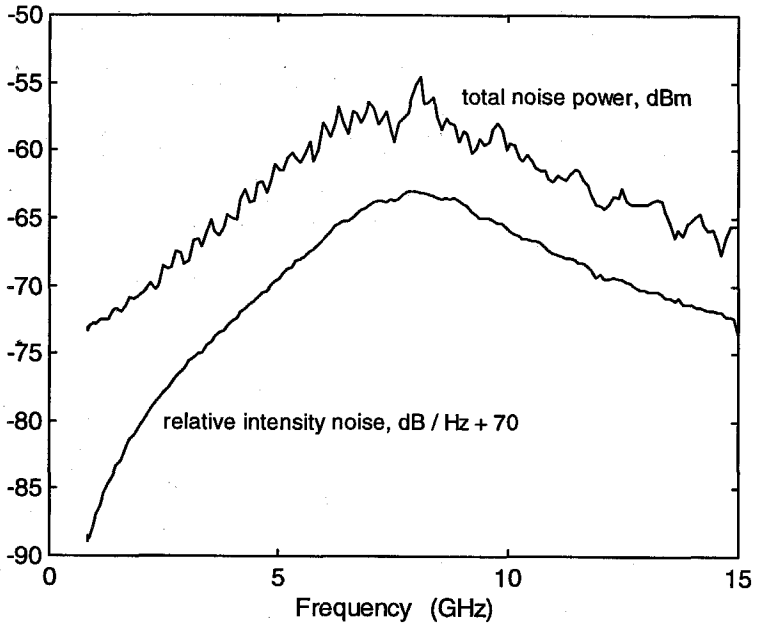

Figure 4.9. Total noise power and RIN versus frequency. Note the scales are different: noise power is measured in dBm, using a 6 MHz resolution bandwidth; and RIN is in dB/Hz, plus 70. The point is that the calibration technique removes the thermal noise and electronic response.

above calibration, we can subtract the thermal noise and shot noise at each frequency, and divide by the electronic response, leaving just the laser RIN, which is a much smoother spectrum. Note the scales are very different--the point is only that this calibration removes the electronic contributions very well and leaves a smooth RIN spectrum.

The RIN spectra measured in this way can be fit to the theory of Chapter 2. Using (2.38), (2.39), and (2.48), we get

$$\mathrm{RIN} = 10\ \log_{10}\left(8K\omega_{ST}\,\frac{\Omega^2 + 1/\tau^2}{\left(\Omega^2 - \Omega_0{}^2\right)^2 + \gamma^2\Omega^2} \right) \tag{4.5}$$

Figure 4.10 shows the measured RIN spectra of a laser at four bias currents, with the fits to (4.5). It is clear that as the bias level increases, the resonant and damping frequencies Ω_0 and γ increase, and the Schawlow-Townes linewidth decreases, as expected. The other parameter τ is fairly constant over this range.

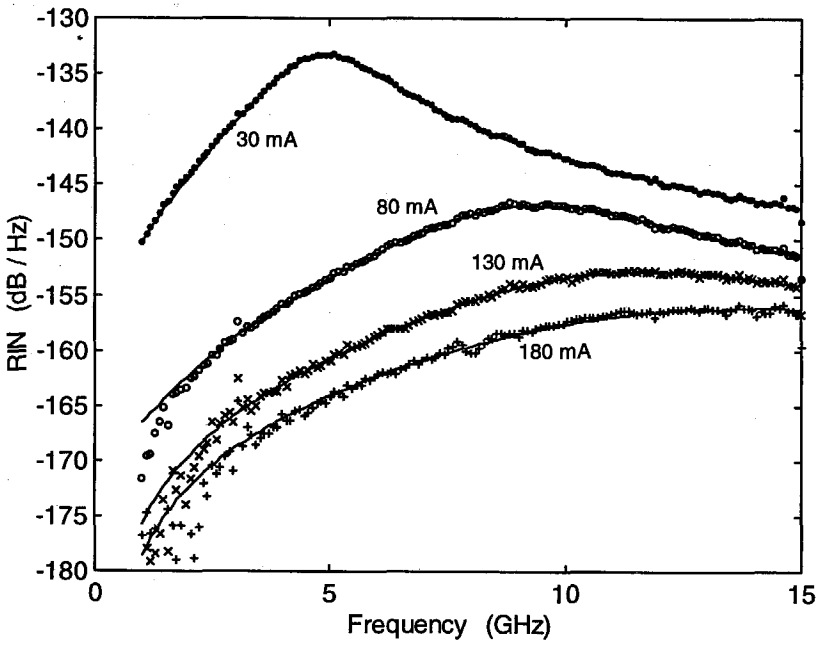

Figure 4.10. RIN spectra of a laser at four different bias currents. The points are experimental data and the lines are fits to equation (4.5).

Fiber transfer function

Finally, we can also measure the change in RIN due to some length of dispersive optical fiber. We can use the calibration coefficients A, B, and C to determine RIN after

the fiber by measuring the photocurrent $\langle i \rangle$ and noise power $\langle i_N^2 \rangle$ after the fiber, and the noise power $\langle i_{N,thermal}^2 \rangle$ with no optical source. Then from (4.2) and (4.3),

$$RIN = \frac{\left(\langle i_N^2 \rangle - \langle i_{N,thermal}^2 \rangle - B\langle i \rangle\right)2e}{B\langle i \rangle^2} \tag{4.6}$$

The results are shown in Figure 4.11 for four different fiber lengths, with fits to (3.41). This lets us measure τ_{ph} and α, providing a nice compliment to the modulation response fiber measurement. For moderate lengths of fiber, the RIN decreases at low frequencies before increasing. For fiber lengths of tens of km, the RIN can increase by 20 dB [35].

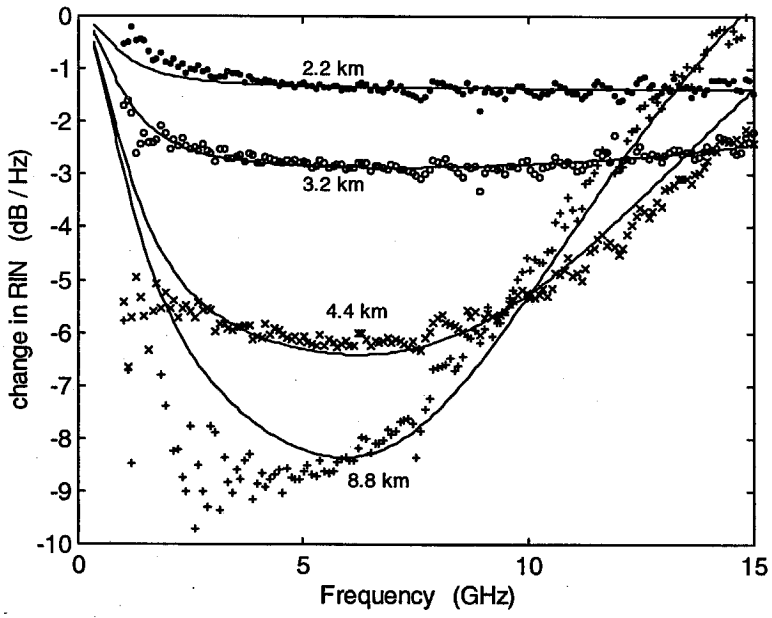

Figure 4.11. Change in RIN due to four lengths of dispersive optical fiber. The points are experimental data and the solid lines are fits to (3.41).

Chapter 5 -- Fiber Bragg Gratings

5.1 Introduction to fiber gratings

A fiber Bragg grating (FBG) is a length of optical fiber in which the refractive index has been periodically modulated, or corrugated, along the length of the fiber. The index corrugation produces a Bragg reflector, coupling forward-propagating waves into the backward-propagating mode whenever the mode wavelength is twice the grating period, analogous to Bragg diffraction of X-rays from a crystal. Typical FBGs are a few cm in length and have center reflectivities of over 99% with minimal scattering losses. FBGs act as very wavelength-sensitive filters, with bandwidths on the order of 1 Å, and have been used in place of mirrors to create entirely fiber-based Fabry-Perot interferometers and erbium-doped fiber lasers [36].

Fiber gratings are also enabling a new generation of high-speed optical communication networks, as they are key components in two of the most important advances in the field in the 1990's. The first is a technique for dispersion compensation, in which several-cm-long fiber gratings are used to recompress pulses that have been broadened by hundreds of kilometers of dispersive optical fiber [37, 38]. The second advance is in wavelength-division multiplexing (WDM), in which a single optical fiber carries several different optical signals, each at a different wavelength [39, 40]. In WDM

networks, fiber gratings usually form the key components of add-drop devices, which are responsible for adding and removing individual wavelengths from the fiber [41]. In either of these applications, as we shall see in the remaining chapters of this thesis, the optical properties of fiber gratings can have a dramatic effect on the behavior of optical signals that pass through them.

Fabrication

The formation of the refractive index corrugation is accomplished by exposing the core of a germanium-doped silica fiber to ultraviolet light. The UV light breaks chemical bonds associated with germanium defects in the crystal; when these bonds are broken, released electrons are then thought to be trapped at hole-defect sites to form color centers [42, 43], changing the absorption of the glass in the UV region and thus refractive index elsewhere. The photosensitivity of the silica can be increased by hydrogen-loading the fiber at high temperature or pressure, resulting in typical index of refraction changes of $2x10^{-3}$. The illumination is usually accomplished from the side with an eximer laser or other coherent UV source, with a transmission mask for example being used to form the periodic intensity pattern. These masks can have non-linear or "chirped" corrugation periods, and tapered or "apodized" intensity profiles. There are many fabrication techniques reported in the technical literature, using holographic masks, interferometric techniques, point-by-point exposure, and single-pulse exposure, in sum allowing for a variety of grating functions to be produced [44, 45, 46, 47, 48].

The fabrication of a grating with a specific index profile is complicated by the saturation dynamics of the index of refraction, which can cause distortion of the intended corrugation and the appearance of higher spatial harmonics. In addition, increasing the amplitude of the index corrugation will increase the average index, thereby changing the local mode wavelength and pulling the Bragg wavelength. Thus a grating whose corrugation profile is tapered, or apodized, will also have a tapered chirp, unless care is taken to maintain a uniform average index by selectively exposing parts of the grating to UV light without the periodic corrugation.

For these reasons, and despite the innovations referenced above, fabricating a mask with a given complicated index profile is still far more difficult than the analysis of said profile. As we will see below, arbitrary grating profiles are very accurately analyzed with numerical solutions to the coupled-mode differential equations. In this chapter, we'll use these equations to calculate the reflection and transmission spectra of fiber gratings, and to analyze the relationship between the phase and amplitude of these spectra.

5.2 Coupled mode equations

The most common analysis of Bragg reflectors is with coupled-mode theory, which describes the coupling of forward-going and backward-going waveguide modes by the grating. A thorough derivation of the coupled-mode differential equations is

presented clearly in [6] and other texts, and we will merely present them and their solutions.

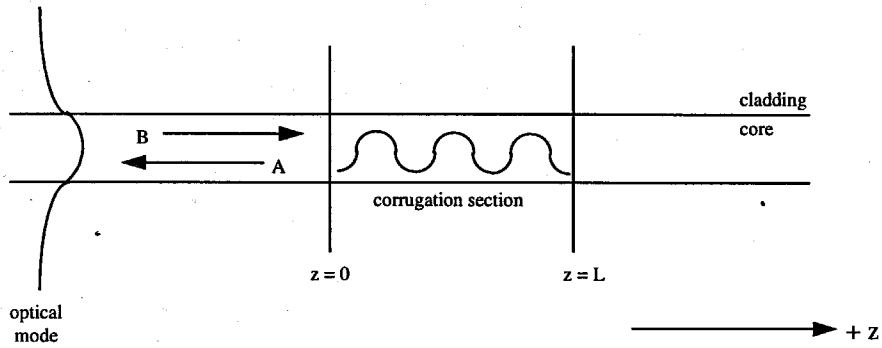

Figure 5.1. Schematic of fiber waveguide and the forward- and backward-propagating mode amplitudes B and A.

We represent the forward and backward propagating modes of the fiber, with wavevectors $\pm\beta$, by the dimensionless envelope functions B(z) and A(z), as shown in Figure 5.1. The electric field is then A or B times some constant E_0. The coupling between modes is described by the differential equations

$$\frac{dA(z)}{dz} = \kappa e^{-i2\Delta\beta z} B(z) \tag{5.1a}$$

$$\frac{dB(z)}{dz} = \kappa^* e^{+i2\Delta\beta z} A(z) \tag{5.1b}$$

where $\Delta\beta$ is the difference between the incident wavevector and the resonant wavevector,

$$\Delta\beta = \beta - \pi / \Lambda \tag{5.2}$$

and Λ is the spatial period of the corrugation. The coupling strength is given by the coupling coefficient κ,

$$\kappa = \frac{i\omega^2}{4\beta c^2}\frac{\Delta\varepsilon}{\varepsilon_0} \tag{5.3}$$

written in terms of the amplitude of the dielectric constant corrugation $\Delta\varepsilon$, or equivalently the change Δn in the fiber refractive index (for small Δn). It is imaginary here, but in general it is complex, allowing for complex $\Delta\varepsilon$, or corrugation of the loss or gain of the waveguide as in some DFB lasers. In deriving κ one only needs to assume the corrugation is slowly-varying compared to the optical wavelength. To analyze tapered gratings, κ is replaced by a position-dependent function $\kappa(z)$ which gives the local mode coupling at each point z along the grating, defined by (5.14) in terms of the local amplitude $\Delta\varepsilon_2$ of the index corrugation at that point.

Uniform gratings

If κ is indeed constant over the entire length of the grating, (5.1a,b) have an analytical solution, giving the field distributions as a function of z in terms of the initial conditions at the ends of the fiber. In the most common uses of fiber gratings in optical communication, the field incident on the grating from the "far" size is zero, A(L) = 0, and we can calculate the quantity of most interest: the electric field reflection and transmission coefficients at the grating ends:

$$r = \frac{E_{left}(0)}{E_{right}(0)} = \frac{(\kappa L)\sinh(sL)}{-i(\Delta\beta L)\sinh(sL) - (sL)\cosh(sL)} \tag{5.4}$$

$$t = \frac{E_{right}(L)}{E_{right}(0)} = \frac{-e^{-i\beta_{Bragg}L}(sL)}{-i(\Delta\beta L)\sinh(sL) - (sL)\cosh(sL)} \tag{5.5}$$

where

$$s^2 \equiv |\kappa|^2 - \Delta\beta^2 \tag{5.6}$$

and $\beta_{Bragg}=\Lambda/\pi$ is the wavevector of the Bragg-matched (on resonance) frequency.

We could add the caveat $\kappa L > \Delta\beta L$ to the above equations, because when $\Delta\beta$ increases beyond κ, s becomes imaginary. Yet equations (5.4) and (5.5) are still valid, provided we recognize $s \rightarrow i\sqrt{\Delta\beta^2 - |\kappa|^2}$ for $\Delta\beta L > \kappa L$, cosh(isL) = cos(sL), and sinh(isL) = i sin(sL). In this case the i factors cancel in the expressions for r and t and they are more clearly written

$$r = \frac{(\kappa L)\sin(|sL|)}{-i(\Delta\beta L)\sin(|sL|) - |sL|\cos(|sL|)} \qquad \Delta\beta L > \kappa L \tag{5.7}$$

$$t = \frac{-e^{-i\beta_{Bragg}L}|sL|}{-i(\Delta\beta L)\sin(|sL|) - |sL|\cos(sL)} \qquad \Delta\beta L > \kappa L \tag{5.8}$$

Here we use the complex magnitude |sL| so that the definition of s in (5.6) is still valid.

Properties

The intensity reflection and transmission coefficients are $R = |r|^2$ and $T = |t|^2$ and it is straightforward to show that R+T = 1. Figure 5.2 shows reflection spectra for three values of κL.

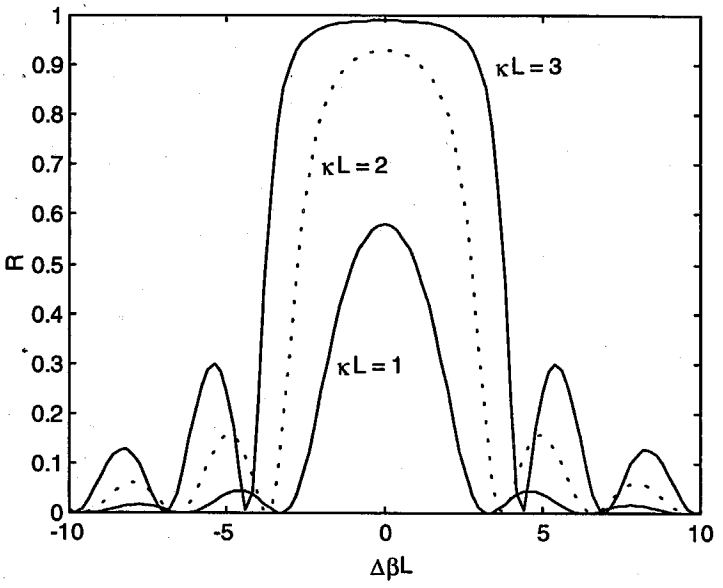

Figure 5.2. Grating reflectivity versus $\Delta\beta L$ for 3 values of κL, from coupled mode theory, using the squared magnitude of equation (5.4).

To convert $\Delta\beta L$ into wavelength or frequency, we use (5.2), which can be written in the useful form

$$\Delta\beta L = \left(\frac{\lambda_{Bragg,air}}{\lambda_{air}} - 1 \right) \pi N_{per} \tag{5.9}$$

Here L is the length of the grating, Λ is the spatial period of the grating, $N_{per} = L/\Lambda$ is the number of periods in the uniform grating, and λ_{air} is the wavelength of the light in air assuming $n_{air} = 1$.

At the Bragg condition, $\Delta\beta=0$ and R is at its largest, and the reflectivity is symmetric about the Bragg wavelength. The strength of the grating is specified by κL, and in fact the functions $r(\Delta\beta L)$ and $t(\Delta\beta L)$ are uniquely determined by κL. As κL is increased, the grating becomes stronger and wider, as Figure 5.2 shows. The reflection

sidelobes on either side of the reflection band are common and usually undesired. They increase in size and number as κL increases. Figure 5.3 shows an experimentally measured transmission spectra for a strong wideband grating, showing several clearly discernible sidelobes.

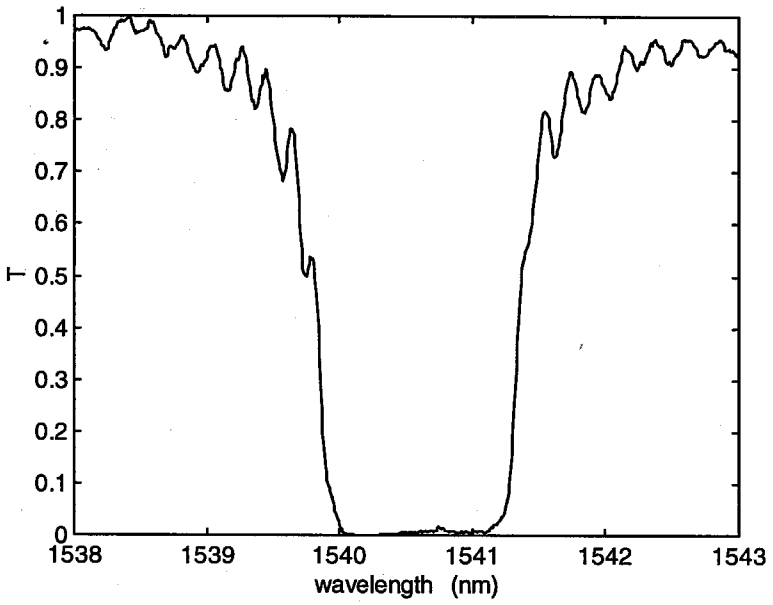

Figure 5.3. Measured reflection spectrum of a strong, wideband grating showing several pronounced reflection sidebands.

Two gratings with different lengths but the same coupling-length product κL will have the same spectra when plotted versus $\Delta\beta L$, but different widths when plotted versus wavelength. The more periods a grating has, the more narrow the grating bandwidth will be, as can be deduced from (5.9). So the length of the grating determines the wavelength or frequency difference corresponding to a given $\Delta\beta L$. As remarked above, s becomes imaginary when $|\Delta\beta L| > \kappa L$ and the fields propagate through the grating instead of being

reflected. This sets the width of the reflection band--using (5.9) we can deduce the forbidden gap width

$$\Delta\lambda_{gap} = \frac{\kappa\lambda_{air}^{\ 2}}{\pi n_{mode}} \qquad \text{or} \qquad \Delta\omega_{gap} = \frac{2\kappa c}{n_{mode}} \tag{5.10}$$

where $n_{mode}=\beta_{Bragg}\lambda_{air}/2\pi$ is the effective index of refraction of the guided mode.

Phase spectra

The phase of the reflectance and transmittance are defined by $r \equiv |r|e^{i\phi_r}$ and $t \equiv |t|e^{i\phi_t}$ and give the time phase, or lag, of the reflected and transmitted wave. Using (5.4) and (5.5),

$$\phi_r = \tan^{-1}\left[\frac{\mathrm{Im}(r)}{\mathrm{Re}(r)}\right] = \tan^{-1}\left[-\frac{\Delta\beta L\sinh(sL)}{(sL)\cosh(sL)}\right] \qquad \Delta\beta L < \kappa L \tag{5.11}$$

$$\phi_t = \tan^{-1}\left[\frac{\mathrm{Im}(t)}{\mathrm{Re}(t)}\right] = -\beta_{Bragg}L + \tan^{-1}\left[-\frac{\Delta\beta L\sinh(sL)}{(sL)\cosh(sL)}\right] \qquad \Delta\beta L < \kappa L \tag{5.12}$$

with similar expressions using sin and cos instead of sinh and cosh for $\Delta\beta L > \kappa L$.

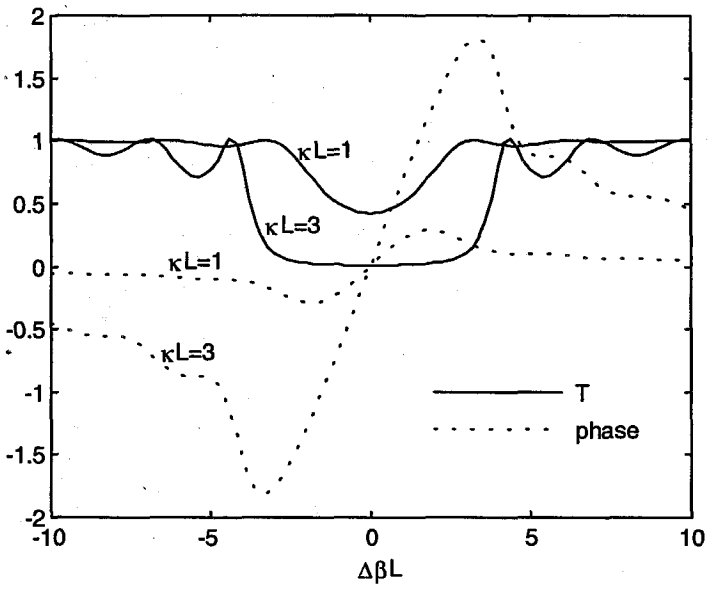

Figure 5.4. Grating transmission (squared magnitude) and phase, versus $\Delta\beta L$ for 2 values of κL, from coupled mode theory, using (5.5).

The transmitted phase appears identical to the reflected phase except for the additive factor of $-\beta_{Bragg}L$, which is exactly the phase accumulated by an on-resonance wave traveling to the right through the length of the grating. However, (5.11) and (5.12) suffer the ambiguity of the arctangent function having a range of $-\pi/2$ to $\pi/2$. To illustrate this point, imagine that a complex number z with phase ϕ_z is multiplied by -1. Both the imaginary and real parts of z change sign, and thus their quotient doesn't, so according to the prescription used in (5.11) and (5.12), the phase of -z is still ϕ_z. Clearly, though, multiplying z by -1 should change its phase by π. With the arctangent function, this change of π gets mapped back into the range $-\pi/2 < \phi_z < \pi/2$. A phase change of π is physically significant but will not be manifest with this method. It is better instead to use

the function arg(z), available on many numerical computing programs, which has a range of $-\pi$ to π, and only physically-insignificant changes of 2π get mapped away.

In light of this, the difference in sign between the numerators of r and t in (5.4) and (5.5) show that ϕ_r and ϕ_t actually differ by $-\beta_{Bragg}L + \pi$. Or, ignoring the phase accumulated in traversing the grating, the transmitted and reflected waves are exactly out of phase at any frequency. Figure 5.4 shows the phase of the transmittance for two values of κL. The phase of r or t becomes more perturbed by the grating as κL increases.

The fact that the phase of the transmitted and reflected waves is not linear with frequency means that the grating has a group velocity dispersion. The second derivative of the phase $\phi'' = d^2\phi/d\omega^2$ plays the role that $\beta''L$ plays in dispersive fiber. Some of the literature uses these analytical expressions to analyze the potential for using gratings for dispersion compensation [52], but for the majority of gratings the phase $\phi(\omega)$ is sufficiently non-quadratic over the bandwidth of interest that using only ϕ'' is a poor approximation. The exception is for wide reflection bandwidth chirped gratings used in reflection, in which case $\phi_r''(\omega)$ is approximately quadratic in the center of the reflection band.

5.3 Numerical solutions

The analytic coupled-mode solutions in the previous section assumed the coupling strength is uniform from z = 0 to z = L. This is not only unrealistic for fiber gratings, it is

often undesirable. By apodizing the corrugation we can eliminate the sidelobes that appear in the spectrum of a uniform grating. In addition, we can broaden the bandwidth of a grating with fixed κ and L by chirping the period of the corrugation. A numerical solution to the coupled-mode equations is required to analyze these effects.

Apodization

Returning to (5.1) we wish to let the coupling strength be a function of position along the grating. We define a dimensionless length variable $x \equiv z/L$, so the grating extends from x = 0 to x = 1, and a dimensionless coupling strength $\xi \equiv \kappa L$, to obtain

$$\frac{dA(x)}{dx} = \xi(x)e^{-i2(\Delta\beta L)x}B(x) \tag{5.13a}$$

$$\frac{dB(x)}{dx} = \xi(x) * e^{+i2(\Delta\beta L)x}A(x) \tag{5.13b}$$

The detuning factor $\Delta\beta L$ now appears as a constant in the exponential. We can define $\xi(x)$ to be any smooth function and integrate these equations numerically from $x = 0 \rightarrow 1$, then use r = A(0)/B(0) and t = B(1)/B(0). To compare the effect of the apodization with the uniform grating, we should make sure that the integrated coupling strengths are the same,

$$\int_0^1 \xi(x)dx = \kappa L \tag{5.14}$$

In addition, we should require that the length of the corrugation section stays the same--if, for example, we let $\xi(x)$ be a Gaussian centered at $x = 1/2$ with a width of $\sigma = 0.1$, the grating has an effective length of $2\sigma = .2$ instead of 1. We would calculate a wider reflection band because of this, which has nothing to do with the apodization.

Figure 5.5 shows corrugation profiles $\xi(x)$ for four different gratings. In each case the integrated coupling strength (5.14) is a constant $\kappa L = 2.0$. In addition, the grating length, defined by the full-width at half-maximum (FWHM) of $\xi(x)$, is 1 for each grating. Note that gratings (c) and (d) extend beyond $x = [0,1]$. Here the equations (5.13) have been integrated along the full length of the function $\xi(x)$, but the definition of L is still from $x = 0$ to $x = 1$. In other words, gratings (c) and (d) are physically longer from end-to-end but do not have a longer FWHM of the apodization profile.

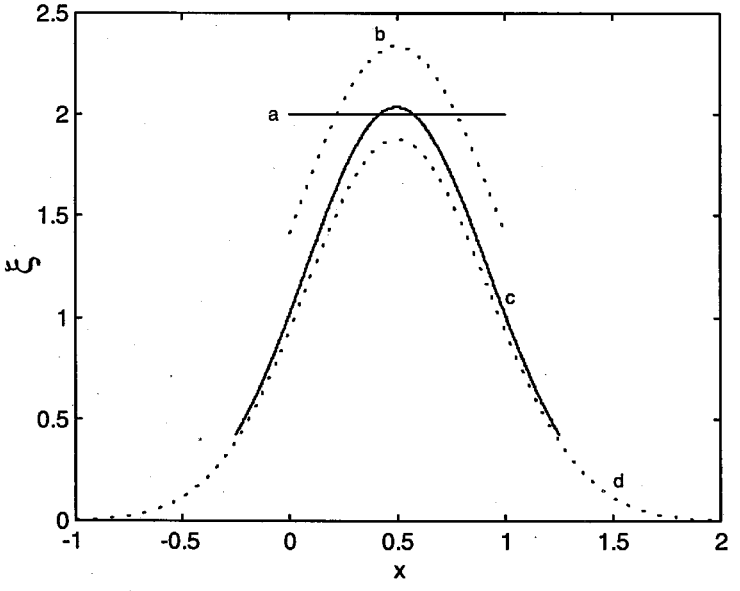

Figure 5.5. Coupling strength profiles $\xi(x)$ for four different gratings. Each grating has an integrated coupling strength of κL=2.0 and a FWHM length of $\Delta x = 1$.

Figure 5.6 shows the resulting reflection spectra of these apodized gratings. To plot R versus wavelength in air, we use (5.9) and assume $\lambda_{Bragg} = 1540$ nm and the number of corrugation periods from x = 0 to x = 1 is $N_{per} = 18{,}000$. (If $n_{mode} = 1.5$ this corresponds to a grating length of 9.2 mm per unit of x in Figure 5.5.) We see that the width of the reflection band varies somewhat between the gratings, but the major effect of the apodization is to reduce the size of the reflection sidelobes and smooth the spectrum. Grating (d), with a Gaussian apodization profile three times longer than the FWHM length, has no discernible sidelobes.

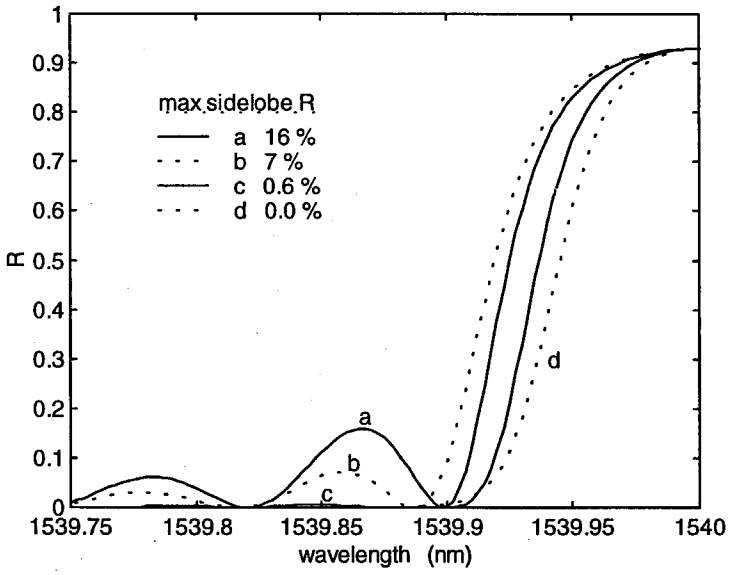

Figure 5.6. Reflection spectra for the four gratings of Figure 5.5. The height of the first reflection sidelobe is listed, showing the effect of apodization.

Chirp

Now suppose we desire to chirp the spatial period of the corrugation. We let the corrugation period Λ be a function of x, through the parameter $\Delta\beta L = (\beta - \beta_0)L$ where $\beta_0 = \pi/\Lambda$ is the Bragg-matched wavevector. Suppose β_0 varies linearly along the grating (assuming the total variation is small, this means Λ is also linear). We write $\beta_0 = \beta_0 + \beta_0' x$, and equations (5.13) become

$$\frac{dA(x)}{dx} = \xi(x)e^{-i2(\Delta\beta L)x}e^{+i2(\beta_0'L)x^2}B(x) \tag{5.15a}$$

$$\frac{dB(x)}{dx} = \xi(x)^* e^{+i2(\Delta\beta L)x}e^{-i2(\beta_0'L)x^2}A(x) \tag{5.15b}$$

which retains the same form as (5.13a,b) with the substitution

$$\xi(x) \rightarrow \xi(x)e^{i2(\beta_0'L)x^2} \tag{5.16}$$

We see that a linear grating chirp can be treated by adding a quadratic complex phase to $\xi(x)$. For a grating with the usual length $\Delta x = 1$, we can show with (5.9) that the parameter $(\beta_0'L)$ is related to the total change along the grating of the local Bragg wavelength $\delta\lambda_{Bragg,air}$ by

$$\beta_0' L = \pi N_{per}\frac{\delta\lambda_{Bragg,air}}{\lambda_{Bragg,air}} = \pi N_{per}\frac{\delta\Lambda}{\Lambda} \tag{5.17}$$

The dimensionless grating profile becomes

$$\xi(x) \rightarrow \xi(x)e^{i2\pi N_{per}f} \tag{5.18}$$

where $f = \delta\lambda_{Bragg,air}/\lambda_{Bragg,air} = \delta\Lambda/\Lambda$ is the fractional change from end-to-end of the local Bragg wavelength or the local corrugation period (assuming $f<<1$). Here N_{per} is the unchirped number, i.e., the number of periods that would be in the grating if $f = 0$.

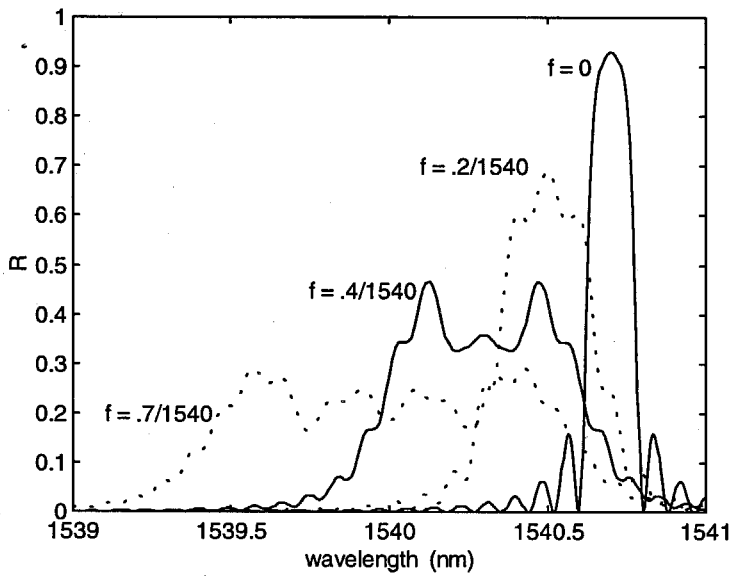

Figure 5.7. Reflection spectra of chirped gratings. The coupling strength magnitude $|\xi(x)|$ is the same for all four, equal to that of the unapodized line (a) in Figures 5.5 and 5.6. They differ by the amount of grating chirp f.

Figure 5.7 shows the effect of chirping the grating. Note that the center wavelength is shifted and the grating is widened, both by approximately $\delta\lambda = f\,\lambda_{Bragg}$. The grating sidebands have also been accentuated to produce a sizable ripple in the grating spectrum, which is undesirable. This does not occur with well apodized gratings: Figure 5.8 shows reflection spectra for the same four chirped gratings, but with the apodization profiles of lines (c) and (d) in Figures 5.5 and 5.6. We see that apodization

smoothes the spectral features of a chirped grating just as effectively as it does an unchirped grating. The figure below illustrates the effect of chirping most clearly--shifting the central wavelength and broadening the bandwidth.

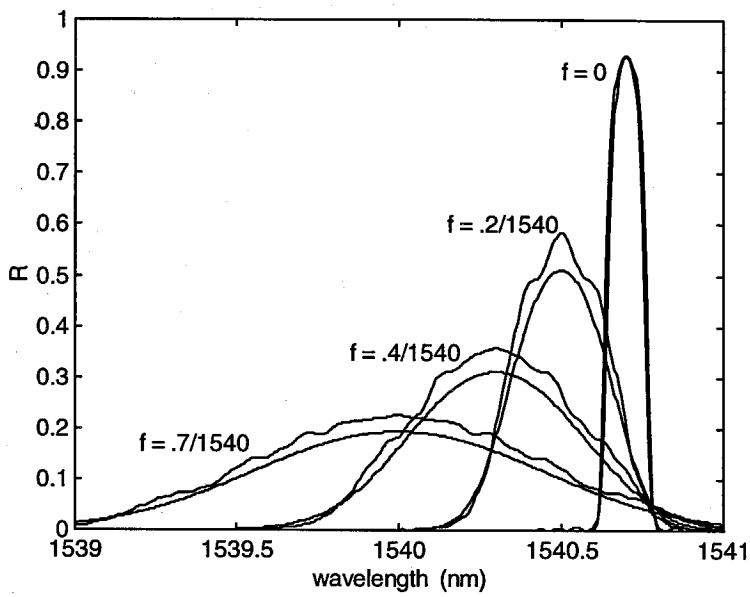

Figure 5.8. Reflection spectra for apodized gratings with different amounts of chirp. For each value of f, two apodizations profiles $|\xi(x)|$ are displayed, corresponding to lines (c) and (d) in Figures 5.5 and 5.6.

The spectra calculated so far have all been symmetric about the peak wavelength, and this is generally true for symmetric grating profiles. It is also true for gratings with chirp but no apodization, or apodization but no chirp. Figure 5.9 shows an example of an asymmetric spectrum, obtained by apodizing only one end of a chirped grating. Lossy chirped gratings will also have asymmetric spectra.

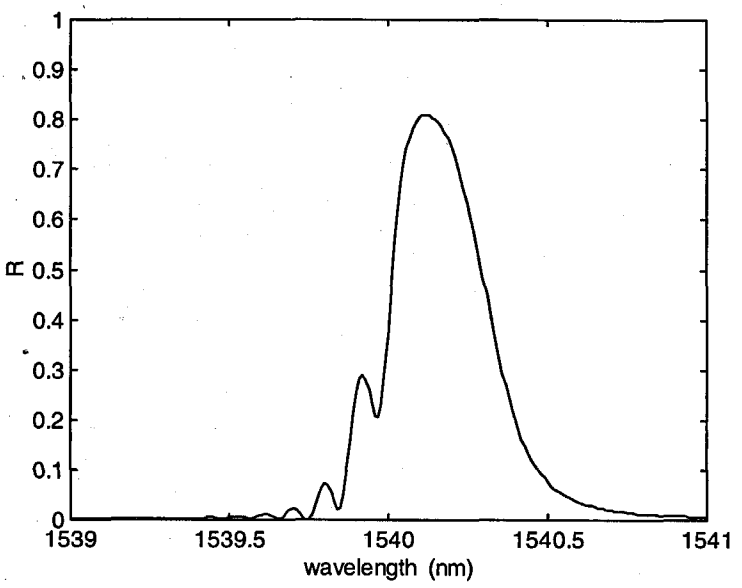

Figure 5.9. Example of an asymmetric reflection spectra. This was formed by apodizing only the long-period side of a uniformly chirped grating, leaving the short-period side of the grating unapodized.

Apodization and chirp provide two valuable tools in constructing gratings for fiber optic applications. The absence of sidelobes makes the optical filtering much more controllable, predictable, and less sensitive to small changes in wavelength. Chirping of the period lets us increase the grating bandwidth beyond the limitations placed by finite mask lengths and refractive index saturation.

Appendix B lists numerical routines, written in Matlab, for solving the coupled mode equations (5.15a,b) for gratings with an arbitrary apodization and chirp.

Finally, we remark that real gratings often have spectra that differ remarkably from anything calculated by coupled-mode equations. They may show imperfections, asymmetries, and peaks and dips of unknown origin. If the exact coupling strength

function $\xi(x)$ were known, the coupled mode equations would presumably give an accurate prediction, but it is very difficult to know the phase of $\xi(x)$ and even the magnitude $|\xi(x)|$ can be uncertain without good control of the UV exposure process. In applications where only the magnitude of the spectrum, $R(\omega)$ or $T(\omega)$, is important, we can simply measure it and not worry about the coupled-mode equations. But as we will see in Chapters 6 and 7, the phase of the spectrum, $\phi_r(\omega)$ or $\phi_t(\omega)$, which is very difficult to measure directly, can have a major influence on the properties of the reflected or transmitted signal. The obvious example is in dispersion compensation applications, in which it is hoped that $\phi_r(\omega)$ is quadratic with ω and opposite to the quadratic phase accumulated by a signal in traversing dispersive fiber. Coupled mode equations allow us to calculate this phase given $\xi(x)$, but unfortunately they cannot be "inverted" to let us deduce $\xi(x)$ from the measured $R(\omega)$ or $T(\omega)$.

One solution is to use the coupled-mode equations assuming a linear chirp and a Gaussian apodization, with the chirp parameter f and the apodization FWHM length chosen so that the calculated $T(\omega)$ roughly matches the observed spectral width and sidelobe heights. Then the calculated phase $\phi_t(\omega)$ will hopefully match the real phase spectrum. A better solution is the subject of the next section.

5.4 Kramers-Kronig relationships

In this section we show that the phase and magnitude of a grating spectrum can be related via Kramers-Kronig relations. The mathematical basis for this is the Titchmarsh theorem, which describes when the relations hold [53, 54]. Here we discuss only the condition (5.19) below and refer the reader to the references to see that the other requirements hold for grating reflection and transmission spectra.

Our theorem is as follows: if a complex-valued function $f(\omega) \equiv f_r(\omega) + i\, f_i(\omega)$ of frequency ω is square-integrable over the ω axis, that is,

$$\int_0^\infty |f(\omega)|^2 \, d\omega = K, \qquad K \text{ finite} \tag{5.19}$$

then the real and imaginary parts of $f(\omega)$ satisfy the following relations:

$$f_r(\omega) = \frac{2}{\pi} P \int_0^\infty \frac{\omega' f_i(\omega')}{\omega^2 - \omega'^2} d\omega' \tag{5.20a}$$

$$f_i(\omega) = -\frac{2\omega}{\pi} P \int_0^\infty \frac{f_r(\omega')}{\omega^2 - \omega'^2} d\omega' \tag{5.20b}$$

Here the P in front of the integral denotes the principal value. These relations tell us that the imaginary part of the grating reflection coefficient $r_i(\omega)$ at any frequency ω can be written as an integral of the real part $r_r(\omega')$ over all frequencies ω'.

Reflectance

A very important caveat is (5.19), which, if we let f(ω) be the reflectivity r(ω), requires that R(ω) be integrable. Fortunately this is true--R(ω) is bound from 0 to 1 and thus has no singularities, and the large-frequency behavior can be gotten from an expansion of (5.7),

$$|r|^2 \xrightarrow[\Delta\beta L\to\infty]{} |\kappa L|^2 \frac{\sin^2(\Delta\beta L)}{(\Delta\beta L)^2} \tag{5.21}$$

Thus R(ω) becomes likes a sinc(ω) function, tending to zero as $1/\Delta\omega^2$, and the integral (5.19) converges. We can therefore calculate the real part of r from its imaginary part or vice versa. Unfortunately the relations are not very useful, since knowledge of the real or imaginary part of r(ω) requires knowledge of the phase. For transmittance the situation is more favorable.

Transmittance

Expanding (5.8) for large ΔβL shows that T approaches 1 for large Δω. The integral of T(ω) does not converge to a finite value and we cannot apply (5.20) on t(ω) directly. However, note that since $t(\omega) = |t(\omega)|e^{i\phi_t(\omega)}$, we have

$$\ln(t(\omega)) = \ln|t(\omega)| + i\phi_t(\omega) \tag{5.22}$$

At large $\Delta\beta L$, the real part $\ln|t(\omega)|$ goes to zero and by itself it is square-integrable, which follows from the fact that $R(\omega)$ goes to zero as $1/\Delta\omega^2$, $T = 1 - R$, and $\ln\left(\sqrt{1-R}\right) \to 1 - R/2$ for small R. However, the imaginary part $i\phi_t(\omega)$ becomes linear--expanding (5.12) for large $\Delta\beta L$ we get

$$\phi_t \xrightarrow[\Delta\beta L \to \infty]{} -\beta_{Bragg} L - \Delta\beta L = -\beta L \tag{5.23}$$

This is exactly the phase accumulated by a wave in propagating a length L of fiber, and this makes sense--far from resonance the corrugation has no effect on the wave and the light propagates through the grating unaffected. This phase does not affect the signal other than to produce the expected time delay $n_{mode}L/c$, and we can factor it out of the transmittance (for example, by defining $t(\omega) = t_{new}(\omega)\, e^{-i\beta L}$ and working only with $t_{new}(\omega)$ hereafter). Ignoring this linear part, the asymptotic behavior of $\phi_t(\omega)$ is determined by the factors $|sL| \to \sqrt{(\Delta\beta L)^2 - |kL|^2}$ in (5.12), and it is only a matter of algebra to show $\phi_t(\omega)$ is also square-integrable. We can thus apply (5.20) to $\ln(t(\omega))$, getting

$$\phi_t(\omega) = -\frac{2\omega}{\pi} P\int_0^\infty \frac{\ln\left(\sqrt{T(\omega')}\right)}{\omega^2 - \omega'^2} d\omega' \tag{5.24}$$

where we have used $\sqrt{T} = |t|$. This very important result tells us that we can calculate the phase spectrum of the transmittance at any frequency by measuring the transmission spectrum $T(\omega)$ and performing a numerical integral. (This cannot be done for the reflectance, as $\ln|R|$ becomes infinite.) The limits of integration are $0 \to \infty$, but in practice

it suffices to measure $T(\omega)$ out to frequencies away from the resonance, and assume T=1 beyond that.

This integral can be performed numerically on any $T(\omega)$ spectrum. If $T(\omega)$ has a constant value T over an interval (ω_a,ω_b), the contribution to (5.24) from that interval is

$$-\frac{2\omega}{\pi}\mathrm{P}\int_{\omega_a}^{\omega_b}\frac{\ln\left(\sqrt{T}\right)}{\omega^2-\omega'^2}d\omega' = \frac{\ln\left(\sqrt{T}\right)}{\pi}\ln\left|\frac{(\omega_b-\omega)(\omega_a+\omega)}{(\omega_a-\omega)(\omega_b+\omega)}\right| \tag{5.25}$$

This result holds whether or not the singular point ω is in the interval, by virtue of the principal value on the left and the absolute value on the right. By splitting the spectrum $T(\omega)$ into many regions, each small enough that T is approximately constant, and adding up the contributions (5.25) from each, the calculation can be made very accurate. Appendix C lists a numerical routine for doing this calculation.

Figure 5.10 shows the transmission spectrum $T(\omega)$ of the grating shown in Figure 5.9, with the phase of the transmittance obtained from the coupled-mode solution, and as calculated from the transform (5.24) performed on an array of $T(\omega)$ values. The slight difference between the two phase spectra is due to the limited number of integration points used (201 across the width of the figure) and the numerical result approaches the exact phase as the number of points is increased.

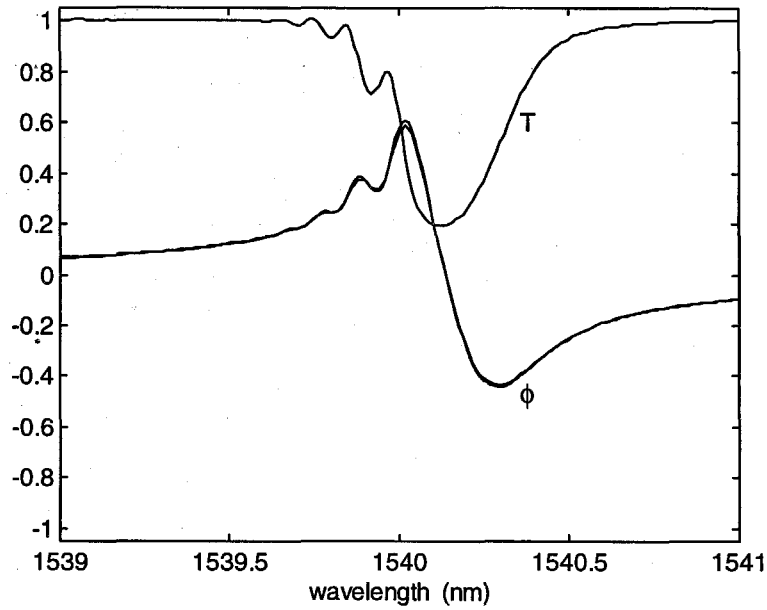

Figure 5.10. The transmitted phase of a chirped, apodized grating. The phase ϕ_t is obtained from both the coupled mode solutions and a Kramers-Kronig integral using 201 points of T.

As T→0 the logarithm becomes large and negative and can have a large effect in the phase spectra. When the transmitted optical power falls below the sensitivity of the optical spectrum analyzer used in the measurement, the T values become noisy and fluctuate between 10^{-2} and 10^{-4}. This causes noise in phase spectrum, as seen in Figure 5.11. If we smooth the measured T when it falls below the detectable limit, the resulting Kramers-Kronig phase spectrum is smoothed.

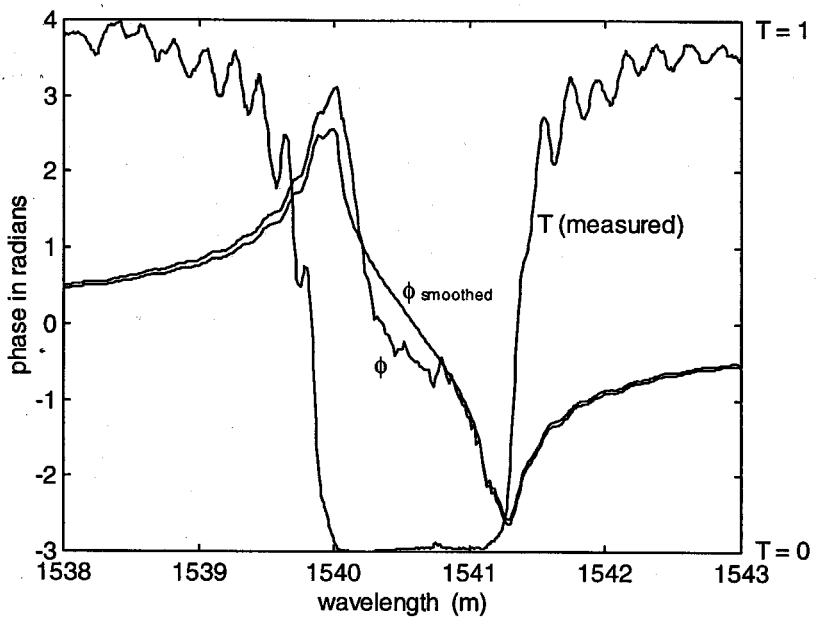

Figure 5.11. Phase calculated from Kramers-Kronig transform on measured T of strong grating. The jagged line ϕ results from the noise in T at low transmitted power. By smoothing T below the detectable limit (from 1540.1 nm to 1540.2 nm) the calculated phase spectrum is smoothed.

Chapter 6 -- Modulation Response Improvement with Fiber Gratings

We saw in Chapter 3 that propagation of a directly modulated laser signal through dispersive fiber will change the modulation response of the laser-fiber system. The change in the AM signal results from the laser frequency modulation (FM), attendant on the AM as a consequence of chirp, being converted into AM and vice versa by dispersive propagation. Recently, Eggleton et al. [58] demonstrated dispersion compensation with an unchirped fiber Bragg grating in transmission. In this chapter, we unite the topics of previous chapters by showing that a fiber grating can convert laser FM into AM, thereby increasing the magnitude of the AM signal. When combined with a dispersive fiber, the grating increases the signal, flattens the frequency response, and increases the system bandwidth, providing a frequency-domain demonstration of dispersion compensation in transmission through an unchirped grating. The frequency-domain analysis of the laser signal, the dispersive fiber, and the fiber grating presented in Chapter 3 accurately predicts the observed results, and allows us to deconstruct the effect into its constituent phenomena.

6.1 Experimental Measurement

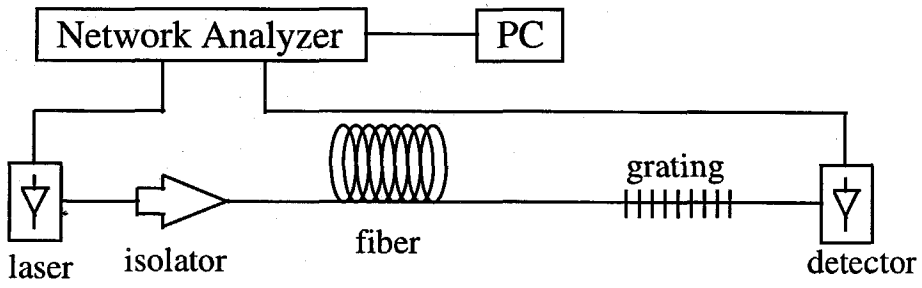

Figure 6.1. Experimental setup used to measure the frequency response of the laser/fiber/grating system.

The experiment consisted of directly current modulating a 1.54 μm commercial (ORTEL Corp.) distributed feedback semiconductor laser at frequencies up to 25 GHz, with the output sent through an optical isolator and into a fiber pigtail (Figure 6.1). After propagation through various lengths of single-mode non-dispersion-shifted fiber and/or an unchirped fiber grating, the signal was detected with a high-speed photodiode and fed to an electronic network analyzer. By comparing the system response to that of the stand-alone laser, we determined the change in the response due solely to the fiber and/or the grating. The laser wavelength was temperature-tuned and stabilized on the short-wavelength side of the grating reflection band.

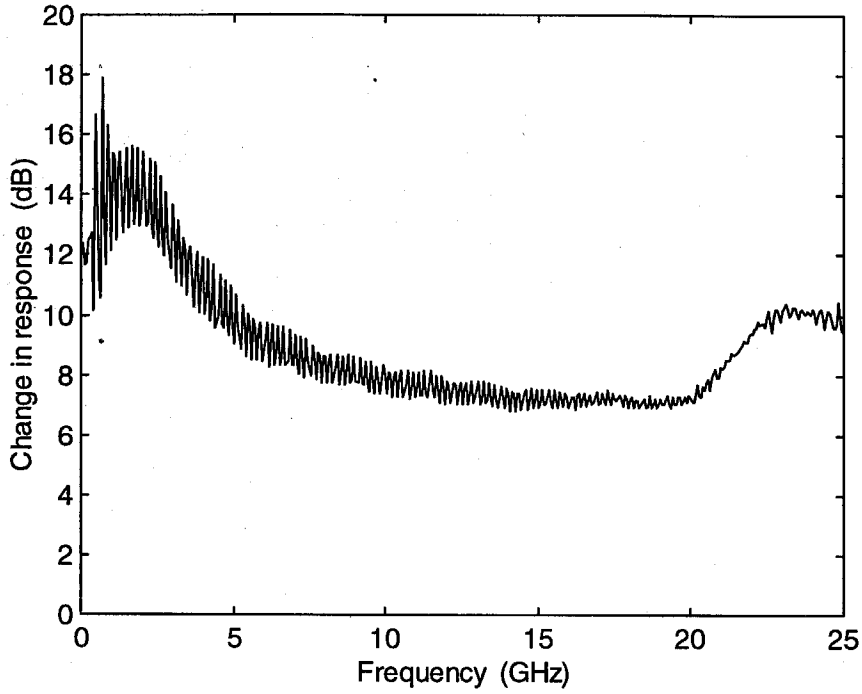

Figure 6.2. Change in modulation response caused by a fiber grating. The signal is increased by 7 to 14 dB at all frequencies.

Transmission through the fiber grating increased the laser modulation response by over 7 dB at all frequencies up to 25 GHz, with a maximum value of 14 dB at low frequencies (Figure 6.2). The optical intensity transmission of the grating was 38% at this wavelength, so that the RF signal increase took place in spite of a drop, by 62%, in the average received optical power. When the laser output was sent through 25 km of fiber alone (Figure 6.3, "25 km fiber"), the AM system response was increased at some frequencies, and decreased at others, a consequence of fiber dispersion. The addition of the grating at the end of the fiber produced an increased signal at low frequencies and a smoothing of the first large "bump" (Figure 6.3, "fiber + grating"). The system

bandwidth was effectively increased too, as the first dip in the system response occurred near 23 GHz, as opposed to 18 GHz without the grating. The small amplitude oscillations, or ringing, in Figure 6.2 at low frequencies was attributed to reflections between the fiber grating and the laser isolator. When the grating in Figure 6.3 was placed ahead of the fiber rather than at its end, the oscillations likewise appeared, but the response was otherwise unchanged. Similar results were obtained with a second grating that had a larger bandwidth. An AM signal increase between 3.5 dB and 7 dB at all frequencies up to 25 GHz was observed. Both gratings were commercially purchased (Bragg Photonics, Inc.) and neither was designed for this experiment.

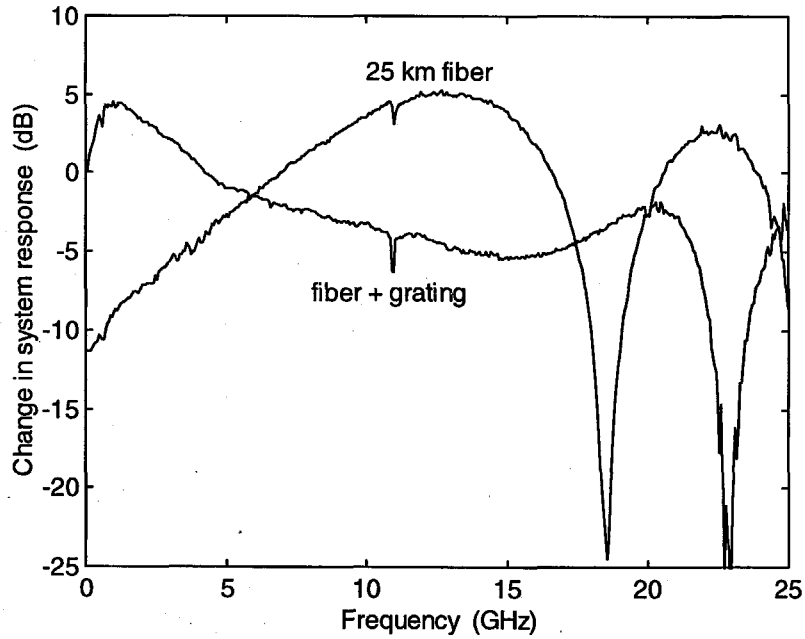

Figure 6.3. Change in system response after 25 km of fiber, with and without the grating.

6.2 Numerical Prediction

The changes in the modulation response of the system produced by the grating can be predicted by the Fourier domain technique of Chapter 3, provided we know the form of the grating's optical transmittance function t(ω). Unfortunately, the grating used in Figures 6.2 and 6.3 was damaged before it could be characterized, but the results from the second grating mentioned above are compelling. Figures 6.4 through 6.6 show the change in the AM response caused by this second grating, with no fiber, 25 km of fiber, and 50 km of fiber. We will compare these results to the Fourier-domain prediction and then extract some physical insight about the phenomenon.

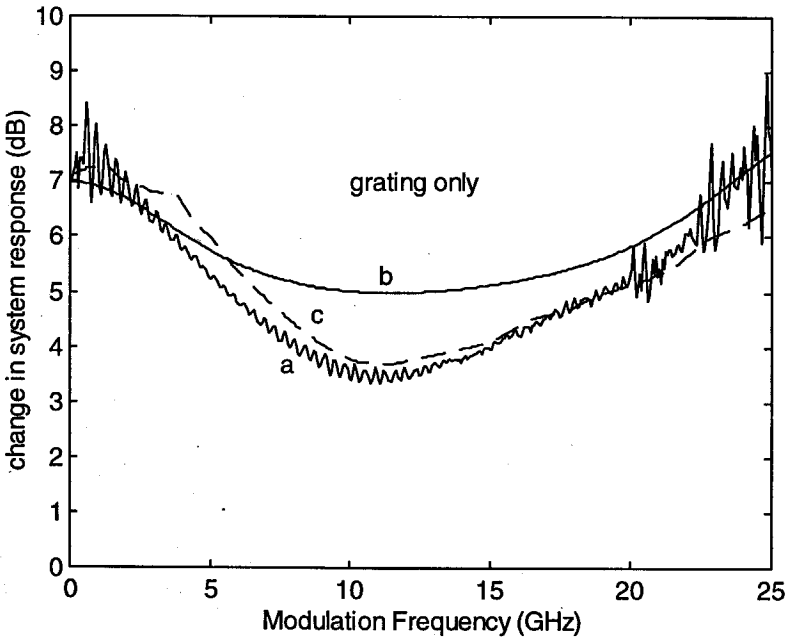

Figure 6.4. Change in system AM response due to a fiber grating. a) Experimental data. b) Numerical simulation using coupled-mode equations to model the grating. c) Numerical simulation using the measured grating transmission spectrum, with the phase of the transmittance being calculated with a Kramers-Kronig integral.

To calculate the effect of the grating on the laser signal, we first specify the signal exiting the laser as in (3.1),

$$E_{in}(t) = E_0 e^{+i\omega t}\sqrt{1+m\sin(\Omega t)}\exp\left[-i\beta\cos(\Omega t+\theta_{FM})\right] \tag{6.1}$$

where $m \cong .05$ is the AM modulation index, β is the phase modulation index, Ω is the modulation frequency, and θ_{FM} is the phase by which the laser FM leads the AM. For a directly modulated laser with a linewidth enhancement factor α, we have as previously,

$$\beta = \frac{|\alpha|}{2} m\sqrt{1+\left(\kappa/\Omega\right)^2} \tag{6.2a}$$

and

$$\theta_{FM} = \tan^{-1}\left(\Omega/\kappa\right) \tag{6.2b}$$

Here $\kappa = \varepsilon P_0 / \tau_{ph}$ is the characteristic frequency separating the adiabatic and transient chirp regimes, where ε is the non-linear gain compression factor, P_0 is the steady-state photon density in the active region, and τ_{ph} is the photon lifetime [19]. κ and α were determined by fitting the change in the modulation response of the laser caused by dispersive fiber to the transfer function (3.30) for dispersive fiber, following [31, 32]. (The data is shown in Figures 6.5 & 6.6 below.) We obtained $|\alpha| = 4.32$ and $\kappa / 2\pi = 8.4$ GHz at the laser operating conditions used in the experiment. Knowing these, we used (6.1) to numerically calculate the Fourier transform $\tilde{E}_{in}(\omega)$. The output optical field from the fiber-grating combination is taken as

$$\tilde{E}_{out}(\omega) = \tilde{E}_{in}(\omega)\, t(\omega)\exp\left[-i\beta''(\omega-\omega_0)^2 L/2\right] \tag{6.3}$$

where $t(\omega)$ is the complex field transmission function of the grating, $\beta'' = \partial^2\beta / \partial\omega^2\Big|_{\omega_0}$ is the fiber dispersion parameter, ω_0 is the center optical frequency, and L is the fiber length. The detected current $I_{out}(t)$ is obtained from $E_{out}(t)$, the inverse Fourier transform of (6.3). The AM system transfer function measured in the figures is the component of the ratio of the output to input signals at the modulation frequency, that is,

$$H_{AM}(\Omega) = \left|\tilde{I}_{out}(\Omega) / \tilde{I}_{in}(\Omega)\right|^2 \tag{6.4}$$

This process is the same outlined in the schematic Figure 3.3.

A crucial step in the above calculation is the model of the fiber grating used to generate the complex optical transmittance $t(\omega) = |t(\omega)|e^{i\phi_t(\omega)}$. The magnitude of the transmittance $T(\omega)$ can be measured with an optical spectrum analyzer using a below-threshold laser as a broadband source. The result is shown in Figure 6.4 (solid line). However, we cannot easily measure the transmittance phase $\phi_t(\omega)$. One solution is to numerically solve the coupled-mode differential equations (5.1a,b) for an unchirped grating, with a Gaussian apodized coupling strength profile chosen to produce the same maximum reflectivity (94.5%) and FWHM (1.9 Å) as measured from our grating. This generates the phase and magnitude of $t(\omega)$ at once, and the resulting spectrum (Figure 6.7, dotted line) is an approximation of the actual spectrum.

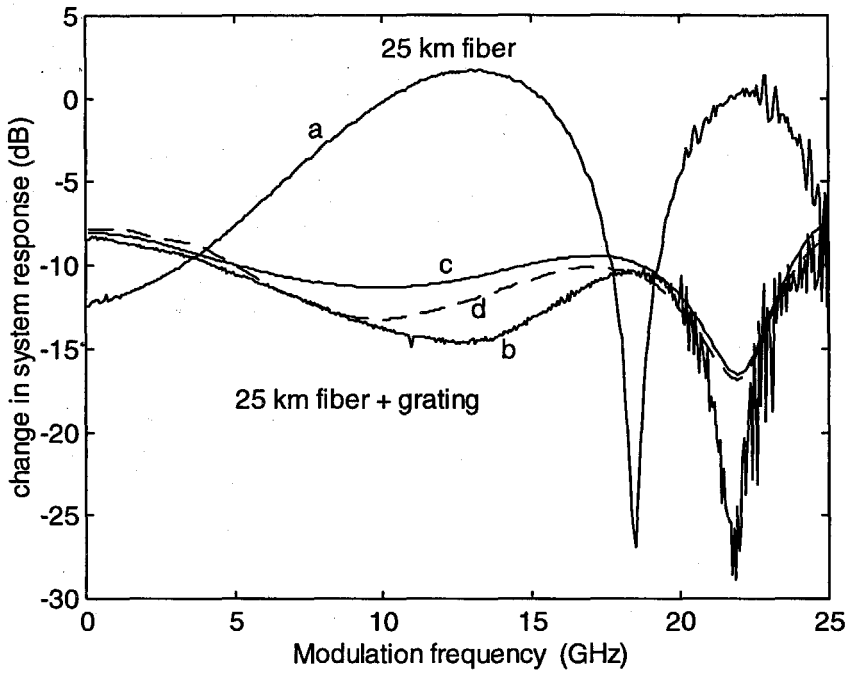

Figure 6.5. Change in system AM response with 25 km of dispersive fiber. a) Experimental data for fiber only. b) Experimental data for fiber and grating. c) Numerical simulation with coupled-mode equations. d) Numerical simulation with Kramers-Kronig integral.

The result of using this coupled-mode transmittance as the optical transfer function is shown in Figures 6.4 through 6.6 (lines "c"). We see an increase in the AM signal due to the grating (Figure 6.4), with the same qualitative shape seen experimentally. For 25 or 50 km of dispersive fiber, we again see a prediction consistent with experiment (Figures 6.5, 6.6), with a larger and flatter system response, and a higher frequency at which the first dip occurs.

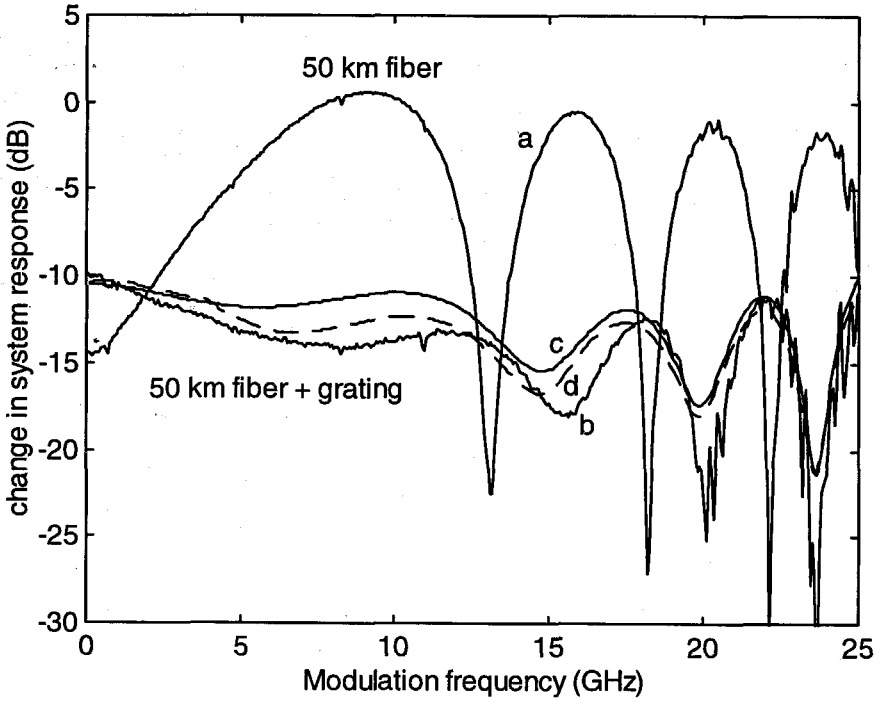

Figure 6.6. Change in system AM response with 50 km of dispersive fiber. a) Experimental data with fiber only. b) Experimental data with fiber and grating. c) Numerical simulation with coupled-mode equations. d) Numerical simulation with Kramers-Kronig integral.

An alternative model for the grating is to use the measured transmission spectrum, with the phase of the transmittance being inferred from its amplitude. Because $\ln(t(\omega))=\ln|t(\omega)| + i\,\phi_t(\omega)$ is square integrable, a Kramers-Kronig integral on the measured spectrum of $\ln(\sqrt{T})$ will give us ϕ_t at any optical frequency. This numerical transform is consistent with coupled-mode solutions for uniform, chirped, or apodized gratings, as described in the previous chapter. The transmission spectrum of our grating was measured at 0.1 Å increments, showing an asymmetric spectrum with sidelobes on either side of the central peak (Figure 6.7). The corresponding phase spectrum was then

generated numerically, and t(ω) values were interpolated for sub-0.1-Angstrom values. The prediction of the system response resulting from this grating model was more accurate than that of the coupled-mode equations (Figures 6.4 through 6.6, dashed lines).

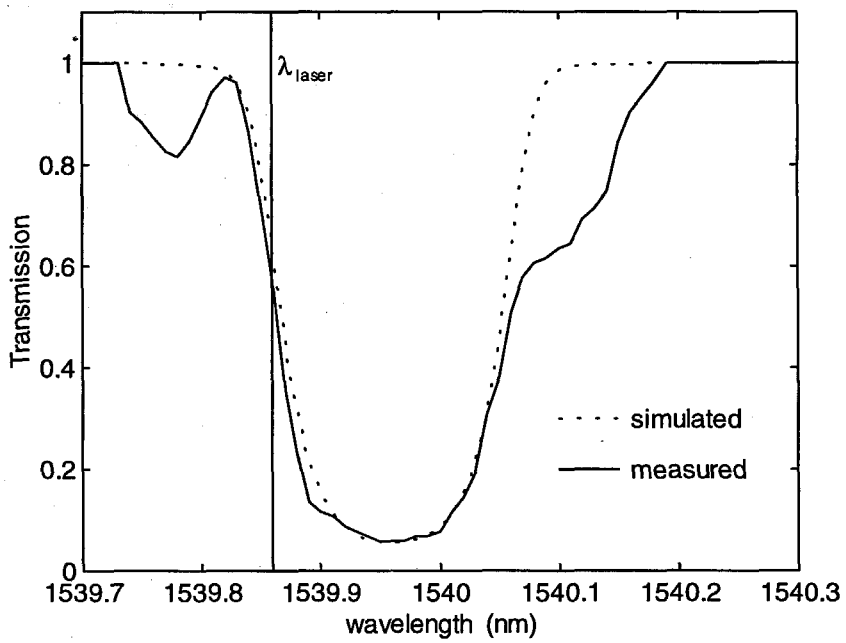

Figure 6.7. Transmission spectrum of grating used in experiment. The "simulated" spectrum is from a numerical coupled-mode equation solution for an apodized grating whose parameters were chosen to match the observed FWHM = 1.76 Å and R_{max} = 94.5% of the real grating. The vertical line marks the laser wavelength λ_{laser} used in the experiment and simulations.

In all of these plots the predicted system response has been corrected for fiber attenuation and connector losses, which were measured away from the Bragg wavelength of the grating. We did not "correct" for the grating transmission at the center wavelength,

$T(\omega_o)$, which was 38% for Figures 6.2 and 6.3, and 46% for Figures 6.4 through 6.6. This does reduce the DC and AM signals, and is accounted for automatically in the Fourier domain calculation.

6.3 Discrimination versus dispersion

The observed changes in the system response are due to a combination of phenomena. The increase in the AM signal from the grating alone can be understood by FM-to-AM conversion in the grating. In a directly modulated semiconductor laser, a frequency modulation (chirp) inevitably accompanies the amplitude modulation [59, 60]. Any frequency discriminator, such as an optical filter or resonant cavity, will convert a varying optical frequency into a varying transmitted power. Using the slope of the grating transmission versus wavelength from Figure 6.7, and the known magnitude of the frequency chirp $\Delta\omega$, we are able to predict an increase in the AM response of about 7 dB at low frequencies, from equation (3.49).

Secondly, the dips in the AM transfer function of the fiber (without the grating) are due to fiber dispersion and occur at modulation frequencies that depend on the fiber dispersion-length product DL. The fact that the use of a grating pushes these dips to higher frequencies is an indication of partial dispersion compensation by the grating, due to the non-linear phase $\phi_t(\omega)$ of the transmittance. Finally, the decrease in the magnitude of these dips, seen most clearly in Figures 6.5 and 6.6, is a result of the partial optical

filtering by the grating of the longer-wavelength sideband [61]. This will also convert FM to AM and increase the AM response, explained by the phasor argument following Figure 3.2.

The frequency discrimination and optical filtering phenomena are not dependent on the phase of the transmittance, and the dispersion compensation is dependent only on the phase. Therefore, we can deduce the relative important of each by repeating the simulation for a phaseless version of the grating, replacing $t(\omega)$ with $|t(\omega)|$, and by doing the opposite, replacing $t(\omega)$ with $t(\omega) / |t(\omega)|$, which has an amplitude of 1 at all frequencies but retains the non-linear phase. Neither of these transmittances are physically possible--the Kramers-Kronig relations show that a frequency-dependent transmission produces a frequency dependent phase, and vice versa. But the exercise allows us to test the intuition above. The results are shown in Figure 6.8 for the grating without fiber.

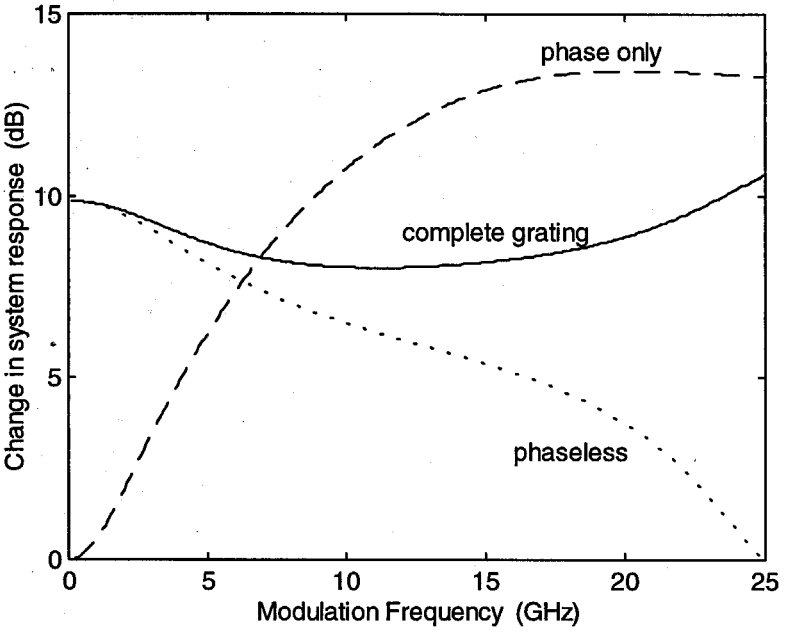

Figure 6.8. Change in laser response due to simulated grating from coupled-mode equations. The solid line uses the compete complex transmittance $t(\omega)$; the dotted line uses the phaseless transmittance $|t(\omega)|$, and the dashed line uses the phase-only transmittance $t(\omega) / |t(\omega)|$.

At low frequencies the phaseless prediction is accurate, as expected from the time-domain frequency discriminator model, which holds only when the signal bandwidth is much less than the grating bandwidth (equal to just under 2 Å, or 25 GHz). At high frequencies it turns out that the optical filtering alone is not sufficient to explain the increase in the signal; rather it is the dispersive phase which is converting laser FM into extra AM to boost the signal. Note the change in the AM signal here is larger than shown in Figure 6.4 because we are no longer subtracting connector losses.

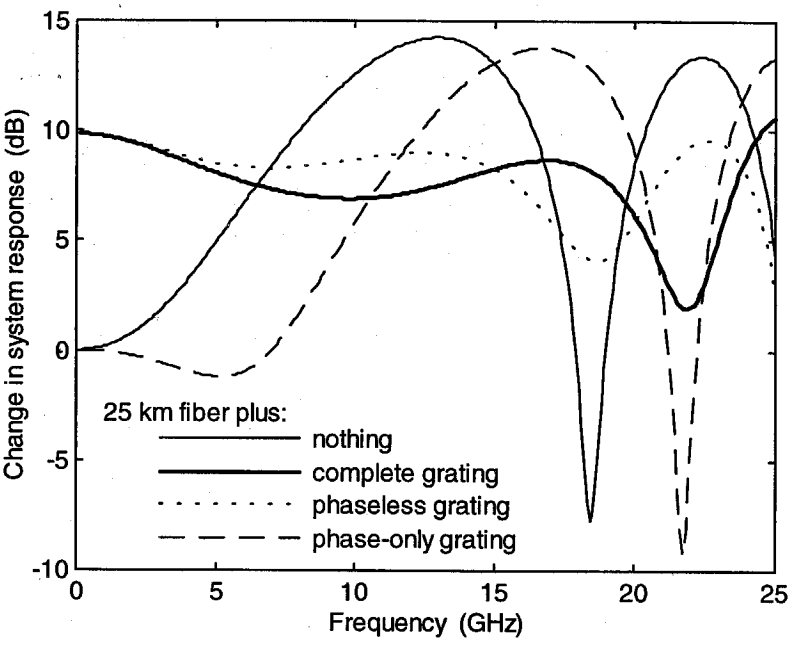

Figure 6.9. Change in laser response due to 25 km of fiber and a simulated grating. The thin solid line is the change due to fiber only; the thick solid line shows fiber plus the compete complex transmittance $t(\omega)$. The dotted line is fiber plus the phaseless transmittance $|t(\omega)|$, and the dashed line is fiber plus the phase-only transmittance $t(\omega) / |t(\omega)|$.

For 25 km of fiber, the phaseless grating predicts most notably the smoothing of the bumps and dips produced by fiber dispersion. In Figure 6.9, the phaseless prediction (dotted line) exhibits the smoothed response, and the phase-only grating doesn't. This supports our intuition that the partial optical filtering of the upper sideband reduces the AM-FM conversion produced by the dispersive fiber, which is the root of those bumps and dips. Note that the dip in the dotted line still occurs at the same frequency, 18 GHz, determined by the fiber dispersion-length product. Thus the phaseless grating does not compensate for dispersion in the technical sense. The phaseless grating does--the dip in

the dashed line of Figure 6.9 occurs at the same 22 GHz frequency as the full prediction, indicating that the phase of the grating alone reduces the quadratic phase of the system. It does not boost the signal or smooth the response.

6.4 Dependence on laser parameters

The 10 dB intrinsic increase in the AM signal shown by this grating is an impressive result, and it is worth considering how the result depends on the laser parameters. In general, we expect a larger $|\alpha|$ parameter will increase the effect because it

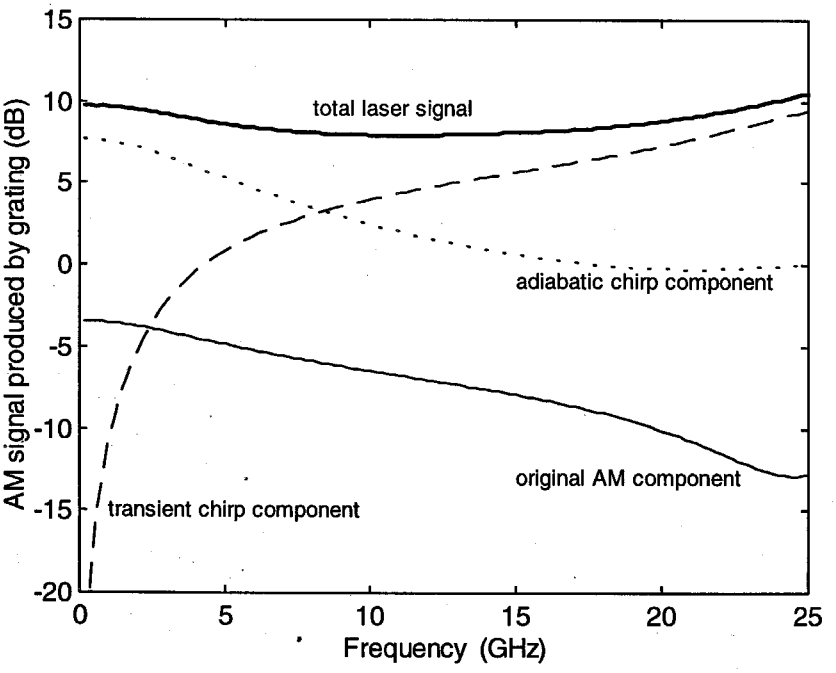

Figure 6.10. AM signal created by the grating from the initial laser signal and its three constituent components.

produces more FM for a given modulation AM. But the full result is a combination of effects on the initial laser AM and the transient and adiabatic components of the FM.

Figure 6.10 shows the laser AM transfer function of our simulated grating (no fiber), broken down by the components of the initial laser signal. Each is compared to the initial AM signal exiting the laser--for example, the adiabatic component has a value of 7.6 dB at 0 GHz; this means that the magnitude of the AM signal produced by the grating from only the adiabatic chirp FM signal is 7.6 dB larger than the initial amount of AM signal exiting the laser. The three component lines do not add to the total transfer function only because the individual AM signals have different phases, much like in equation (3.29)--if we use the complex transfer functions, they do sum to the total transfer function. We expect this because our system is linear, and with the small modulation index m = .05, the input electric field E(t) of equation (3.1) can be written as a sum of three small-signal terms.

The AM component can again be interpreted with the intuition developed in Chapter 3. At $\Omega = 0$, both sidebands and the carrier wave are at the optical frequency and pick up a factor $t(\omega_0)$ through the grating. There is no AM-FM conversion but they are attenuated by the transmission at this frequency, and the AM electrical signal is down by a factor $T(\omega_0)^2 = (0.67)^2 = -3.5$ dB. As Ω increases, the phases of the two sidebands start differing, converting some of the AM into FM and decreasing the signal further, producing the downward sloping line.

At low frequencies, the transient contribution is smaller than the adiabatic because $\Delta\omega_{transient} \propto \Omega$ and $\Delta\omega_{adiabatic} \propto$ (constant). At $\Omega = \kappa = 8.4$ GHz the two chirp components are equal in magnitude and produce the same size AM contribution (though with different phases). If a laser has a smaller non-linear gain parameter ε, then, the low-frequency AM signal after the grating will be smaller, because the adiabatic chirp is responsible for this low-frequency signal increase.

In short, the initial AM plays little role in the final AM, which is produced primarily by the conversion of transient FM into AM at low frequencies and adiabatic FM into AM at high frequencies.

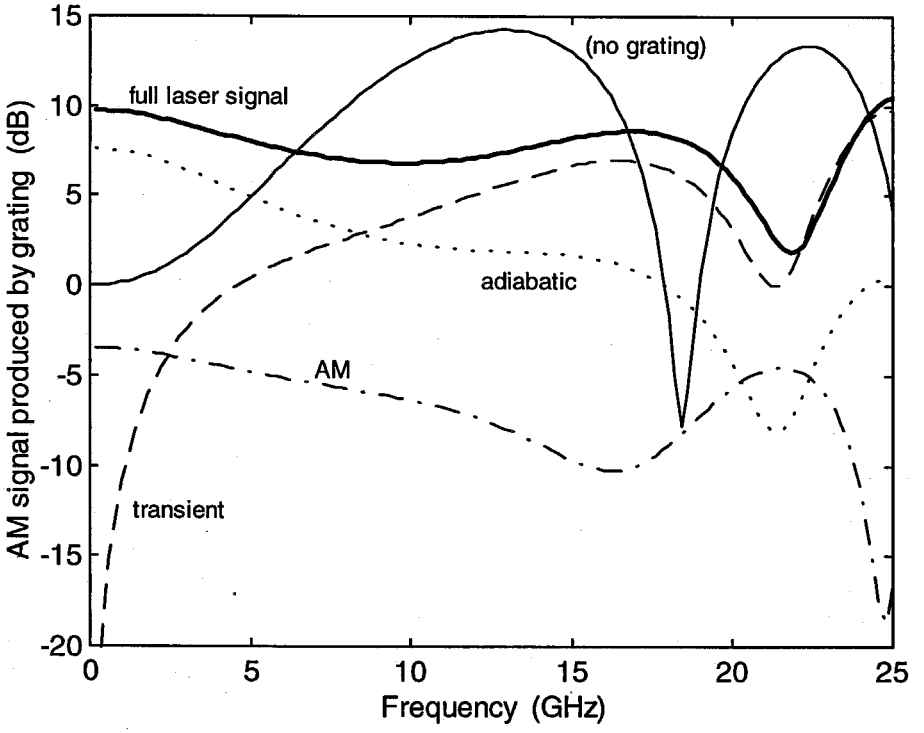

Figure 6.11. AM signal produced by simulated grating after 25 km of fiber, for the total laser signal and its individual components. For reference, the change in response due to the fiber alone is represented by the thin solid line.

The same analysis is presented in Figure 6.11 for the change caused by the grating after 25 km of dispersive fiber. Note the dispersion compensation, represented by the increase in the "dip" frequency, is the same for both chirp components. Again the initial AM signal is of little consequence once the grating has been added, as its magnitude is small compared to the adiabatic and transient chirp contributions.

The AM system response was found to depend strongly on the detuning of the optical frequency from the grating center frequency. When the laser was temperature-tuned by only 10% of the grating FWHM, the change in the system response could be made to increase or decrease monotonically with modulation frequency or be negative. Likewise, the dips in the system response could be increased or decreased in magnitude and in the frequencies at which they occurred. In general, as expected, the system response changes were found experimentally and numerically to be larger for gratings with smaller bandwidths and larger reflectivities.

To be useful in optical communication systems, the laser wavelength must be carefully controlled, and optimized with the grating for a given length of fiber. The advantage of this system is that unchirped gratings are less expensive than chirped gratings, and the transmission geometry avoids the need for optical circulators. Finally, we reiterate that the signal increase in Figures 6.2 and 6.4 were accompanied by a decrease in the average optical power. Since shot noise is proportional to the average detector photocurrent, which was reduced by over 50% due to the gratings, the shot noise power decreased while the signal power increased. This does not mean that the system

signal-to-noise ratio (SNR) will increase, though, because the same mechanism that converts FM into AM will also convert laser frequency noise into excess amplitude noise [35]. This is the subject of the next chapter.

Chapter 7 -- Effect of Fiber Gratings on RIN

We saw in Chapter 6 that fiber Bragg gratings can convert frequency modulated (FM) semiconductor laser signals into amplitude modulated (AM) signals and vice versa. This is due to the frequency dependence of both the transmitted amplitude (referred to as frequency discrimination) and the phase (dispersion). The phenomenon is similar in dispersive fiber, in which, as we saw in Chapter 3, FM-to-AM conversion will also mix frequency and intensity noise, and can increase or decrease the relative intensity noise (RIN) of the laser depending on the fiber length and the laser dynamic parameters [35]. The effect relies on intrinsic correlations between intensity noise and frequency noise, which have been exploited to reduce laser RIN using a Michelson interferometer [63, 64].

In this chapter we investigate the effect of transmission through a fiber grating on the relative intensity noise of semiconductor laser light, thereby uniting again the topics of previous chapters. We use our model of the grating as a linear frequency discriminator to correctly explain observed increases in intensity noise of up to 30 dB at low frequencies, obeying an inverse-square frequency dependence. We will also show that there exist conditions under which a grating can reduce intensity noise, and we demonstrate 2 dB of RIN reduction at frequencies up to 15 GHz. The Fourier-domain calculation used in the last chapter, which incorporates the phase of the grating transmittance, correctly predicts these results.

7.1 Experimental Measurement

The experimental measurements were performed by biasing a 1.54 μm commercial (ORTEL Corp.) distributed feedback laser with a low-noise constant-current controller. The laser output was sent into a fiber pigtail and through an optical isolator (> 60 dB), through a variable optical attenuator and into a high-speed photodiode (Figure 7.1). The detected photocurrent was electronically amplified and fed to an electronic

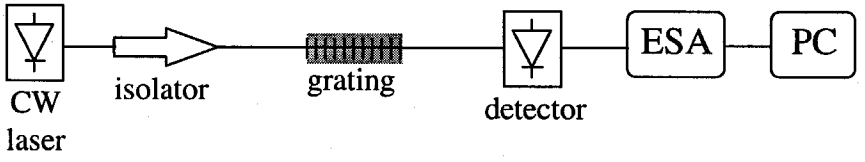

Figure 7.1. Experimental setup used to measure laser intensity noise. The ESA is an electronic spectrum analyzer.

spectrum analyzer. From the experimental plots of noise power versus photocurrent we extracted the thermal noise (constant part), shot noise (linear part), and laser noise (quadratic part) at each electronic frequency, as in Chapter 4. We then replaced the attenuator with a fiber grating and compared the RIN with and without the fiber grating to determine its effect.

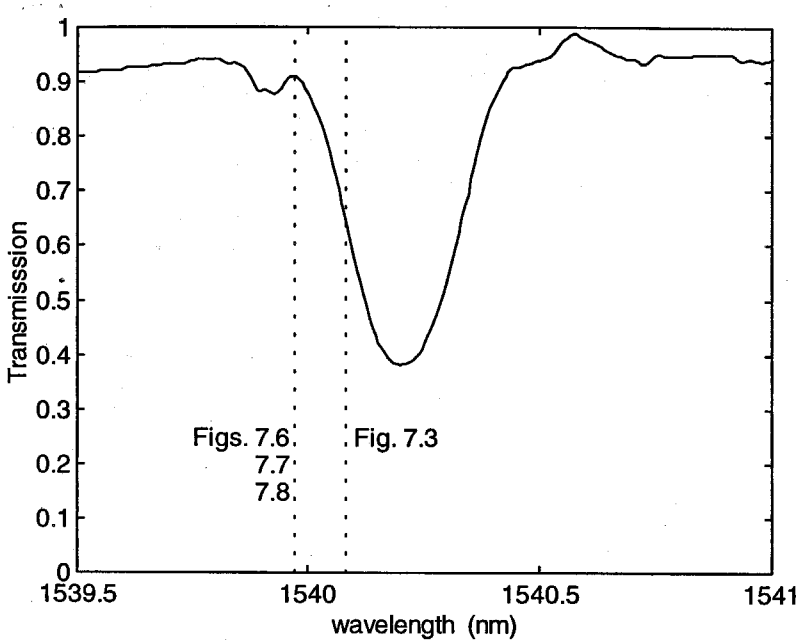

Figure 7.2. Transmission spectrum of grating used in experiments. The right vertical line marks the laser wavelength used in taking the data of Figure 7.3; the left one marks the laser wavelength for Figures 7.6 through 7.8.

The laser wavelength was temperature-tuned and stabilized during the experiment at different parts of the grating transmission spectrum. Figure 7.2 shows the spectrum of one such grating. First we tuned the laser wavelength to the steep, linear part of the transmission spectrum on the low-wavelength side of the reflection band, marked by the right vertical line in the figure. The change in RIN produced by the grating at this wavelength is shown in Figure 7.3. The dramatic increase in noise, over 20 dB at low frequencies, is due to the frequency discrimination of the grating, which converts laser frequency fluctuations into transmitted intensity fluctuations.

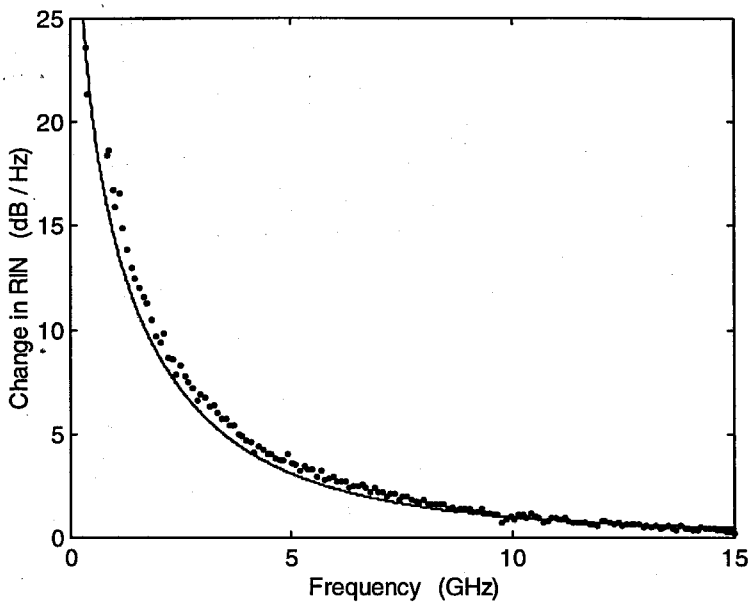

Figure 7.3. Change in RIN due to fiber grating, with the laser tuned to the steep linear part of the grating transmission spectrum. The points are experimental data and the line is equation (7.6).

7.2 Time-domain model

To make this more explicit, suppose a constant optical power P_{inc} is incident on the grating with an instantaneous frequency deviation $\Delta\omega(t) = \omega(t) - \omega_0$. The frequency-dependent transmission produces a transmitted optical power deviation of

$$\Delta P_{trans}(t) = P_{inc}\, T'\, \Delta\omega(t) \qquad (7.1)$$

where $T' = dT / d\omega|_{\omega_0}$ is the slope of the grating transmission versus frequency at the center wavelength ω_0. This model of the grating as a (phaseless) linear frequency discriminator, discussed in Chapter 3, is sufficient for explaining Figure 7.3 and much of

the observed results, by using (7.1) and specifying the nature of the frequency fluctuations. The discussion below extracts the essentials of the discussion in Chapter 2.

The dominant source of laser noise is spontaneous emission into the laser mode and its spectral density can be derived from the rate equations. We represent the component of the spontaneous emission field that is in phase with the laser field by a Langevin force $F_{\|}(t)$, which perturbs the laser intensity; and the other quadrature of the spontaneous emission field by a Langevin force $F_{\perp}(t)$, which perturbs the laser phase. The in-phase or parallel component $F_{\|}(t)$ produces an output power fluctuation $\Delta P_{\|}(t)$ with spectral density $S^{\|}_{\Delta P}(\Omega)$, and a frequency fluctuation $\Delta\omega_{\|}(t)$ with spectral density (from 2.42)

$$S^{\|}_{\Delta\omega}(\Omega) = \left(\frac{|\alpha|\Omega_0^{\,2}}{2P_0\Omega}\right)^2\left[\frac{(\tau_{ph}\Omega)^2+1}{(1/\tau\Omega)^2+1}\right]S^{\|}_{\Delta P}(\Omega) \tag{7.2}$$

Here α is the linewidth enhancement factor, Ω_0 is the laser resonant frequency, τ_{ph} is the photon lifetime, τ is the carrier lifetime, and P_0 is the optical output power. The intensity and frequency fluctuations produced by $F_{\|}(t)$ are correlated, and $\Delta\omega_{\|}(t)$ leads $\Delta P_{\|}(t)$ by a phase given in (2.43),

$$\theta^{\|} = \frac{\pi}{2} + \tan^{-1}\left(\frac{(1/\tau\Omega)+\tau_{ph}\Omega}{1-(\tau_{ph}/\tau)}\right) \tag{7.3}$$

For the laser conditions used in Figure 7.3, the laser parameters were determined by a fit to the RIN spectrum (without a grating) and to the change in RIN after a fiber of known dispersion, as in [35], giving $1/2\pi\tau$ = .39 GHz and $1/2\pi\tau_{ph}$ = 31 GHz. For frequencies in

the range $1/\tau << \Omega << 1/\tau_{ph}$, as in this experiment, the quantity in brackets in (7.2) is nearly 1 and $\theta^{\parallel}$ is nearly $\pi/2$. Thus the intensity and frequency fluctuations produced by $F_{\parallel}(t)$ are 90 degrees out of phase, and we can simply add the intensity noise power created by the grating from $S^{\parallel}_{\Delta\omega}(\Omega)$ to the initial intensity noise power $S^{\parallel}_{\Delta P}(\Omega)$ caused by $F_{\parallel}(t)$ directly.

The spontaneous emission term $F_{\perp}(t)$ produces no initial intensity fluctuations, but does create frequency fluctuations that are uncorrelated with $F_{\parallel}(t)$ and have a spectral density $S^{\perp}_{\Delta\omega}(\Omega) = 2K\omega_{ST}$, where ω_{ST} is the Schawlow-Townes linewidth and K is the Petermann enhancement factor for DFB lasers [23]. This too gets converted by the grating into an intensity noise power that adds with $S^{\parallel}_{\Delta P}(\Omega)$.

Putting $S^{\perp}_{\Delta\omega}(\Omega)$ and $S^{\parallel}_{\Delta\omega}(\Omega)$ into (1), we get the intensity noise spectral density after the grating,

$$S^{grating}_{\Delta P}(\Omega) = S^{initial}_{\Delta P}(\Omega)\left[T^2 + \left(\frac{T'\alpha{\Omega_0}^2}{2\Omega}\right)^2\right] + \left(P_0 T'\right)^2 2K\omega_{ST} \tag{7.4}$$

The last term above is independent of frequency and represents a new noise floor created by the grating from $S^{\perp}_{\Delta\omega}(\Omega)$. It is usually smaller than either the initial intensity noise (attenuated by T^2) or that created by the grating from $S^{\parallel}_{\Delta\omega}(\Omega)$. Ignoring it, we arrive at a simple expression for the change in RIN due to the grating:

$$\Delta RIN(\Omega) = 10\log_{10}\left\{1 + \left(\frac{T'\alpha{\Omega_0}^2}{2T\Omega}\right)^2\right\} \tag{7.5}$$

Figure 7.3 shows a plot of this expression (solid line), using the independently measured values of the grating transmission T and slope T' and the laser parameters Ω_0 and α, showing very good agreement with the experimental data.

There is an important lesson in the experiment and theory contained in Figure 7.3. It is that semiconductor lasers possess an intrinsic frequency noise, caused by spontaneous emission, which has a $1/\Omega^2$ behavior not shared by the intensity noise produced from the same spontaneous emission, and thus is very large at low frequencies. A frequency discriminator can convert this frequency noise into excess intensity noise that is orders of magnitude larger than the original intensity noise. This is a dramatic consequence of laser chirp, and surprisingly does not depend on the non-linear gain parameter ε, which is normally associated with adiabatic or low-frequency chirp--see (2.40), from which (7.2) comes. Also note that this low-Ω frequency noise is not brought out by dispersive fiber, which also converts frequency noise into amplitude noise. The reason is that the transfer function $H_{\|}(\Omega)$ of (3.36), which describes this conversion, has a $\sin^2\theta(\Omega)$ term whose low-frequency behavior goes as Ω^2 and thus cancels the $1/\Omega^2$ behavior of the frequency noise source--a fortunate coincidence for fiber optic communication systems.

7.3 RIN Reduction

Equation (7.5) predicts that RIN will always increase with a grating, due to the phase $\theta' \approx \pi/2$ between the correlated frequency and intensity noise. This is not always the case. For frequencies that are low ($\Omega<<1/\tau$) or high ($\Omega>>1/\tau_{ph}$) the frequency fluctuations $S^{\parallel}_{\Delta\omega}(\Omega)$ are independent of frequency and π out of phase with the intensity fluctuations. Thus a grating for which T increases linearly with ω (e.g., on the short-wavelength side of the reflection band) will compensate an increased intensity with a decreased transmission. The intensity noise from $F_{\parallel}(t)$ is eliminated completely when the grating slope is $T'/T = 2/(|\alpha|\Omega_0^2\tau)$ at low frequencies or $T'/T = 2/(|\alpha|\Omega_0^2\tau_{ph})$ at high frequencies.

In addition, there are other sources of noise that can be eliminated with a linear frequency discriminator. Carrier fluctuations not involving spontaneous emission into the lasing mode, including those from pump current noise, produce frequency fluctuations that are in phase with the intensity fluctuations when $\Omega<<\varepsilon P_0/\tau_{ph}$ (in the adiabatic chirp regime, typically up to several GHz), where ε is the nonlinear gain compression factor. The intensity noise from this source will be removed completely when the grating slope is $T'/T = -2\tau_{ph}/|\alpha|\varepsilon P_0$. For $\Omega>>\varepsilon P_0/\tau_{ph}$, the transient chirp regime, the intensity and frequency fluctuations are $\pi/2$ out of phase and a frequency discriminator can only increase the intensity noise from this source. We have also neglected mode partition

noise, which is important at low frequencies and is affected differently by dispersive optical elements [65].

The discussion thus far has neglected the phase $\phi_t(\omega)$ of the complex grating transmittance $t(\omega)$, which is a good approximation when the transmittance is linear over the bandwidth of interest. In all other cases we must include the effect of grating dispersion on the RIN. The phenomenon is the same in principle as in dispersive fiber, in which AM and FM noise are inter-converted by a mixing angle $\theta(\Omega) = \beta''L\Omega^2/2$, where $\beta'' = \partial^2\beta / \partial\omega^2\big|_{\omega_0}$ is the fiber dispersion parameter and L the fiber length. For the case of a grating, the mixing angle is, from (3.23),

$$\theta(\Omega) = \left[\phi_t(\omega_0 + \Omega) + \phi_t(\omega_0 - \Omega) - 2\phi_t(\omega_0)\right] / 2 \qquad (7.6)$$

An expression similar to (7.4) can be derived to include $\theta(\Omega)$, along the lines of equation (3.43), but an analytic treatment is intractable for fiber gratings, and the numerical Fourier-domain calculation shown schematically in Figure 3.3 is preferred.

7.4 Numerical predictions: discrimination versus dispersion

The intensity noise after the grating is calculated from $\tilde{E}_{out}(\omega) = \tilde{E}_{in}(\omega)t(\omega)$, with $\tilde{E}_{in}(\omega)$ obtained from the Fourier-transformed rate equations containing $F_{\|}(t)$ and $F_{\perp}(t)$ as sources. Measuring the magnitude of the transmittance spectrum $|t(\omega)| = \sqrt{T(\omega)}$ lets

us infer the phase $\phi_t(\omega)$ numerically via a Kramers-Kronig integral as before [1]. This numerical calculation allows us to treat more narrow spectral features of a grating.

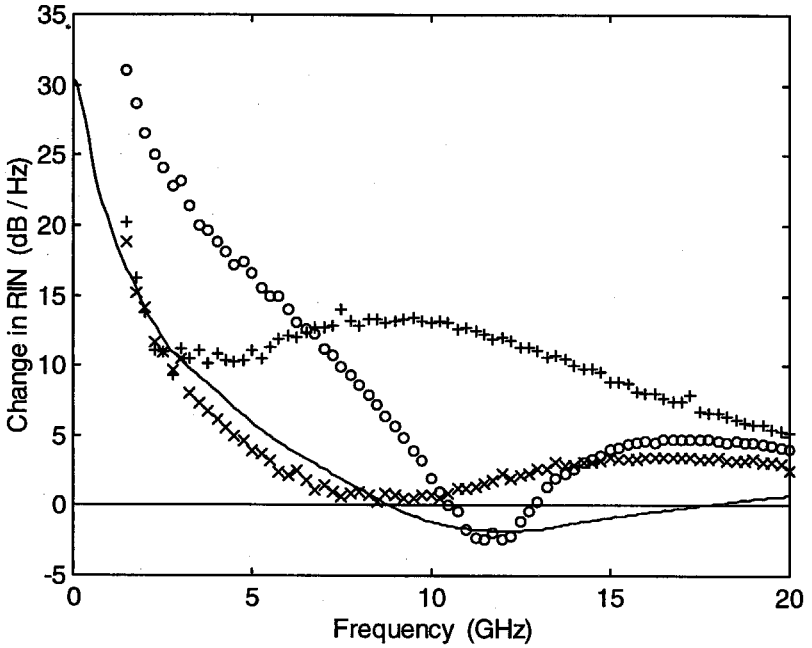

Figure 7.4. Change in RIN due to fiber grating, with the laser tuned to three different wavelengths among the weak sidelobes of the reflection spectrum. The symbols +, o, and x are experimental data and the solid line is a typical numerical calculation using the measured grating spectrum.

As an example, Figure 7.4 shows RIN changes from a grating at three different wavelengths, each among the weak reflection sidelobes on the long-wavelength side of the grating spectrum shown in Figure 7.5 and marked by the vertical lines. The RIN increased at low frequencies but deviated from the $1/\Omega^2$ dependence of equation (7.5) and even decreased at some frequencies (Figure 7.4, circles). The numerical calculation

(solid line) incorporating the measured spectrum reflects these effects qualitatively but is limited by the resolution of our optical spectrum analyzer (10 GHz), which essentially smoothes the transmission function used in the calculation and fails to predict the more frequency-sensitive features of $\Delta RIN(\Omega)$. The laser parameters, which affect the change in RIN due to the grating, were measured as described in Chapter 4 and for the above experiment had the values $\Omega_0 = 7.0 \times 10^{10}\ s^{-1}$, $\gamma_0 = 5.3 \times 10^{10}\ s^{-1}$, $|\alpha| = 8.0$, $\tau_{ph} = 5 \times 10^{-12}$ s, $\tau = 5 \times 10^{-10}$ s, and $K\omega_{ST} = 4 \times 10^5\ s^{-1}$.

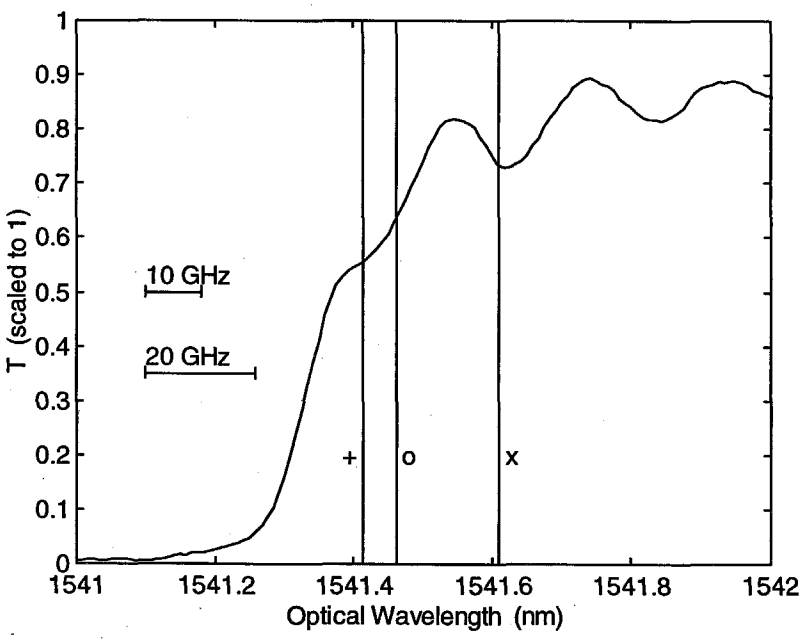

Figure 7.5. Transmission spectrum of the grating that produced the data in Figure 7.4. The three vertical lines mark the wavelength to which the laser was tuned for the three sets of data in Figure 7.4, labeled by the symbols +, o, and x in both figures.

The grating phase plays an important role in changing the RIN and can reduce the RIN when T' is small. Figure 7.6 shows a RIN reduction of 2 dB obtained with the grating shown in Figure 7.2. The laser was tuned to the low-wavelength side of the spectrum near the weak sidelobe, as indicated in Figure 7.2. The solid line is the full numerical calculation incorporating this spectrum and its Kramers-Kronig-generated phase. The low-Ω prediction is somewhat artificial, given the limited resolution of $t(\omega)$, and the variations in the data below 3 GHz might result from a fine structure in the grating spectrum that we cannot resolve. The laser parameters used in the simulation were $\Omega_0 = 4.8 \times 10^{10}\ s^{-1}$, $\gamma_0 =$

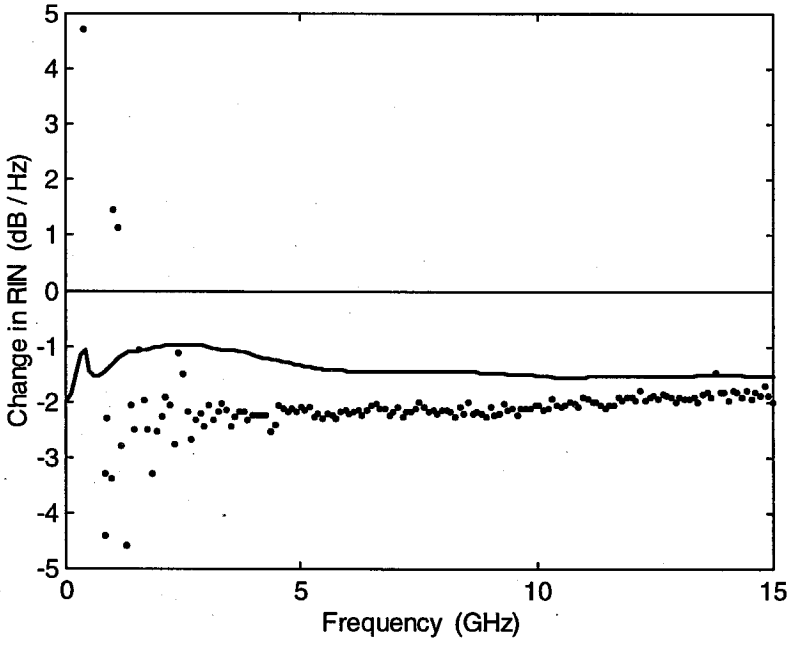

Figure 7.6. Change in RIN due to the grating of Figure 7.2, showing a decrease in the laser intensity noise. The points are experimental data and the solid line is the numerical calculation using the measured grating spectrum.

2.4×10^{10} s^{-1}, $|\alpha| = 4.1$, $\tau_{ph} = 5.1\times10^{-12}$ s, $\tau = 4.1\times10^{-10}$ s, and $K\omega_{ST} = 3.9\times10^{5}$ s^{-1}. Note that these parameters were not fit to match the simulations in this or any of the previous figures, but rather were all measured independently.

The numerical calculation in Figure 7.6 can be repeated using the a phaseless version of the grating transmittance, $|t(\omega)|$. In this case the predicted RIN is larger than both the prediction of the full transmittance $t(\omega)$ and the experimental data (Figure 7.7, dotted line), demonstrating that the RIN reduction is influenced by the grating phase. But the phase alone is also inadequate to predict the RIN reduction, as seen from the result of using the phase-only transmittance $t(\omega)/|t(\omega)|$. Figure 7.7 is hardly compelling, and only serves to justify the conclusion that neither the frequency discrimination of the grating, represented by the phaseless model, nor the dispersion of the grating, represented by the phase-only model, are adequate to explain the RIN reduction observed. Instead, the full complex transmittance is required, involving a combination of the two effects.

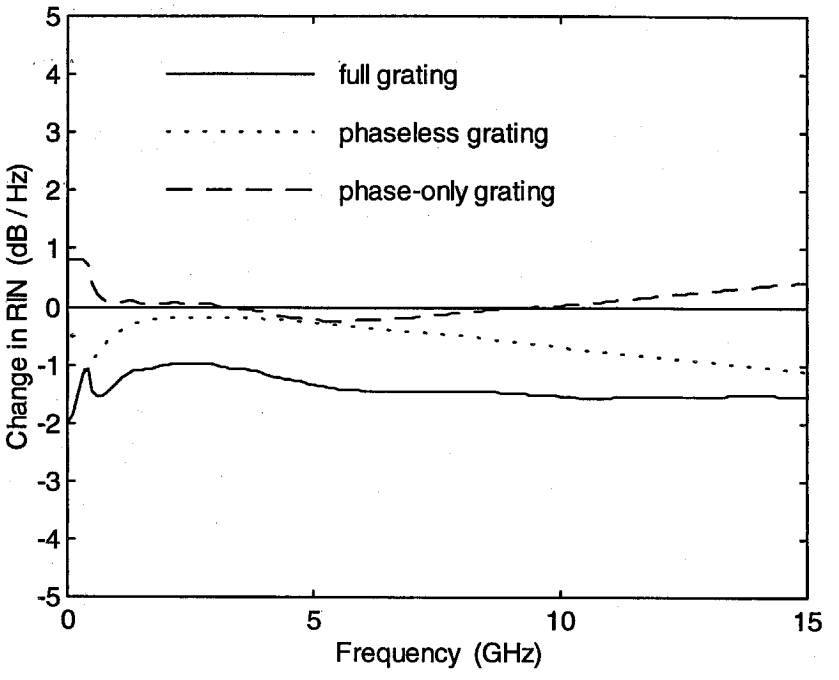

Figure 7.7. Change in RIN caused by the grating of the previous figure, calculated using the exact transmittance $t(\omega)$ as well as the phaseless version $|t(\omega)|$ and the phase-only version $t(\omega)/|t(\omega)|$. Here both frequency discrimination and dispersion participate in RIN reduction.

The situation is a little more clear if we repeat this analysis using the experiment of Figure 7.4. We see in Figure 7.8 that the $1/\Omega^2$ increase in RIN is fully predicted by the phaseless grating model, justifying our frequency discriminator explanation of this behavior and the time-domain calculation. And this phaseless prediction fails to dip below zero like the full prediction (and some experimental data) does. In this case it appears that the dispersive effect of the grating is responsible for the reduction of RIN.

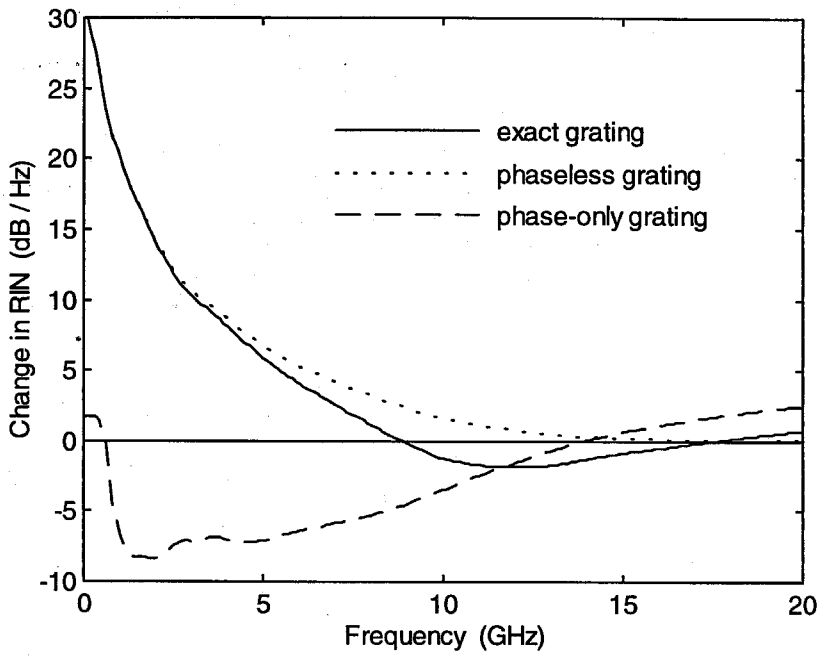

Figure 7.8. Change in RIN caused by a grating, using the exact transmittance $t(\omega)$ as well as the phaseless version $|t(\omega)|$ and the phase-only version $t(\omega)/|t(\omega)|$. The grating and laser parameters are the same as in Figure 7.4.

7.5 Incorporation of fiber

Aside from being necessary to predict RIN reduction, the numerical calculation is required if we wish to incorporate the effects of dispersive fiber, which complicates the relationship between amplitude and frequency noise and renders the time-domain model intractable. The reduction of RIN produced by the grating of Figure 7.6 is still present after 8.8 km of fiber, as Figure 7.9 shows. Here the fiber itself reduces the RIN by almost 10 dB at some frequencies, identical to what is discussed in Chapter 4, but the grating

enhances the phenomenon. Again a numerical calculation incorporating the measured spectrum adequately models the combined fiber-grating result.

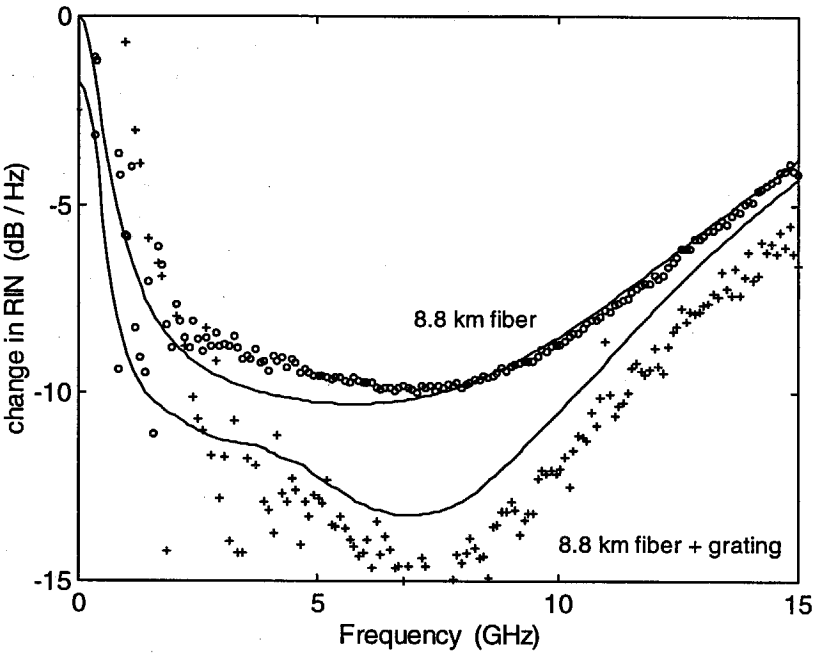

Figure 7.9. Change in RIN with fiber and fiber plus grating. The laser parameters and grating used are the same as in Figure 7.4. The open circles and upper line are experimental data and numerical simulation for 8.8 km fiber; the plus symbols and lower line are data and simulation for fiber plus the grating.

Unfortunately, the result does not persist with any fiber length, and in fact is almost gone beyond 25 km of fiber. Figure 7.10 shows the data and simulation for the effect of the grating after 25 km of fiber. The grating only changes the RIN by about 1 dB either way, close enough to the uncertainty in the simulation that the solid line follows the experimental data only roughly.

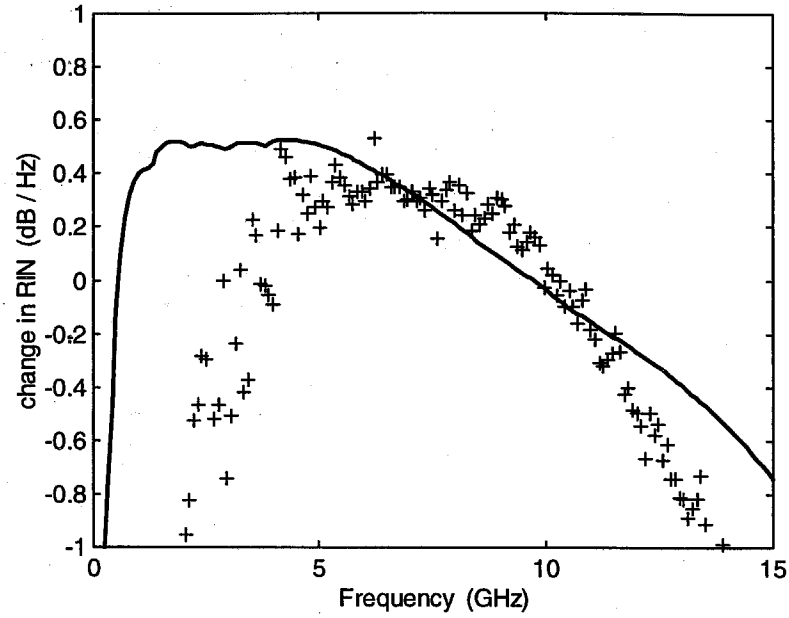

Figure 7.10. Change in RIN due to grating after 25 km of fiber. The points are experimental data and the solid line is the numerical calculation. Here the grating has little effect on the RIN (less than ±1 dB).

We cannot conclude that fiber eventually washes out the effect of a grating on the RIN--only that in it did in the above example. For a counter-example, we compute the effect on the RIN of the apodized ("simulated") grating of Figure 6.7, after 25 km of fiber, shown below. Not surprisingly, the familiar $1/\Omega^2$ increase in RIN is concomitant with the large AM increase this grating produced (Figure 6.4), both being a consequence of the strong frequency discrimination. The fiber has a rapid increase in RIN below 1 GHz characteristic of long fiber lengths, then dips at 20 GHz where $H_{\|}(\Omega)$ of (3.36) is near zero. The grating moves the dip to a higher frequency, just like with the modulation

response data, providing a second manifestation of the grating's dispersion compensation. With a phaseless version of this grating, the dip frequency is unchanged.

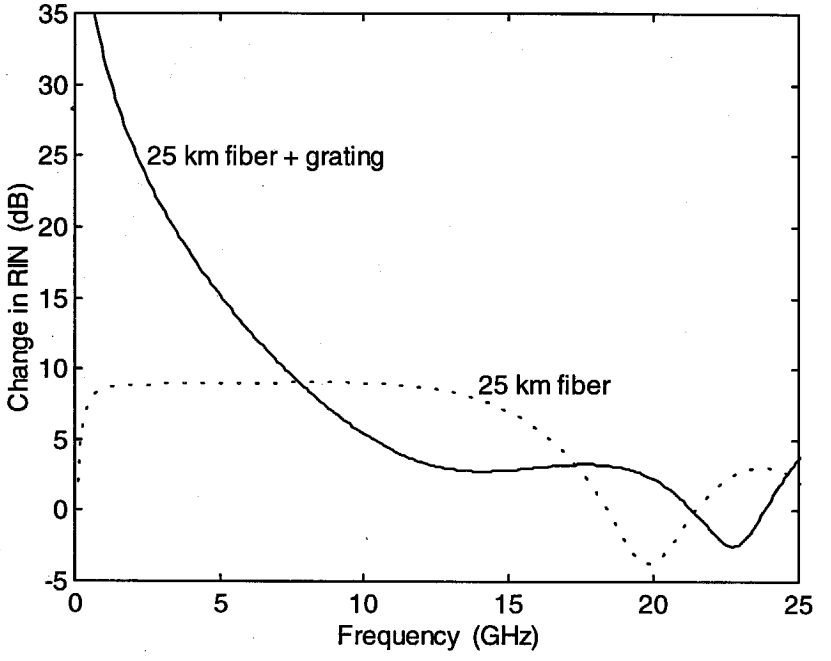

Figure 7.11. Change in RIN for 25 km of fiber, and fiber plus the simulated grating of Figure 6.7. Note the $1/\Omega^2$ RIN increase and the movement of the dip to higher frequency, the latter a manifestation of dispersion compensation.

The above sets of figures are presented as case studies in the different ways gratings can affect laser noise. It is unfortunate that the effect is a complicated interplay of laser dynamics and propagation effects which can often only be accurately predicted with an elaborate Fourier-domain calculation. We have tried to extract some intuition into the effect where it can be found.

7.6 Laser parameters and grating design

Designing a grating for RIN reduction requires a good amount of trial and error using the numerical calculations described above. As guiding principles, first note that the grating transmission cannot be too large, or else it will create the large intensity noise increase described by (7.5). A small transmission slope can reduce the RIN if it has the correct sign, but because of the importance of the grating phase, this time domain analysis is successful only if the transmission is linear over a bandwidth much larger than the signal. Finally, one should aim for well-apodized gratings to reduce the reflection sidelobes in the grating spectrum and the peculiarities they cause, as in Figure 7.4. Our numerical calculation indicates that this laser should be capable of more than 5 dB of RIN reduction with an appropriate grating. Reductions of 7 dB have been achieved with a Michelson interferometer at low frequencies [63], and there is no physical reason why this result could not be duplicated with a fiber grating.

Unfortunately, there appears to be no simple algorithm for choosing grating parameters for RIN reduction given a set of laser parameters. It is clear that the design of a grating will need to take those parameters into consideration, as changing them in the calculations above changes the RIN curves. We can deduce some of these relationships from our analytical expressions. In (7.4) the $S^{\perp}(\omega)$ term creates a new noise floor that was ignored in (7.5). We can test this assumption with the numerical calculations.

Figure 7.12 shows the RIN before and after the grating of Figure 7.4 (the difference between the "before grating" and "after grating" lines in Figure 7.12 equals the calculated change in RIN of Figure 7.4). The contribution from the "perpendicular" term $S_{\Delta P}^{\perp}(\omega)$ to the RIN after the grating is also shown, and is more than 15 dB smaller than the $S_{\Delta P}^{\parallel}(\omega)$ contribution, which is almost identical to the full RIN. Thus the approximation is a good one, and furthermore, the change in the RIN will not be sensitive to the overall noise constant $K\omega_{ST}$. This can be seen from (7.4). However, the change in RIN is sensitive to α and the relaxation frequency Ω_0, which change the optimum slope needed to reduce the RIN (see 7.5).

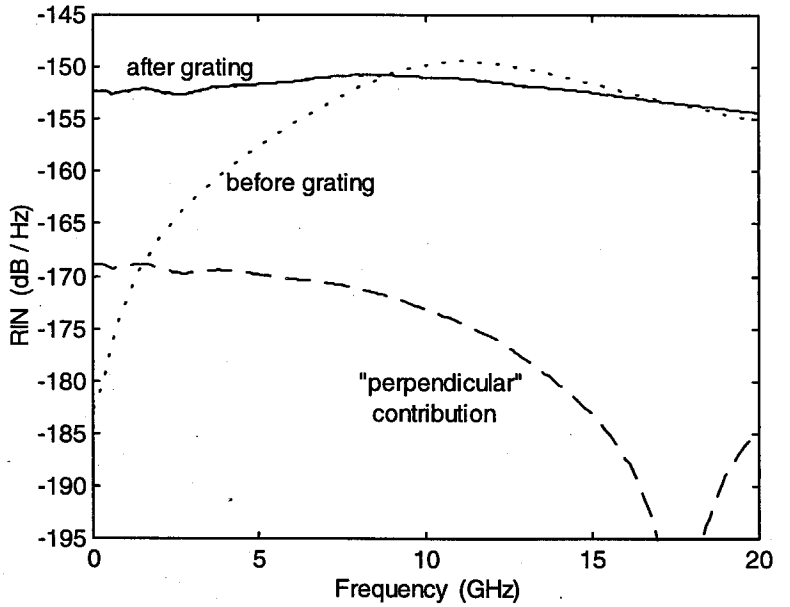

Figure 7.12. RIN before and after the grating of Figure 7.3. The "perpendicular" contribution $S_{\Delta P}^{\perp}(\Omega)$ is negligibly important in this case; the RIN after the grating is dominated by $S_{\Delta P}^{\parallel}(\Omega)$.

The situation is the same for the grating of Figure 7.6--the $S^{\parallel}_{\Delta P}(\omega)$ contribution and the total RIN are more than 20 dB larger than the $S^{\perp}_{\Delta P}(\omega)$ contribution. However, we are prevented again from drawing a general conclusion by the presence of a counter-example. Figure 7.13 shows the change in RIN due to 8.8 km of fiber and the grating of Figure 7.9, broken down by "parallel" contribution $S^{\parallel}_{\Delta P}(\omega)$ and "perpendicular" contribution $S^{\perp}_{\Delta P}(\omega)$. Both terms contribute to the overall noise strength, and thus the change in RIN does depend on the value of $K\omega_{ST}$. Note that $\kappa = \varepsilon P_0 / \tau_{ph}$ does not enter into (7.4) or our simulations at all, which is somewhat surprising. The dependence of the change in RIN on output power comes via Ω_0 and not the adiabatic chirp parameter.

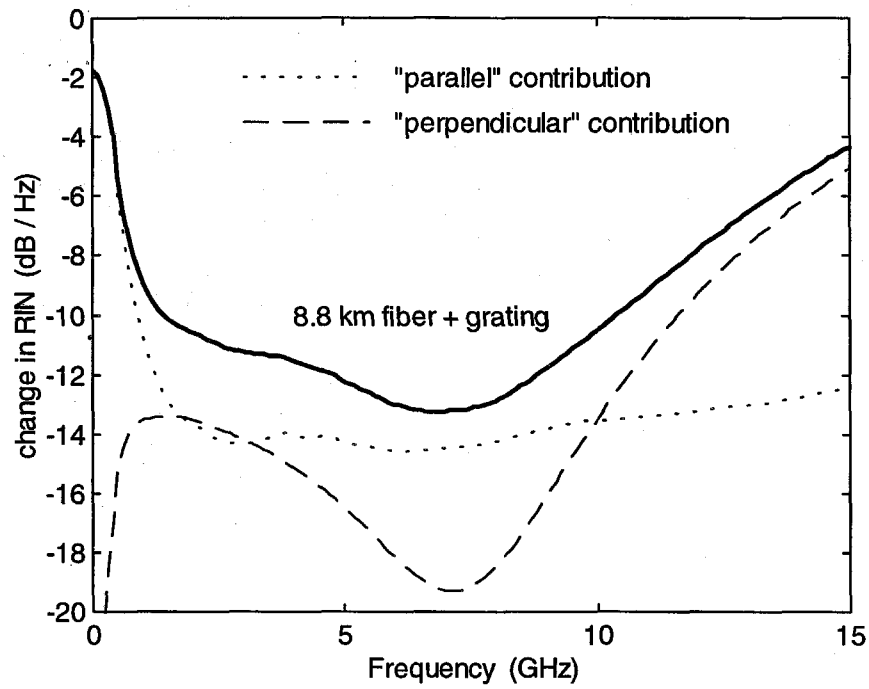

Figure 7.13. The simulation for the fiber + grating line of Figure 7.9, broken down by components. This is an example of a case in which the "perpendicular" contribution $S_{\Delta P}^{\perp}(\omega)$ is not negligible.

Chapter 8 -- Fiber Gratings in Communication Systems

The previous two chapters have shown that fiber gratings can be used to increase the AM signals of directly modulated lasers and to decrease their RIN. The natural question is whether these can both be done at once. All the investigations of the author indicate that they cannot. It seems that when a grating increases the AM signal, it also increases the RIN, although we cannot prove that this is always true. We can show, though, that in many cases the AM signal can increase by more than the RIN increases, thereby improving their ratio. The outlook is further improved when we consider the ratio that matters the most in real systems, that of signal to total noise, including shot noise and amplifier noise. We take up these calculations in this chapter.

Another alternative heretofore unconsidered is the use of digital modulation schemes, or optical pulses. In this context, fiber dispersion is manifested in the temporal broadening of pulses as they travel along a fiber. We will show in the second half of this chapter that here too an advantage can be gained by propagation through a fiber grating.

8.1 Signal to RIN ratios

We start with the simplified metric of signal-to-RIN ratios. Does a fiber grating that increases a laser signal do so by more than it increases the RIN? Or does a grating

which reduces the RIN do so by more than it reduces the signal? In many real systems we need the answer of one of these to be yes for the grating to be of practical use. (Many, but not all; for example, if a laser is externally modulated, we might insert a grating after the laser but before the modulator to reduce the RIN, without worrying what the grating would do to a direct-modulation signal.)

We start by looking at the example of the simulated grating of Figure 6.4, chosen because it produced an impressive ~10 dB increase in AM signal for the laser with which it was measured (without subtracting connector losses). Figure 8.1 shows this same result plus the change in RIN the grating would produce, calculated from the numerical routine of Chapter 7 with the same laser parameters measured experimentally. The strong frequency discrimination of the grating that boosts the signal also produces the $1/\Omega^2$ increase of noise. However, above 10 GHz, the signal is increased by more than the RIN–the change in the signal-to-RIN ratio is positive here, reaching a maximum of 6 dB above 20 GHz.

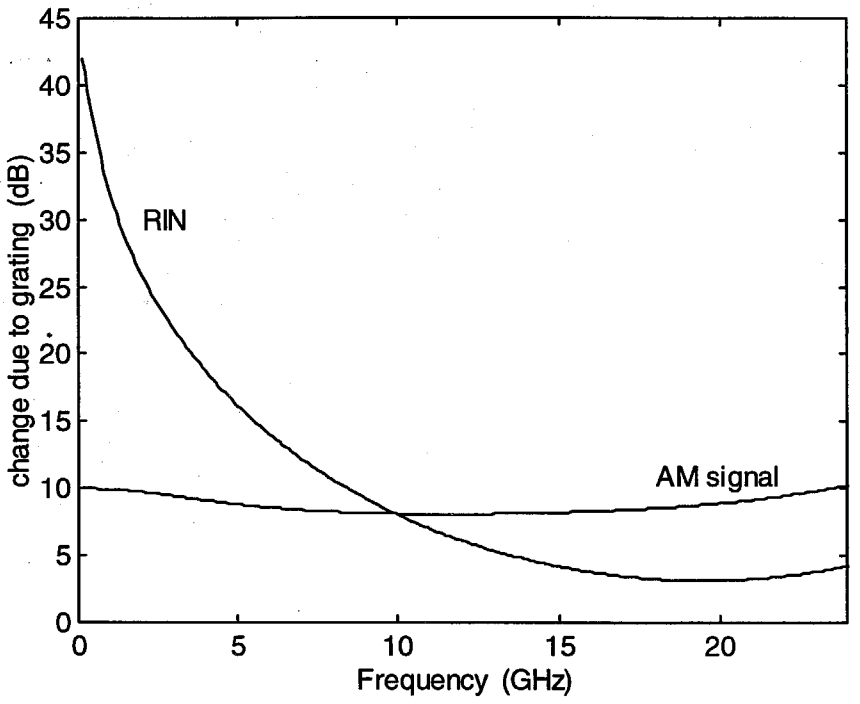

Figure 8.1. Change in RIN and AM signal due to the simulated grating of Chapter 6. The AM signal is boosted by the ~10 dB seen earlier, and the RIN exhibits a familiar $1/\Omega^2$ increase. Above 10 GHz, though, the signal is increased by more than the RIN is.

The above plot is the effect of the grating only, and for optical communication systems we of course have to include fiber. We saw in Chapter 6 that this grating smoothes out the dips and peaks of the fiber transfer function, and we saw in Chapter 7 that this grating postpones the dip in RIN that fiber causes and adds a $1/\Omega^2$ RIN increase (Figure 7.11). If we combine the two and calculate a signal-to-RIN ratio with and without fiber, we get Figure 8.2.

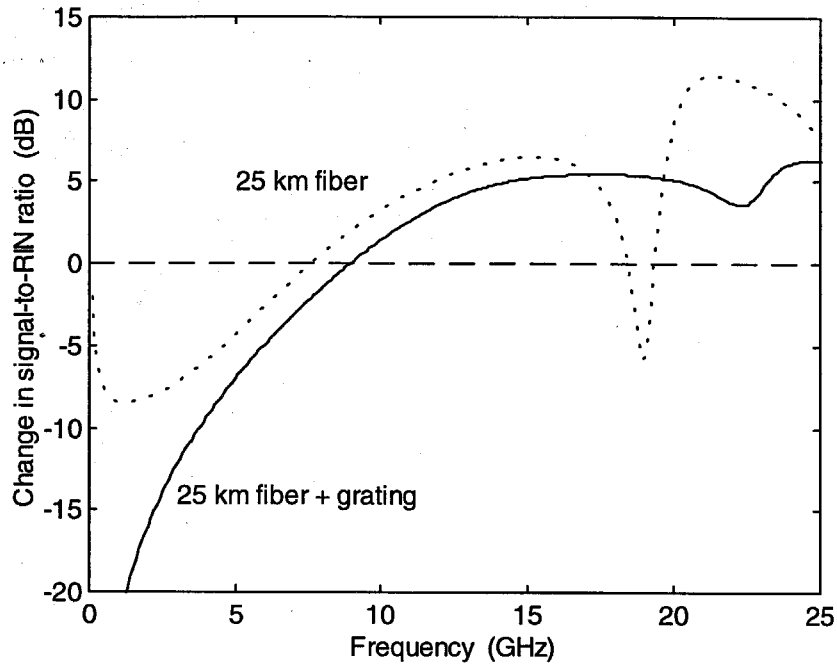

Figure 8.2. Change in signal-to-RIN ratio after 25 km of fiber, with and without the simulated grating of Chapter 6.

We see the grating hurts the ratio of signal to RIN at low frequencies, because of the $1/\Omega^2$ increase in RIN, but it smoothes the dip at 18 GHz. For 50 km of fiber, the situation is the same--the grating makes the ratio generally worse after fiber, but the big dips in the ratio, caused by the near-zeroes in $H_{||}(\Omega)$, are removed. This could be of benefit in intraband modulation schemes--those in which the signal applied to the laser contains an electronic carrier wave, in the 10 GHz range for satellite relay links, whose frequency may fall in a dip produced by dispersive fiber.

Suppose that instead of choosing a grating that increased the signal (using that of Figure 6.7) we choose one that lowers the laser noise (like that of Figure 7.2). Below we

see the AM signal and RIN after the grating of Figure 7.6. The RIN is decreased by the ~1.5 dB seen before, and the AM signal is decreased by approximately the same amount up to 15 GHz, at which point the signal increases and the signal-to-RIN ratio is benefited by the grating. If we add 10 km of fiber, the RIN is reduced more than the signal is, making the fiber plus grating combination better than fiber alone. However, the difference is only a few dB, and the lesson is that gratings which increase the signal or decrease the RIN may end up with a better signal-to-RIN ratio than with fiber alone, but only over a limited frequency range and only by several dB.

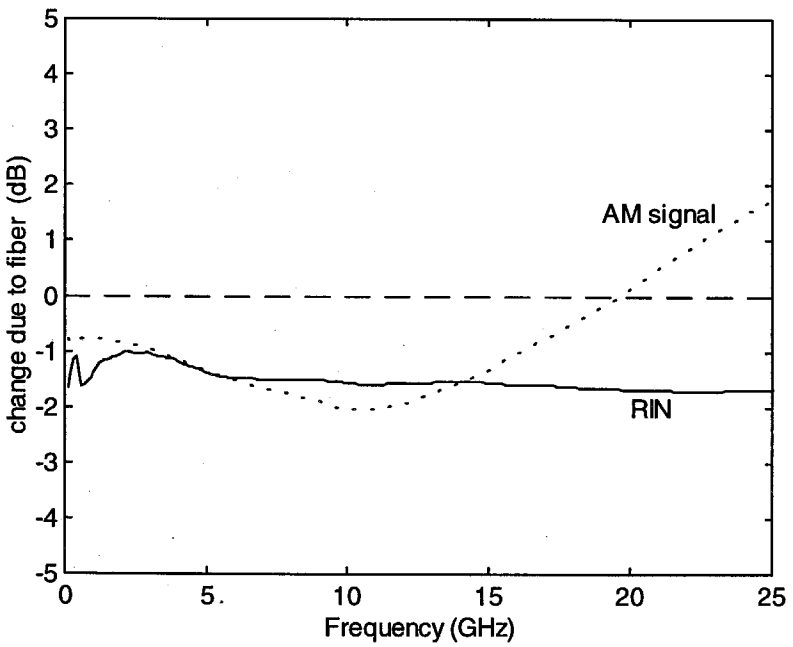

Figure 8.3. Change in signal and RIN due to the grating of Figure 7.4, which lowered RIN, and the signal too, but not prohibitively. The grating is useful only above 15 GHz. No fiber is included here.

8.2 SNR and fiber attenuation

Although the ratio of signal to RIN before and after the addition of a grating can tell us that a grating is useful, it cannot always tell us that a grating is not useful. The reason is that shot noise and amplifier noise may be the dominant portion of the total system noise, so an increase in RIN caused by the grating might have no impact on the total noise level. To calculate the total system noise and thus the signal-to-noise ratio (SNR), we have to quantify the amplifier and detector noise of a system, as described in Chapter 4. From (4.2),

$$\langle i_N^2 \rangle = G(\nu)\Delta\nu\left[f_N(\nu) + 2e\langle i\rangle + [RIN]\langle i\rangle^2\right] \tag{8.1}$$

we see the detected DC photocurrent <i> will affect the magnitude of these noise powers differently--the amplifier noise is constant with photocurrent, the shot noise linear, and the laser noise quadratic. In Figure 8.4 we see the result of this calibration done for our system. The figure shows $\langle i_N^2 \rangle$ versus <i> for different values of laser RIN.

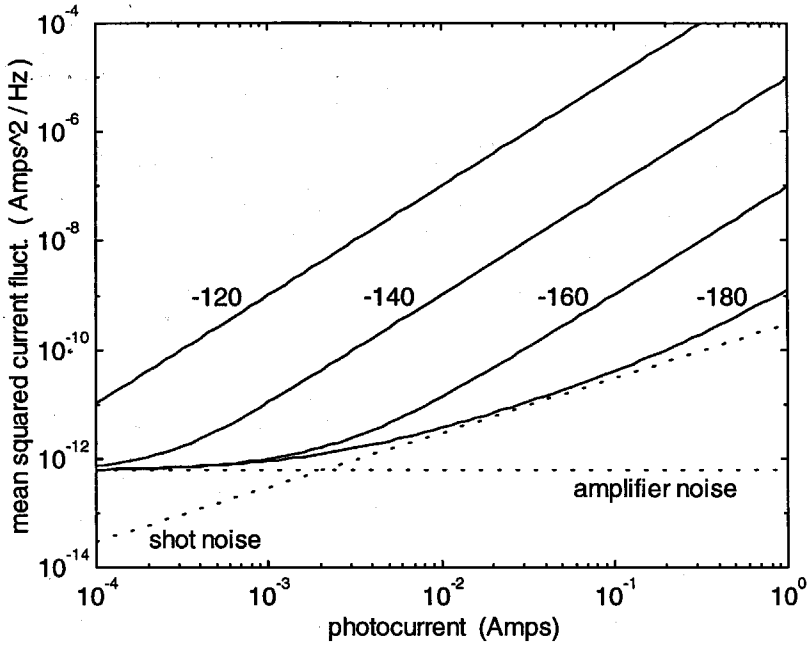

Figure 8.4. Mean square current fluctuations versus photocurrent for different values of the RIN, using the detector and amplifier characteristics measured for our system.

At RIN = -120, the total noise is comprised entirely of the laser noise. At -140, the laser noise dominates except below a current of about 0.3 mA, at which point the amplifier noise is apparent. At no point is shot noise important for this RIN value. At RIN = -180, the limiting noise is from the amplifier at low current, shot noise from 2 mA to 300 mA, and laser noise above that. A good RIN to calibrate the coefficients of (8.1), as explained in Section 4.3, would be -160, using photocurrents from 0.1 mA to 10 mA. This range would cover the amplifier noise, shot noise, and laser noise regimes all pretty well, and allow a good fit for the constant, linear, and quadratic terms.

Note that the shot noise level can be lowered only by changing $G(\nu)\Delta\nu$ in (8.1), and the other noise terms change by the same amount. The amplifier noise can be

lowered with a lower noise figure amplifier, and one would like the amplifier noise power to remain smaller than the shot noise power for as low a photocurrent as possible. We would also prefer as low a RIN as possible, but for a given maximum photocurrent, there's a minimum RIN below which improvements in RIN make no difference. For example, in Figure 8.4, if we know our photocurrent will always be less than 100 mA, lowering the RIN below -180 dB/Hz will not lower the total noise power, since shot noise and amplifier noise already dominate.

Figure 8.4 is the characterization of the system that allows us to convert RIN and AM signal data into a SNR. Returning to the grating of Figure 8.1, we have measured the grating by its effect on RIN and AM signal. We convert this into a change in SNR by assuming a detector photocurrent--the result of three different values is shown in Figure 8.5. At each frequency Ω, we've calculated both the signal and the RIN before and after the grating, then we use the assumed photocurrent and the RIN *at that frequency* to calculate the total system noise à la Figure 8.4, and then the SNR. The lower the photocurrent is, the less of the total noise is determined by the laser noise (RIN), so the less we're penalized for the $1/\Omega^2$ increase in RIN the grating produces. If the current is below 0.5 mA, the SNR is increased by the grating at all frequencies.

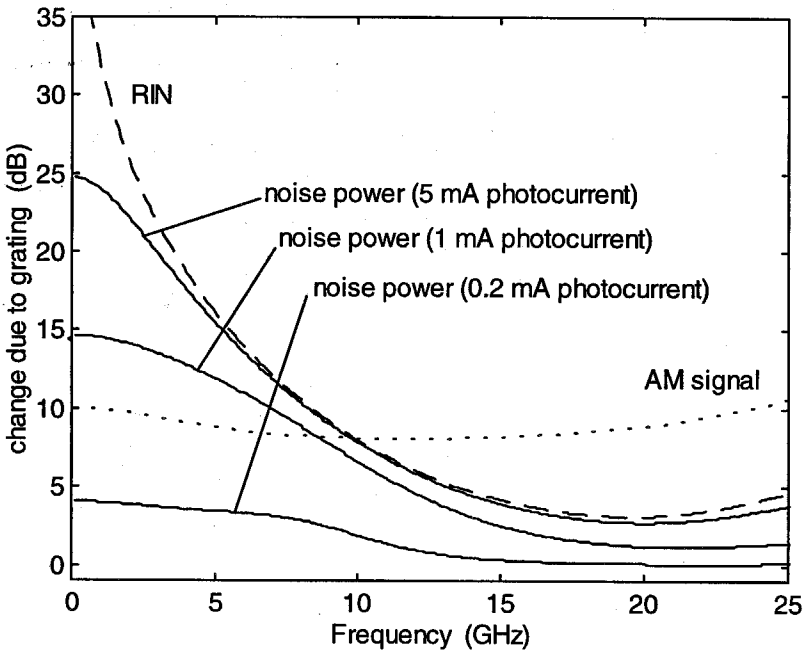

Figure 8.5. Change in RIN, AM signal, and total noise power for different photocurrents, using the grating and laser parameters of Figure 8.1. At a photocurrent of 0.5 mA, the SNR is increased at all frequencies.

Keep in mind that Figure 8.5 only indicates the *change* in SNR due to the grating. Though the grating helps the most at low photocurrents, it does not mean we should artificially lower the photocurrent when we have a grating. If the optical intensity transmission of a medium is T (where $T < 1$ corresponds to attenuation), the electrical power of the AM signal carried by the light is lowered by a factor T^2 in traversing the medium. This has been included in all of the grating/AM signal calculations so far. The RIN of the light is unchanged by the attenuation, since it measures noise *relative* to the DC intensity--we can see from (8.1) if <i> is lowered by a factor T, and RIN is unchanged, the laser noise power is lowered by T^2. Thus in the regime where laser noise

determines the system noise, attenuating the beam has no effect on the SNR, since both signal and noise decrease by T^2. But since shot noise is lowered by T and amplifier noise not at all, in these regimes the signal power is attenuated by more than the noise power. Thus it never helps the SNR to attenuate the beam, and it mostly hurts; Figure 8.5 merely shows that in these low-photocurrent regimes, a grating can be useful.

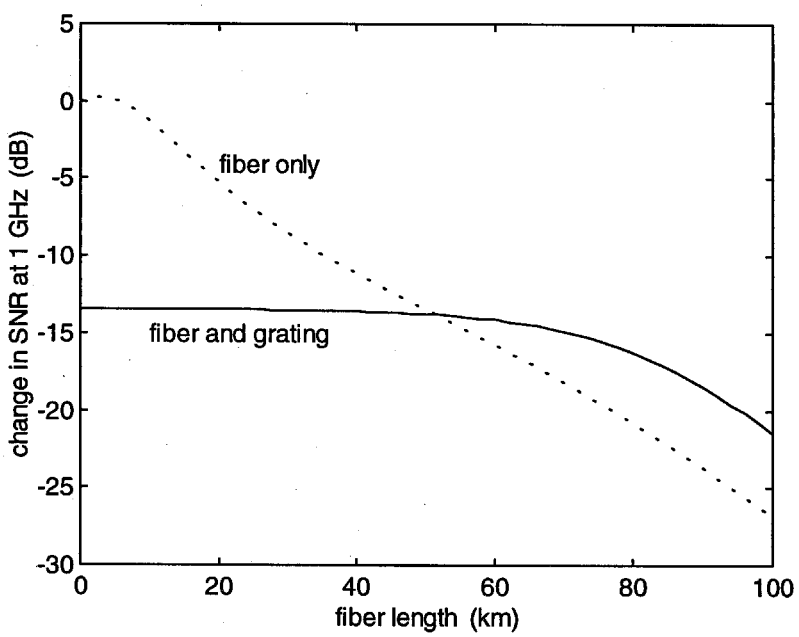

Figure 8.6. Change in SNR at 1 GHz, versus fiber length, with and without the grating of Chapter 6.

The final step in assessing the benefit of the grating is to include the effect of fiber. The fiber changes both the signal and the RIN because of dispersion, and we can use our previous studies to quantify this. In addition, the fiber attenuates the beam,

typically by -0.2 dB per kilometer at 1550 nm, changing the received photocurrent and thus the calculation of SNR. Figure 8.6 shows the change in SNR versus fiber length at 1 GHz (typical cable TV application) for the same laser and grating used in Figure 8.5. We have assumed an initial optical power adequate to produce 10 mA of detector photocurrent with no fiber; this then attenuates by -0.2 dB per km of fiber, or -0.4 dB/km for the electrical signal power. With fiber only, the laser is mostly limited by amplifier noise at 1 GHz, and the SNR drops quickly with fiber length. The small ripples in the fiber curve are caused by the AM-FM conversion of both the signal and the RIN. For the fiber plus the grating, the SNR is immediately much worse, because of the huge increase in RIN at 1 GHz caused by the grating. Since the system is now limited by laser noise, the SNR is constant as the beam is attenuated. At about 50 km, the total noise drops down to the shot noise level, and we start to reap the benefit of the 10 dB increase in the signal. Beyond this distance of fiber, we are better off using the fiber grating.

To decide whether to use a fiber grating in a real system, then, one needs to know the laser characteristics (noise, modulation response, chirp), the fiber length needed, the optical power to be used, and the noise characteristics of the amplifier. Given this, one can use the above numerical techniques to calculate the change in the SNR due to dispersive fiber, and compare that to fiber plus a grating. For the above example, the grating helps--and keep in mind that the simulations above were for an off-the-shelf grating purchased without this purpose in mind. It is very likely that by trial-and-error design of the grating, one can achieve significant (more than 5 dB) improvement in SNR with an inexpensive grating.

8.3 Pulse broadening and re-narrowing

We will conclude this chapter, and this thesis, with a look at an as yet unexamined method of optical communication, in which information is transmitted not via analog AM signals but in discreet pulses. In this context fiber dispersion manifests itself though the temporal broadening of narrow optical pulses. If the initial pulse has a Gaussian intensity profile (a common simplifying assumption) of the form

$$I(t) = \frac{C}{\sqrt{2\pi\sigma^2}} \exp\left(\frac{-t^2}{2\sigma^2}\right) \tag{8.2}$$

where $\sigma >> 1/\omega_0$ measures the pulse width and C is the integrated energy of the pulse, then the width after a length L of fiber with dispersion constant D is given by [49]

$$\sigma_{\text{after fiber}} = \sigma\sqrt{1+\left(\frac{DL\lambda^2 \ln 2}{\pi c \sigma^2}\right)^2} \tag{8.3}$$

The more narrow a pulse is originally, the more quickly it broadens as a function of fiber length.

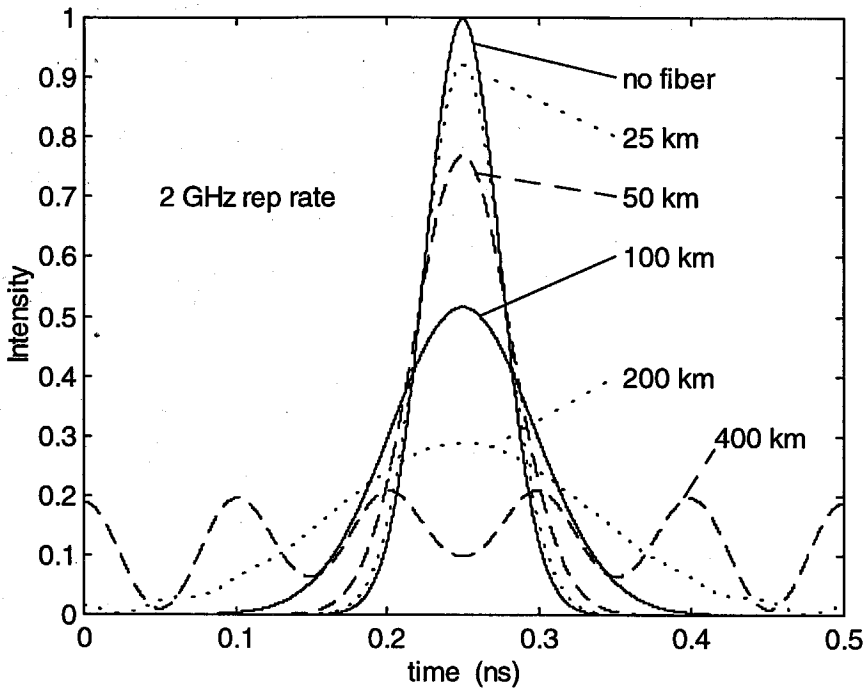

Figure 8.7. Gaussian pulses after various lengths of dispersive fiber. The integrated intensities of each pulse are the same.

Figure 8.7 illustrates this for a train of pulses with initial width of $2\sigma = 49$ ps and a repetition rate of 2 GHz. As the length of fiber is increased, the pulses become broader, and begin to overrun each other, producing ripples that are minor at 200 km and all that remain at 400 km. The integrated intensity of each pulse is the same, because energy is conserved as the pulse broadens. These pulses were calculated using the numerical Fourier-transform technique depicted in Figure 3.3, using an input electric field E(t) consisting of a carrier wave and an envelope function whose square (the intensity I(t)) is of the form (8.2) above. Unlike the previous analysis, there are no laser dynamics that go

into this--we can imagine the pulses are created by a chirp-free external optical modulator.

The effect of transmission through a grating is calculated in the familiar way, using the grating transmittance t(ω) to calculate the Fourier-transformed output field $\tilde{E}_{out}(\omega)$. We will use for comparison's sake the same grating of the previous chapters: that of Figure 6.7 (dotted line, the coupled-mode solution), with the laser center wavelength as indicated in the Figure 6.7. Figure 8.8 shows the result for an input pulse

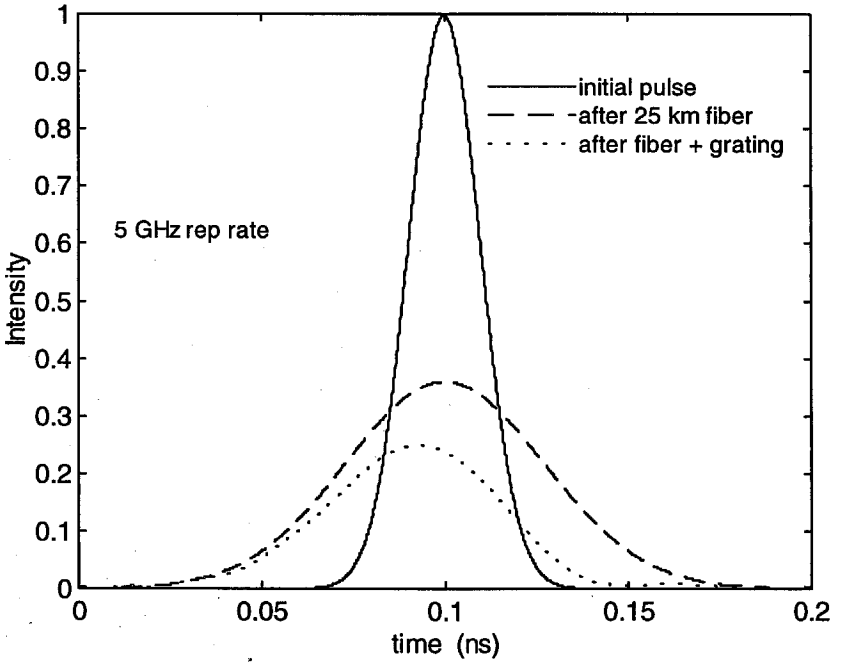

Figure 8.8. Gaussian pulse after 25 km of fiber and after 25 km of fiber plus a fiber grating. For comparison, the grating is identical to the simulated grating of Chapter 6. Note the trailing red edge of the pulse is clipped more than the leading blue edge.

train with a 5 GHz repetition rate. The pulse is broadened after 25 km of fiber, but has the same integrated intensity. If we put a grating after the fiber, the pulse is re-narrowed, mostly by a loss of intensity in the trailing half of the pulse.

The integrated intensity of the pulse after the fiber grating is 60% of its initial value, reflecting the grating loss. (The optical transmission at the carrier frequency is $T(\omega_0) = 0.68$, but the transmission is not linear and the average across the pulse bandwidth is 0.60.) The smaller pulse energy can be remedied with an optical amplifier--it's easier to increase the energy of a pulse than to narrow its width. If we re-scale each pulse by its maximum value to simulate this amplification, we see more clearly the narrowing of the pulse by the grating, as shown in Figure 8.9.

Note that the pulse shape is distorted somewhat by the grating--there is a satellite peak following the main pulse, though in this case it looks negligible. The pulse is clearly attenuated in the back edge more than the front. This is because the dispersive fiber not only broadens the pulse but gives it a linear frequency chirp [49]. Recall from the discussion following (3.27) that in standard fiber blue components of a signal travel faster than the red components (where $D > 0$). Thus the leading edge of the fiber-broadened pulse in Figure 8.9 has a more blue instantaneous frequency than the trailing edge. We see from the grating spectrum in Figure 6.7 that the blue components are preferentially transmitted and the red reflected; thus this frequency discriminator narrows the pulse by shaving off the trailing red edge.

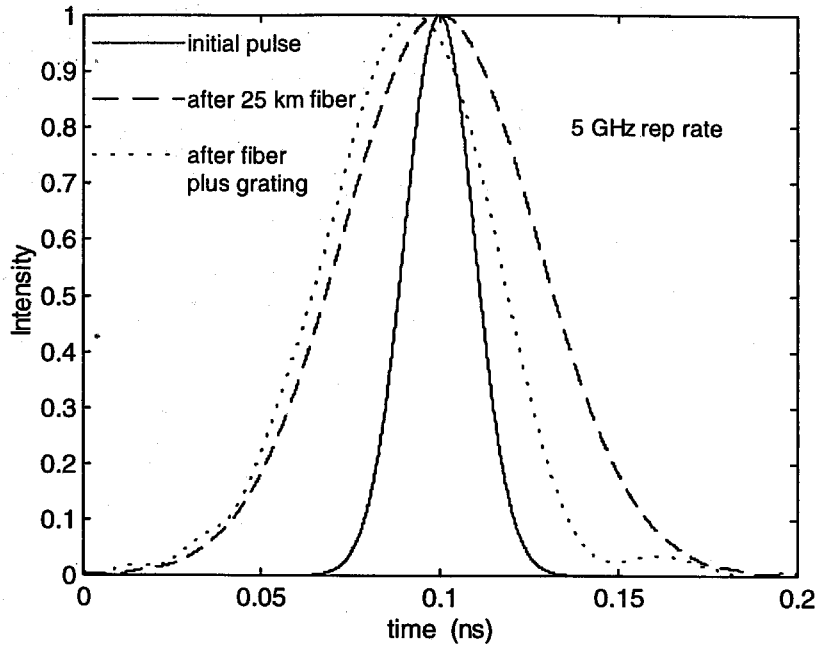

Figure 8.9. The three pulses of Figure 8.8 scaled to have the same maximum value. The grating clearly re-narrows the dispersion-broadened pulse somewhat.

The grating does not produce a uniformly more narrow pulse after any length of fiber; in fact, with no fiber, the grating widens the pulse, because the initial pulse is unchirped (and thus can't be narrowed by our frequency discriminator) and the grating's own dispersion only broadens the pulse. Figure 8.10 shows the pulse width versus fiber length with and without this grating; we see that below 7.1 km, we are better off not using the grating. The repetition rate is 5 GHz.

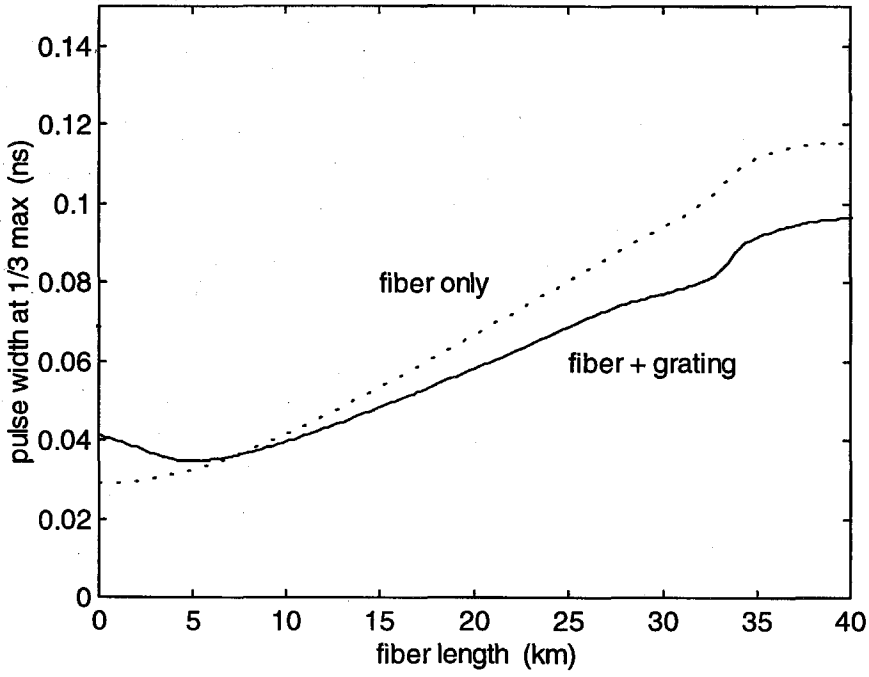

Figure 8.10. Pulse width (full width at one-third max) versus fiber length. The dotted line is for fiber only; the solid line is for fiber followed by a grating.

As the pulse widens, it accumulates ripples in its leading and trailing edge that grow in size with fiber length. Eventually they become a sizable fraction of the pulse height and must be considered as contributing to the pulse width (for a clear example of these ripples, look ahead to Figure 8.13). The width by which the pulse is measured in Figure 8.10 is the full width at 1/3 of the maximum intensity. We cannot use the Gaussian width σ because, after the distortion of the grating, the pulse is no longer Gaussian. We could use the full width at half-max, but we chose a more conservative estimate which is more sensitive to the ripples and satellite peaks created by the grating.

As the pulse broadens, the size of the secondary bump in Figure 8.9 produced by the grating becomes larger compared to the main peak. Eventually it reaches 1/3 of the maximum pulse intensity and the width measured by this yardstick will leap upward. The bumps in the width vs. fiber length plot of Figure 8.10 are caused by successive ripples in the pulse reaching 1/3-max height. (For a Gaussian pulse, the full width at 1/3-max is 2.96σ).

8.4 Chirped pulses and frequency discrimination

Because the blue components of a signal travel faster in standard fiber, the front edge of the pulse is more blue than the trailing edge, and the instantaneous frequency decreases linearly with time as the pulse passes. If the pulse is initially pre-chirped in the opposite direction, so that the leading edge is more red and the blue components are launched last, the pulse will first be narrowed by the dispersion before broadening again. In this case, the grating turns out to be almost uniformly better than no grating--now even with no fiber the pulse has a linear chirp, and the frequency discriminator can selectively transmit one half of the pulse. Figure 8.11 shows the pulse width of a pre-chirped pulse whose initial instantaneous wavelength decreases linearly at a rate of 1 Å per full-width (2σ = 49 ps) of the pulse. We see the fiber first narrows the pulse before rebroadening it, and the grating only helps matters. At the minimum pulse width occurring at about 16

km of fiber, the grating makes no difference, because at this point the fiber has removed the frequency chirp and the grating frequency discrimination is not beneficial.

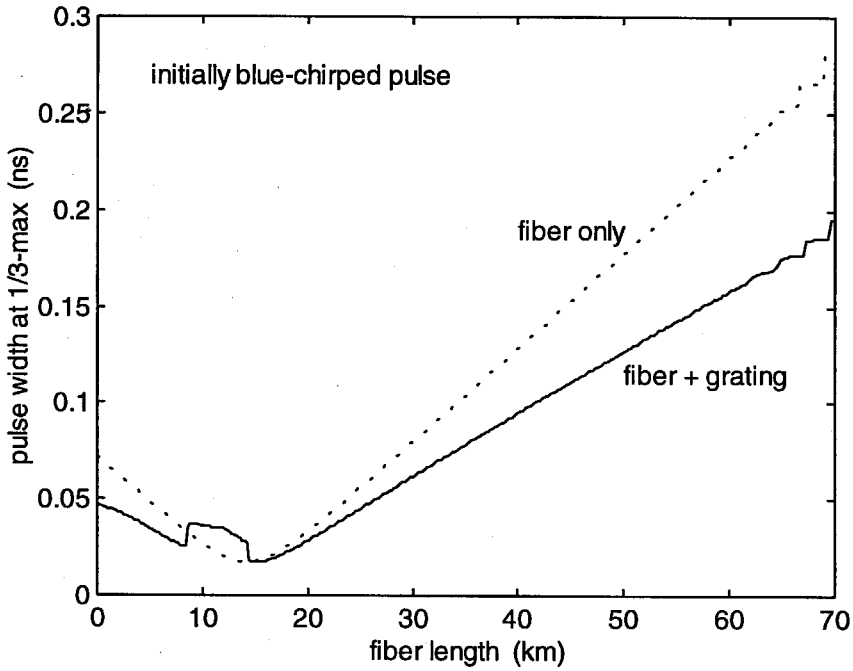

Figure 8.11. Pulse width at one-third maximum versus fiber length for an initially blue-chirped pulse, with and without the grating. The grating narrows the pulse but produces satellite peaks which can become unacceptable.

The only problem with the grating is the satellite peak it produces. Figure 8.12 shows this in the time domain for 8 km of fiber--that is, the data plotted at 8 km in Figure 8.11 are exactly the full width at 1/3-max of the pulses shown in Figure 8.12. We see the satellite peak on the leading edge of the pulse, and for fiber lengths between about 8 and 13 km, its height is more than 1/3 the maximum pulse intensity, causing the discontinuity in the "fiber + grating" line of Figure 8.11. The 1/3-max criteria is arbitrary, but it is

clear that some measure of the contributions of the secondary peaks to the pulse width must be used to demonstrate the disadvantage of the grating. Despite this, for a broad range of fiber lengths, the grating can be useful to combat dispersion broadening.

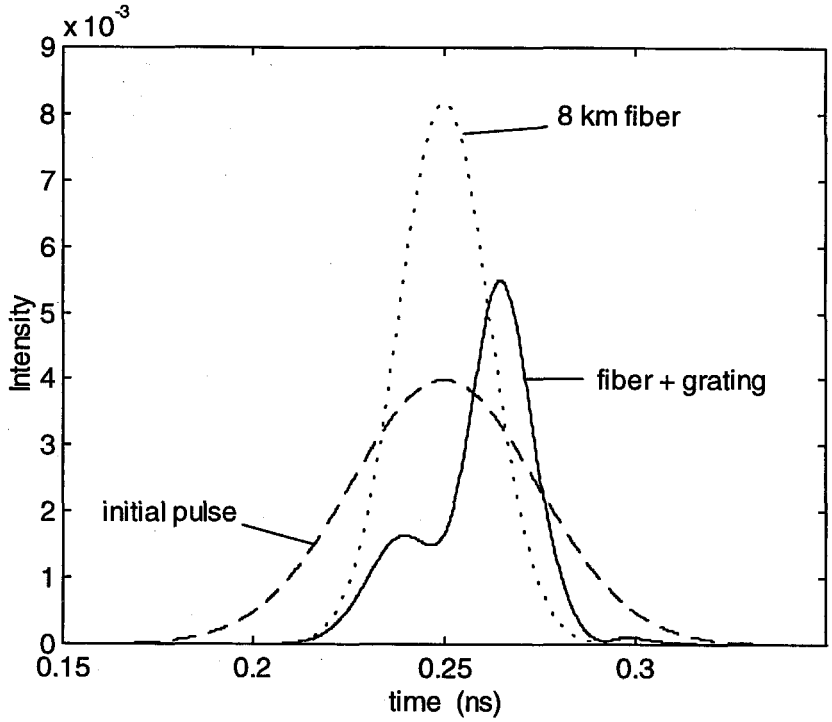

Figure 8.12. Pulse shapes after 8 km of fiber, with and without the grating, for initially blue-chirped pulse. The satellite peak on the front of the pulse, formed by the grating, serves to widen the pulse.

Note that the "fiber + grating" pulse in Figure 8.11 has less intensity in the leading edge than the training edge, compared to the fiber-broadened version. This is the opposite of the previous example--this pulse has been initially blue-chirped (meaning the

instantaneous wavelength gets more blue with time), so the leading edge is red at 0 km. The grating at 0 km narrows the pulse by shaving (reflecting) the leading red edge. This is still the situation after 8 km of fiber. After 13 km, the minimum width distance, the blue-chirp is gone and the fiber has created a red-chirp, and the grating now blocks the trailing red edge. Figure 8.13 shows the same pulse after 70 km of fiber, demonstrating the loss of the red trailing edge. Here the satellite peaks have been replaced by ripples.

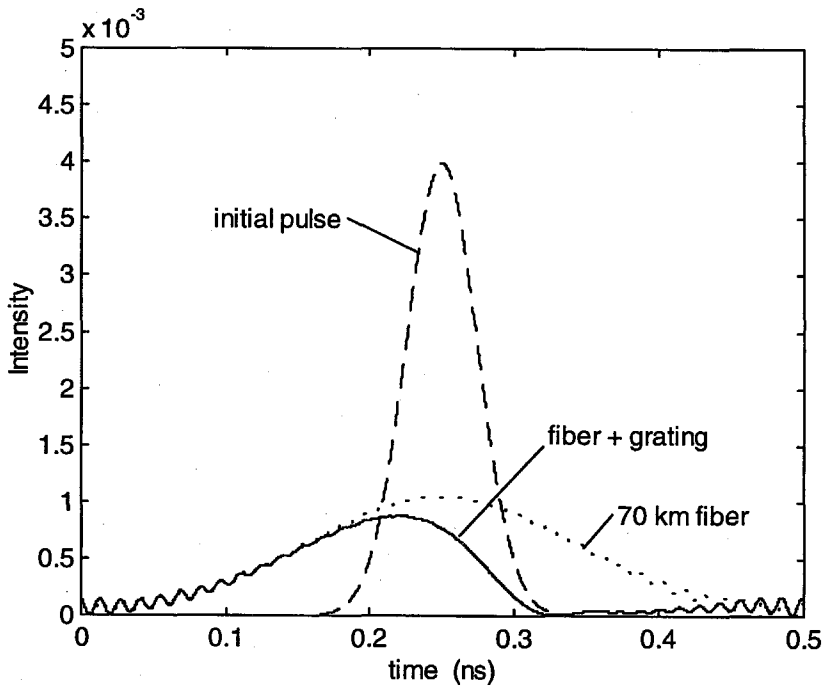

Figure 8.13. Pulse width after 70 km fiber, with and without grating, for initially blue-chirped pulse, now red-chirped by the fiber.

We have been assuming a pulse train thus far, and the ripples we see in the leading edge of Figure 8.13 are a consequence of this--they are caused by the overlap of

this pulse with its neighbor. This is a real phenomenon and will occur if the adjacent pulse is coherent with the first, which will happen when the laser coherence time is longer than the repetition rate. Since a typical DFB laser linewidth is tens of MHz and the repetition rate is GHz, this is true by a wide margin. We can recalculate the time-domain evolution for a much slower repetition rate to remove those ripples.

Figure 8.14 shows the same two pulses as Figure 8.13--initially blue-chirped, after 70 km of fiber and fiber plus the grating--without the effect of neighboring pulses. The ripples are gone, and the grating distortion is manifested in a trailing satellite peak, which may be of concern if it is large enough. The pulse is decidedly more narrow, and it will depend on the particular detection and decoding scheme whether the satellite peak is less desirable than the narrower pulse. In the case of this pulse, the secondary peak has a maximum intensity that is 10.02% of the global maximum, and contains 7.23% of the entire pulse's integrated intensity. It is probably negligible, or at worst removable with an electronic discriminator after the detector.

Figure 8.14 also shows the pulses that would result from a phaseless and phase-only version of our grating. We see the pulse narrowing is due to the frequency discrimination of $|t(\omega)|$--the phase of the grating has a rather small effect on the final pulse shape. This confirms the claim made so far that the narrowing is due to the frequency discrimination of the grating, rather than dispersion compensation, which we would attribute to the non-linear grating phase.

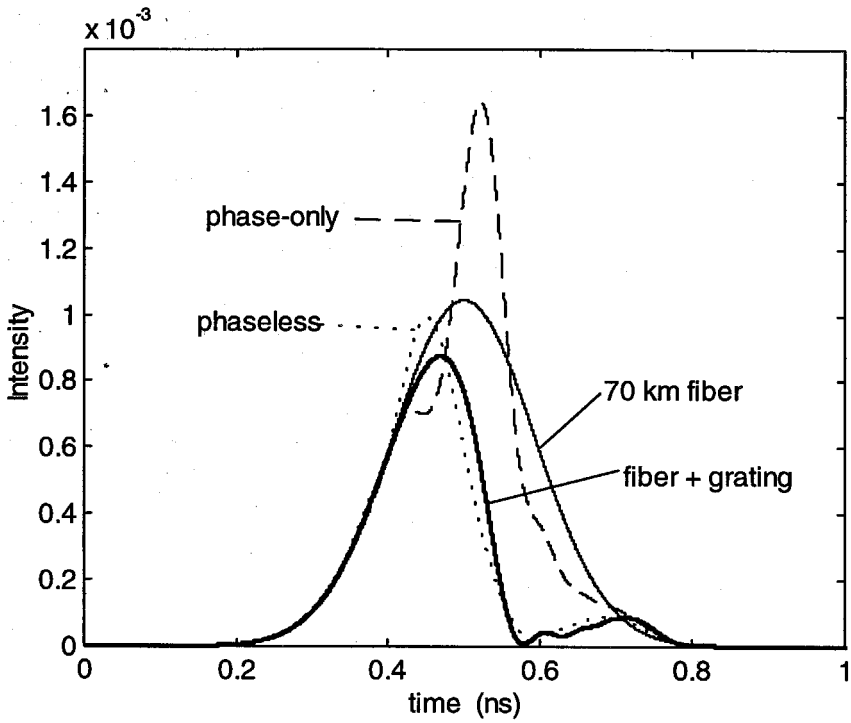

Figure 8.14. A close-up of Figure 8.13: the thin solid line is the pulse after 70 km of fiber, and the thick solid line is after fiber plus the grating. The dotted and dashed lines show the result of the simulation using a phaseless grating transmittance $|t(\omega)|$ and a phase-only transmittance $t(\omega) / |t(\omega)|$. The frequency discrimination of $|t(\omega)|$ clips the red trailing edge.

The preceding pulses have all be chirpless or with an initial linear frequency up-chirp. In a directly modulated laser, we are not so lucky, as the chirp is determined by the adiabatic and transient chirp phenomena of the laser. For large signal modulation schemes, which pulsed system necessarily are, the small-signal rate equations we used to derive the nature of that chirp no longer hold. We can get a feel for the complications introduced by the laser chirp by making some crude approximations and interpreting the results only qualitatively. We assume our laser has a CW output power of P_0 and a

"small-signal" pulsed output $\Delta P(t)$ that goes from 0 to P_0 and back to 0. We used (2.29) to calculate the instantaneous optical phase perturbation accompanying this direct modulation pulse.

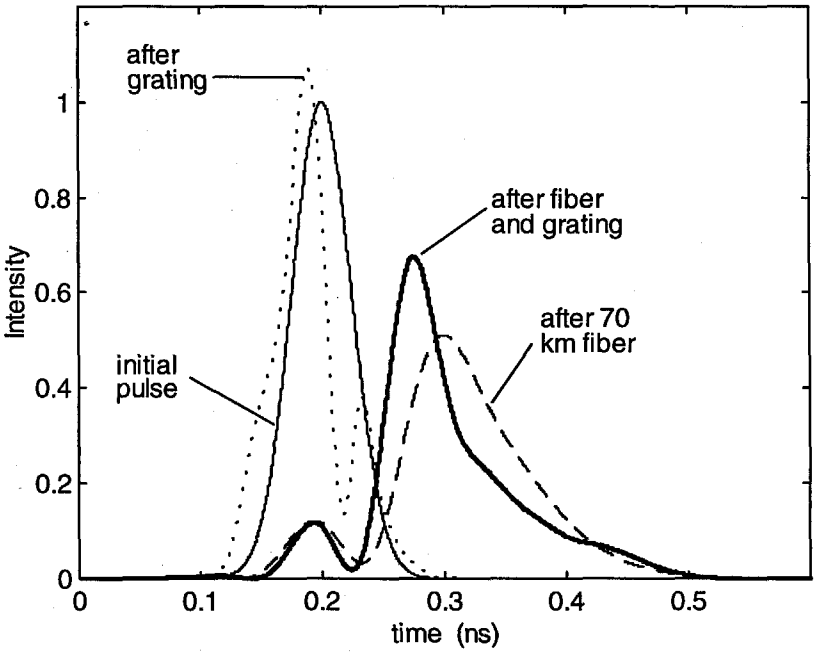

Figure 8.15. Evolution of a pulse from a directly modulated laser, showing (crudely) the complications of adiabatic and transient chirp. The intensity is measured by $\Delta P(t) / P_0$ and we've taken $|\alpha| = 4.32$ and $\kappa = 8.4$ GHz. It is not clear that the grating helps matters.

Figure 8.15 shows the result. The pulse is of course no longer linearly chirped, either before or after the fiber, and the effect of the grating is not intuitive. Although the grating gives the pulse a larger maximum intensity after 70 km of fiber, and the leading bump may be negligible, it is far from clear that the grating-produced pulse is preferable

to the fiber-broadened pulse. The point is that a grating is most advantageous for re-narrowing pulses whose frequency chirp is a result of dispersive fiber; in direct modulation schemes with large-signal laser chirp, it is unlikely we can derive the same advantage.

8.5 Summary of system applications

We conclude with a summary of where fiber gratings would be useful in real optical communication systems, incorporating the lessons of the previous three chapters. All of the applications we've analyzed involve gratings in a transmission geometry, which avoids the need for optical circulators (couplers and isolators), conserving optical power, and can remain entirely fiber-based.

A grating can increase the size of an AM laser signal by converting laser chirp into excess AM signal power. This allows one to increase the optical modulation depth of a signal without increasing the electrical (injection current) modulation index--for example, to avoid laser non-linearities and stay in the small-signal regime. Combined with fiber, the grating can flatten the dispersion-distorted frequency response of the system, smoothing out the maxima and nulls the fiber produces. For an intraband modulation scheme in which the electronic carrier wave frequency falls at a null of the fiber transfer function, adding a grating to boost the system response at this frequency may be cheaper than adding more fiber to change the dip frequency.

Gratings can reduce the RIN of a laser. If the optical signal is generated with an external modulator, the change in the directly-modulated AM signal this grating would cause is irrelevant, and the RIN reduction is useful outright. The RIN can be lowered after a fixed length of fiber also, and the peaks and dips in the RIN curve after a length of fiber can be adjusted with a grating.

The signal-to-noise ratio of a directly modulated laser and fiber system can be improved with a grating, either in certain frequency ranges and/or in systems which are limited by amplifier or shot noise. This may reasonably include systems with fiber lengths in the tens of kilometers.

A grating can compensate for dispersion by virtue of its dispersive transmittance phase, or, more markedly in the case of dispersion-broadened pulses, by virtue of their frequency discrimination. This is most useful with low-chirp external modulators, which is the preferred method of digital modulation, rather than with direct modulation. An optical amplifier may be necessary to recover power removed by the grating.

Incorporation of gratings into useful systems will require grating design aided by a numerical calculation and trial and error, but guided by intuition into the roles of frequency discrimination and dispersion, AM/FM inter-conversion, and the dynamics of laser modulation, chirp, and noise.

Appendix A -- Numerical Propagation Routine

In this appendix we give a listing of a routine which performs the numerical calculation described in Figure 3.3. The result is the transfer function for a fiber grating that describes the change in a directly modulated laser signal. The routine is written for the Matlab mathematics software package, and makes use of a function t_gauss which calculates the complex transmittance of a grating, described in Appendix B.

```
%     gratCALC.M

lairB = 1540.00e-9;      % Bragg lambda in air
lairopt = 1539.898e-9;   % optical lambda in air

% [this is used if lairopt is swept]
%Hg1GHz = [];
%lairopt_arr = [];
%for lairopt = 1539.70e-9 : .01e-9 : 1540.0e-9  ;

N = 2^10;          % elements in FFT arrays

Nper = 22500;            % periods in Bragg grating

c = 3e8;
wB = c*2*pi/lairB;       % Bragg (optical) freq
wopt = c*2*pi/lairopt;   % center optical freq of carrier wave

n = [ 1 : N ];

Hg = [];          % AM transfer functions
Hf25 = [];
Hf50 = [];
Hf100 = [];
Hf25g = [];
Hf50g = [];
Hf100g = [];


Omega_arr = [];

for Omega = 0.2e9 : 0.2e9 : 25e9;      % modulation freq

      Omega/1e9    % to display while working
```

```
alpha = 4.32;            % laser parameters
BL = 1.9641e-20;
kappa = 8.4e9;

m = 0.50;          % AM index...FM index
beta = alpha/2*m*sqrt(1 + (kappa/Omega)^2);

theta_FM = atan(Omega/kappa); % FM phase lead

Et = sqrt(1 + m*sin(2*pi*n/N)).*...
      exp(-i*beta*cos(2*pi*n/N + theta_FM));
It= abs(Et).^2;

Ef = fft(Et);
If = fft(It);

% Fiber Field Transfer Function:
% positive sign in exponent should intrisically
% be negative, but I use BL>0 above...
% for fiber, BL<0 physically, so it's okay
Hopt_fib25 = exp(i*1/2*BL*( (n-N/2-1)*Omega).^2);
Hopt_fib50 = exp(i*1/2*2*BL*( (n-N/2-1)*Omega).^2);
Hopt_fib100 = exp(i*1/2*4*BL*( (n-N/2-1)*Omega).^2);


% Note: the nth element of Ef is the size of
% freq. component of Et with (n-1) periods in
% the Et array.
% e.g. n=1 is DC, n=2 is the fundemental
% "harmonic" with one period across the array.
% After the fftshift, the nth element of
% fftshift(Ef) is the component with (n-N/2-1)
% periods.  Hence the above factor in Hopt.
% This way we correctly account for negative
% sidebands (left side of the carrier wave).

clear Hopt_gra;
Hopt_gra(N) = 0;
for j = N/2-7 : N/2+9;
      (j - N/2 -1)       % to display while working
      dBL = (wopt - wB + 2*pi*(j-N/2-1)*Omega)*...
            (lairB*Nper/2/c);
      Hopt_gra(j) = t_gauss(dBL);
end;

% GRATING
Efdisp_g = fftshift( Hopt_gra.*fftshift(Ef) );
Etdisp_g = ifft(Efdisp_g);
Itdisp_g = abs(Etdisp_g).^2;
Ifdisp_g = fft(Itdisp_g);
Hg = [Hg, 10*log10( ( abs(Ifdisp_g(2)/If(2)) )^2 ) ];

% FIBER
Efdisp_f = fftshift( Hopt_fib25.*fftshift(Ef) );
Etdisp_f = ifft(Efdisp_f);
Itdisp_f = abs(Etdisp_f).^2;
Ifdisp_f = fft(Itdisp_f);
Hf25 = [Hf25, 10*log10( ( abs(Ifdisp_f(2)/If(2)) )^2 ) ];
```

```
      Efdisp_f = fftshift( Hopt_fib50.*fftshift(Ef) );
      Etdisp_f = ifft(Efdisp_f);
      Itdisp_f = abs(Etdisp_f).^2;
      Ifdisp_f = fft(Itdisp_f);
      Hf50 = [Hf50, 10*log10( ( abs(Ifdisp_f(2)/If(2)) )^2 ) ];

      Efdisp_f = fftshift( Hopt_fib100.*fftshift(Ef) );
      Etdisp_f = ifft(Efdisp_f);
      Itdisp_f = abs(Etdisp_f).^2;
      Ifdisp_f = fft(Itdisp_f);
      Hf100 = [Hf100, 10*log10( ( abs(Ifdisp_f(2)/If(2)) )^2 ) ];

      % GRATING + FIBER
      Efdisp_fg = fftshift( Hopt_fib25.*Hopt_gra.*fftshift(Ef) );
      Etdisp_fg = ifft(Efdisp_fg);
      Itdisp_fg = abs(Etdisp_fg).^2;
      Ifdisp_fg = fft(Itdisp_fg);
      Hf25g = [Hf25g, 10*log10( ( abs(Ifdisp_fg(2)/If(2)) )^2 ) ];

      Efdisp_fg = fftshift( Hopt_fib50.*Hopt_gra.*fftshift(Ef) );
      Etdisp_fg = ifft(Efdisp_fg);
      Itdisp_fg = abs(Etdisp_fg).^2;
      Ifdisp_fg = fft(Itdisp_fg);
      Hf50g = [Hf50g, 10*log10( ( abs(Ifdisp_fg(2)/If(2)) )^2 ) ];

      Efdisp_fg = fftshift( Hopt_fib100.*Hopt_gra.*fftshift(Ef) );
      Etdisp_fg = ifft(Efdisp_fg);
      Itdisp_fg = abs(Etdisp_fg).^2;
      Ifdisp_fg = fft(Itdisp_fg);
      Hf100g = [Hf100g, 10*log10( ( abs(Ifdisp_fg(2)/If(2)) )^2 ) ];


      Omega_arr = [Omega_arr, Omega] ;

end;

% [following lines are for lairopt sweep]
%Hg1GHz = [Hg1GHz,Hg(1)];
%lairopt_arr = [lairopt_arr,lairopt*1e9-1500];
%end;  % of lairopt sweep



%[for lairopt sweep]
%plot(lairopt_arr,Hg1GHz)

figmake2
```

Appendix B -- Numerical Coupled Mode Routine

This Appendix shows a listing of a numerical routine used for solving the coupled mode equations (5.33a,b) with an arbitrary apodization and chirp function. The routine, written for the mathematics software package Matlab, is a function that returns the complex field reflectivity r, with the detuning parameter $\Delta\beta L$ passed in when the function is called. The dimensionless coupling strength function $\xi(x)$ of Chapter 5 is represented as the array Q.

```
function r = r_gauss(dBL)
%     r_gauss(dBL) returns the complex field reflection r of a
%     gaussian (or other) apodized grating by numerically solving
%     coupled mode DEs.  Grating parameters are set inside below.

N_steps = 1000;          % number of integration steps along grating
KL_tot = 2.00;           % total integrated coupling constant kappa*L

x_start = 0;             % integration starting point
x_stop = 1;              % integration ending point

f = -0/1540;       % the chirp parameter-- see section 6.4

Nper = 18000;      % needed only to translate f into a quadratic phase

dx = (x_stop-x_start)/N_steps;       % distance b/t integration points
x = [x_start : dx : x_stop ];        % creates an array of x values

sigma = 0.5/sqrt(2*log(2));   % width (length) of grating apodization

% dimensionless coupling strength array
% first part gives gaussian apodization
% second part adds phase for chirp
Q = exp( -(x-.5).^2 ./ (2*(sigma)^2) ).*exp(2*pi*i*Nper*f*x.^2);

Q_norm = sum( abs( Q(1:N_steps) )*dx );   % normalization factor of Q(x)
Q = Q*KL_tot/Q_norm;           % rescale so integrated coupling is KL_tot

% integrate DE's to generate field strength arrays

% A(j) and B(j) are field amplitudes at point x(j) travelling
% in positive and negative direction.  x=0 is left side of grating
```

```
% we integrate backwards, from far end of grating x=1 to near side x=0.

      A(N_steps+1) = 0; %creates and initializes array
      B(N_steps+1) = 1;

      for j = (N_steps) : -1 : 1;
            % integrate coupled mode DE's for one step
            A(j) = A(j+1) - ...
                  dx*Q(j+1)*B(j+1)*exp(-i*2*dBL*j*dx);
            B(j) = B(j+1) - ...
                  dx*conj(Q(j+1))*A(j+1)*exp(i*2*dBL*j*dx);
      end;

% return complex reflectivity

r =  A(1)/B(1) ;        % for t we return 1/B(1)
```

Appendix C -- Numerical Kramers-Kronig Routine

Below is a numerical routine that calculates the Kramers-Kronig integral (5.20b) by adding up contributions (5.25). It is intended for calculating the phase of a grating field transmittance as in (5.24) and the variable names reflect this. An array of frequencies and a corresponding array of $\ln(\sqrt{T})$ are passed in when the function is called, along with the single frequency at which the phase ϕ_t is desired. If no single frequency is passed in, the routine calculates an array of phases corresponding to the array of $\ln(\sqrt{T})$. The routine is further complicated by the capacity to handle an unevenly spaced frequency array, which often results when the frequency array is converted from a wavelength array as part of an experimental measurement. It is written for the Matlab mathematics software package.

```
function impart = kkre2im(freq,repart,w0)
%KKRE2IM    converts real values to imag via Kramers-Kronig
%     returns impart = kkre2im(freq,repart,w0)
%     freq is an array of frequencies, in radians/sec
%     repart is an array of real parts that corresponds to freq
%     impart is the imaginary part at w0
%     if w0 is not passed in, impart is an array corresponding to freq

if ~all(size(freq)==size(repart)) error('freq and repart wrong sizes');
end;
if ~(min(size(freq))==1) error('freq and repart wrong sizes');
end;

N = max(size(freq)) ;
dw = (freq(N) - freq(1)) / (N-1);  % approx...we don't assume constant
spacing below

if (nargin==3)
      impart = 0;
      % determine which element in freq is closest to w0
      if (w0 < freq(1) ) error('w0 is below range of freq array');
```

```
    elseif (freq(N) < w0) error('w0 is above range of freq array');
    end;  % of if (freq(1)...)
    j = 1;
    while (freq(j) < w0) j=j+1; end;
    if (freq(j)==w0)    % use exact w0
        for m=1:N;
            % set w1 and w2, bounds of sub-integral...
            % assumes freq(j) may not be evenly spaced....
            if ( m==1 | m==N)
                w1 = freq(m)-dw/2;
                w2 = freq(m)+dw/2;
            else
                w1 = (freq(m)+freq(m-1))/2;
                w2 = (freq(m+1)+freq(m))/2;
            end; % of if-else;
            % calculate contribution from this sub-integral
            impart = impart + repart(m)*...
            log(abs( (w2-w0)*(w1+w0)/((w1-w0)*(w2+w0)) ))/pi;
        end; % of m loop
    else  % extrapolate between two closest freq values "a" and "b"
        w0a = freq(j-1);
        imparta = 0;
        for m=1:N;
            % set w1 and w2, bounds of sub-integral...
                assumes freq(j) may
            % not be evenly spaced....
            if ( m==1 | m==N)
                w1 = freq(m)-dw/2;
                w2 = freq(m)+dw/2;
            else
                w1 = (freq(m)+freq(m-1))/2;
                w2 = (freq(m+1)+freq(m))/2;
            end; % of if-else;
            % calculate contribution from this sub-integral
            imparta = imparta + repart(m)*...
            log(abs( (w2-w0a)*(w1+w0a)/((w1-w0a)*(w2+w0a)) ))/pi;
        end; % of m loop
        w0b = freq(j);
        impartb = 0;
        for m=1:N;
            % set w1 and w2, bounds of sub-integral...
            % assumes freq(j) may
            % not be evenly spaced....
            if ( m==1 | m==N)
                w1 = freq(m)-dw/2;
                w2 = freq(m)+dw/2;
            else
                w1 = (freq(m)+freq(m-1))/2;
                w2 = (freq(m+1)+freq(m))/2;
            end; % of if-else;
            % calculate contribution from this sub-integral
            impartb = impartb + repart(m)*...
            log(abs( (w2-w0b)*(w1+w0b)/((w1-w0b)*(w2+w0b)) ))/pi;
        end; % of m loop
        impart = imparta + (impartb-imparta)*(w0-w0a)/(w0b-w0a);
    end;  % of if (freq(j)==w0)

elseif (nargin==2)      %...i.e. in this case return an array
    for n=1:N;
```

```
            n
            w0 = freq(n);
            impart(n) = 0;

            % for limited calculation
            % if( (n > N/2-20) & (n < N/2+20))

            for m=1:N;
                  % set w1 and w2, bounds of sub-integral...
                  % assumes freq(j) may
                  % not be evenly spaced....
                  if ( m==1 | m==N)
                        w1 = freq(m)-dw/2;
                        w2 = freq(m)+dw/2;
                  else
                        w1 = (freq(m)+freq(m-1))/2;
                        w2 = (freq(m+1)+freq(m))/2;
                  end; % of if-else;
                  % calculate contribution from this sub-integral
                  impart(n) = impart(n) + repart(m)...
                  *log(abs( (w2-w0)*(w1+w0)/((w1-w0)*(w2+w0)) ))/pi;
            end; % of m loop

            % for limited calculation
            % end;  % of if (n>N/2+...) loop

      end; % of n loop

else error('wrong number of argin');

end;  % of if-elseif-else
```

References

1) Matt McAdams, Eva Peral, Dan Provenzano, W. K. Marshall, Amnon Yariv, "Improved modulation response by frequency modulation to amplitude modulation conversion in transmission through a fiber grating," Applied Physics Letters, **71**, pp. 879-881 (1997).

2) Matt McAdams, Dan Provenzano, Eva Peral, W. K. Marshall, Amnon Yariv, "Effect of transmission through fiber Bragg gratings on semiconductor laser intensity noise," Applied Physics Letters, **71**, pp. 3341-3343 (1997).

3) Govind P. Agrawal, Fiber-Optic Communication Systems, John Wiley & Sons, 1992.

4) Ivan P. Kaminow, Thomas L. Koch, Optical Fiber Telecommunications IIIA, Academic Press, 1997, copyright Lucent Technologies.

5) Ivan P. Kaminow, Thomas L. Koch, Optical Fiber Telecommunications IIIB, Academic Press, 1997, copyright Lucent Technologies.

6) Amnon Yariv, Optical Electronics in Modern Communications, 5th ed., Oxford University Press, 1997, Sections 13.3 to 13.6.

7) Y. Arakawa, Amnon Yariv, "Quantum well lasers--gain, spectra, dynamics," IEEE Journal of Quantum Electronics, **QE-22**, pp. 1887-1899 (1986).

8) M. Asada, Y. Suematsu, "Density-matrix theory of semiconductor-lasers with relaxation broadening model - gain and gain-suppression in semiconductor-lasers," IEEE Journal of Quantum Electronics, **21**, pp. 434-442 (1985).

9) M. Willatzen, A. Uskov, J. Mork, H. Oleson, B. Tromborg, A.P. Jauho, "Nonlinear gain suppression in semiconductor-lasers due to carrier heating," IEEE Photonics Technology Letters, **3,** pp. 606-609 (1991).

10) Bin Zhao, T. R. Chen, Amnon Yariv, "The gain and carrier density in semiconductor lasers under steady-state and transient conditions," IEEE Journal of Quantum Electronics, **28**, pp. 1479-1486 (1992).

11) J. Manning, R. Olshansky, D.M. Fye, W. Powazinik, "Strong influence of nonlinear gain on spectral and dynamic characteristics of ingaasp lasers," Electronics Letter, **21**, pp. 496-497 (1985).

12) R. J. Lang, A. Yariv, "Semiclassical theory of noise in multielement semiconductor lasers," IEEE Journal of Quantum Electronics, **22**, pp. 436-449 (1986).

13) R. J. Lang, A. Yariv, "Analysis of the dynamic response of multielement semiconductor lasers," IEEE Journal of Quantum Electronics, **21**, pp. 1683-1688 (1985).

14) Amnon Yariv, Optical Electronics in Modern Communications, 5th ed., Oxford University Press, 1997, Sections 15.5 and 15.6.

15) Larry A. Coldren, Scott W. Corzine, Diode Lasers and Photonic Integrated Circuits, Wiley-Interscience, 1995, Chapter 5.

16) G.P. Agrawal, "Spectral hole-burning and gain saturation in semiconductor-lasers - strong-signal theory," Journal of Applied Physics, **63**, pp. 1232-1234 (1988).

17) Larry A. Coldren, Scott W. Corzine, Diode Lasers and Photonic Integrated Circuits, Wiley-Interscience, 1995, Appendix 5.

18) G.P. Agrawal, "Fundamental limitation on large-signal modulation of semiconductor-lasers and its implications for lightwave transmission," Electronics Letters, **26**, pp. 916-918 (1990).

19) T. L. Koch, R. A. Linke, "Effect of nonlinear gain reduction on semiconductor laser wavelength chirping," Applied Physics Letters, **48**, pp. 613-15 (1986).

20) C. H. Henry, "Theory of the phase noise and power spectrum of a single-mode injection laser," IEEE Journal of Quantum Electronics, **19**, pp. 1391-1397 (1983).

21) C.H. Henry, "Theory of the linewidth of semiconductor-lasers," IEEE Journal of Quantum Electronics, **18**, pp. 259-264 (1982).

22) C. H. Henry, "Theory of spontaneous emission noise in open resonators and its application to lasers and optical amplifiers," Journal of Lightwave Technology, **4**, pp. 288-297 (1986).

23) J. Wang, N. Schunk, K. Petermann, "Linewidth enhancement for DFB lasers due to longitudinal field dependence in the laser cavity," Electronics Letters, **23**, pp. 715-717 (1987).

24) George Arfken, Mathematical Methods for Physicists, 3rd ed., Academic Press, 1985, p. 585.

25) S. Yamamoto, N. Edagawa, H. Taga, Y. Yoshida, H. Wakabayashi, "Analysis of laser phase noise to intensity noise conversion by chromatic dispersion in intensity modulation and direct detection optical-fiber transmission," Journal Of Lightwave Technology, **8**, pp. 1716-1722 (1990).

26) C. C. Bradley, J. Chen, R.G. Hulet, "Instrumentation for the stable operation of laser-diodes," Review Of Scientific Instruments, **61**, pp. 2097-2101 (1990).

27) K. G. Libbrecht, J. L. Hall, "A low-noise high-speed diode laser current controller," Review of Scientific Instruments, **64**, pp. 2133-2135 (1993).

28) P. A. Morton, T. Tanbun-Ek, R. A. Logan, A. M. Sergent, P. F. Sciortino Jr., D. L. Coblentz, "Frequency response subtraction for simple measurement of intrinsic laser dynamic properties," IEEE Photonics Technology Letters, **4**, pp. 133-136 (1992).

29) G.P. Agrawal, "Effect of gain nonlinearities on the dynamic-response of single-mode semiconductor-lasers." IEEE Photonics Technology Letters, **1**, pp. 419-421 (1989).

30) R. Olshansky, D.M. Fye, J. Manning, C.B. Su, "Effect of nonlinear gain on the bandwidth of semiconductor-lasers," Electronics Letters, **21**, pp. 721-722 (1985).

31) A. Røyset, L. Bjerkan, D. Myhre, L. Hafskjær, "Use of dispersive optical fibre for characterization of chirp in semiconductor lasers," Electronics Letters, **30**, pp. 710-11 (1994).

32) R. C. Srinivasan, J. C. Cartledge, "On using fiber transfer function to characterize laser chirp and fiber dispersion," Photonics Technology Letters, **7**, pp. 1327-29 (1995).

33) B. Wedding, "Analysis of fibre transfer function and determination of receiver frequency response for dispersion supported transmission," Electronics Letters, **30**, pp. 58-59 (1994).

34) Amnon Yariv, Optical Electronics, 4th ed., Saunders College Publishing, 1991, Chapter 10.

35) W. K. Marshall, J. Paslaski, A. Yariv, "Reduction of relative intensity noise of the output field of semiconductor lasers due to propagation in dispersive optical fiber," Applied Physics Letter, **68**, pp. 2496-98 (1996).

36) William W. Morey, Gary A. Ball, Gerald Meltz, "Photoinduced Bragg gratings in optical fibers," Optics and Photonics News, **5**, pp. 8-14 (1994).

37) W. H. Loh, R. I. Laming, X. Gu, M. N. Zervas, M. J. Cole, T. Widdowson, A. D. Ellis, "10 cm chirped fiber Bragg grating for dispersion compensation at 10 Gbit/s over 400 km of non-dispersion shifted fiber," Electronics Letters, **31**, pp. 2203-2204 (1995).

38) P. A. Krug, T. Stephens, G. Yoffe, F. Ouellette, P. Hill, G. Dhosi, "Disperson compensation over 270 km at 10 Gbit/s using an offset-core chirped fiber Bragg grating," Electronics Letters, **31**, pp. 1091-1093 (1995).

39) Mike J. O'Mahony, "Optical multiplexing in fiber networks: progress in WDM and OTDM," IEEE Communications Magazine, December 1995, pp. 82-88.

40) Stephen B. Alexander, "WDM network operation calls for close control of parameters," Lightwave, June 1997, pp. 27-32.

41) Sergei S. Orlov, Amnon Yariv, Scott Van Essen, "Coupled-mode analysis of fiber-optic add-drop filters for dense wavelength-division multiplexing," Optics Letters, **22**, pp. 688-690 (1997).

42) K. O. Hill, B. Malo, F. Bilodeau, D. C. Johnson, "Photosensitivity in Optical Fibers," Annual Review of Materials Science, **23**, pp. 125-157 (1993).

43) Govind Agrawal, Nonlinear Fiber Optics, 2nd ed., Academic Press, 1991, p. 449.

44) K. O. Hill, B. Malo, F. Bilodeau, D. C. Johnson, J. Albert, "Bragg gratings fabricated in monomode photosensitive optical fiber by UV exposure through a phase mask," Applied Physics Letter, **62**, pp. 1035-1037 (1993).

45) Gerald Meltz, William W. Morey, W. H. Glenn, "Formation of Bragg gratings in optical fibers by a transverse holographic method," Optics Letters, **14**, pp. 823-825 (1989).

46) J. D. Prohaska, E. Snitzer, S. Rishton, V. Boegli, "Magnification of mask fabricated fiber Bragg gratings," Electronics Letters, **29**, pp. 1614-1615 (1993).

47) B. Malo, K. O. Hill, F. Bilodeau, D. C. Johnson, J. Albert, "Point-by-point fabrication of micro-Bragg gratings in photosensitive fiber using single excimer pulse refractive-index modification techniques," Electronics Letters, **29**, pp. 1668-1669 (1993).

48) M. A. Putnam, C. G. Askins, G. M. Williams, E. J. Friebele, M. Baskansky, J. Reintjes, "Single-pulse fabrication of fiber Bragg gratings using a phase-conjugated KrF excimer laser," Electronics Letters, **31**, pp. 885-886 (1995).

49) Amnon Yariv, Optical Electronics, 4th ed., Saunders College Publishing, 1991, pp. 61-64.

50) Henry W. Wyld, Mathematical Methods for Physics, Addison-Wesley, 1976, Section 2.8.

51) George Arfken, Mathematical Methods for Physicists, 3rd ed., Academic Press, 1985, Chapter 9.

52) F. Ouellette, "Limits of chirped pulse compression with an unchirped Bragg grating filter," Applied Optics, **29**, pp. 4826-29 (1990).

53) George Arfken, Mathematical Methods for Physicists, 3rd ed., Academic Press, 1985, pp. 421-426.

54) E. C. Titchmarsh, Introduction to the Theory Fourier Integrals, 2nd ed., Oxford University Press, 1937.

55) Hermann A. Haus, Waves and Fields in Optoelectronics, Prentice-Hall, Inc., 1984, Section 3.3.

56) Pochi Yeh, Optical Waves in Layered Media, John Wiley and Sons, Inc., 1988, Section 5.3.

57) John D. Jackson, Classical Electrodynamics, John Wiley & Sons, Inc., 1975, pp. 249-251.

58) B. J. Eggleton, T. Stephens, P.A. Krug, G. Dhosi, Z. Brodzeli, F. Ouellette, "Dispersion compensation using a fiber grating in transmission," Electronics Letters, **32**, pp. 1610-11 (1996).

59) C. Harder, K. Vahala, A. Yariv, "Measurement of the linewidth enhancement factor α of semiconductor lasers," Applied Physics Letters, **42**, pp. 328-330 (1983).

60) Larry A. Coldren, Scott W. Corzine, Diode Lasers and Photonic Integrated Circuits, Wiley-Interscience, 1995, pp. 207-213.

61) J. Park, W. V. Sorin, K. Y. Lau, "Elimination of the fibre chromatic dispersion penalty on 1550 nm millimetre-wave optical transmission," Electronics Letters, **33**, pp. 512-13 (1997).

62) Amnon Yariv, Optical Electronics in Modern Communications, 5th ed., Oxford University Press, 1997, p. 509.

63) Kerry J. Vahala, Mickael A. Newkirk, "Intensity noise reduction in semiconductor lasers by amplitude-phase decorrelation," Applied Physics Letters, **57**, pp. 974-976 (1990).

64) Michael A. Newkirk, Kerry J. Vahala, "Amplitude-phase decorrelation: a method for reducing intensity noise in semiconductor lasers," IEEE Journal of Quantum Electronics, **27**, pp. 13-22 (1991).

65) Xiao Lin Lu, C. B. Su, R. B. Lauer, "Increase in laser RIN due to asymmetric nonlinear gain, fiber dispersion, and modulation," Photonics Technology Letters, **4**, pp. 774-777 (1992).

66) Amnon Yariv, Optical Electronics, 4th ed., Saunders College Publishing, 1991, pp. 1-3.

67) George Arfken, Mathematical Methods for Physicists, 3rd ed., Academic Press, 1985, p. 425.

68) D.C. Hutchings, M. Sheikbahae, D.J. Hagan, E.W. Vanstryland, "Kramers-Kronig relations in nonlinear optics," Optical and Quantum Electronics, **24**, pp. 1-30 (1992).